COLLECTIVE PLASMA STRUCTURES WITH KINETIC NONLINEARITY: THEIR COHERENCE, INTERACTION AND STABILITY

By

Debraj Mandal

PHYS06201204006

INSTITUTE FOR PLASMA RESEARCH, GANDHINAGAR

A thesis submitted to the
Board of Studies in Physical Sciences

In partial fulfillment of requirements
for the Degree of

DOCTOR OF PHILOSOPHY
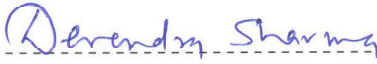
of

HOMI BHABHA NATIONAL INSTITUTE

October 2017

Homi Bhabha National Institute

## Recommendations of the Viva Voce Committee

As members of the Viva Voce Committee, we certify that we have read the dissertation prepared by **Debraj Mandal** entitled " COLLECTIVE PLASMA STRUCTURES WITH KINETIC NONLINEARITY: THEIR COHERENCE, INTERACTION AND STABILITY " and recommend that it may be accepted as fulfilling the thesis requirement for the award of Degree of Doctor of Philosophy.

--- Date : 09/ 01/ 2018

Chairman : Prof. S. Mukherjee

--- Date : 09/ 01/ 2018

Guide/ Convener : Dr. Devendra Sharma

--- Date : 09/ 01/ 2018

Examiner : Dr. Prateek Sharma

--- Date : 09/ 01/ 2018

Member : Dr. Joydeep Ghosh

--- Date : 09/ 01/ 2018

Member : Prof. P. K. Chattopadhyay

--- Date : 09/ 01/ 2018

Member : Prof. Y. C. Saxena

Final approval and acceptance of this thesis is contingent upon the candidate's submission of the final copies of the thesis to HBNI.

I hereby certify that I have read this thesis prepared under my direction and recommend that it may be accepted as fulfilling the thesis requirement.

Date : 09/ 01/ 2018

Place: IPR, Gandhinagar

Dr. Devendra Sharma

Guide

STATEMENT BY AUTHOR

This dissertation has been submitted in partial fulfillment of requirements for an advanced degree at Homi Bhabha National Institute (HBNI) and is deposited in the Library to be made available to borrowers under rules of the HBNI.

Brief quotations from this dissertation are allowable without special permission, provided that accurate acknowledgement of source is made. Requests for permission for extended quotation from or reproduction of this manuscript in whole or in part may be granted by the Competent Authority of HBNI when in his or her judgment the proposed use of the material is in the interests of scholarship. In all other instances, however, permission must be obtained from the author.

Debraj Mandal

DECLARATION

I, hereby declare that the investigation presented in the thesis has been carried out by me. The work is original and has not been submitted earlier as a whole or in part for a degree / diploma at this or any other Institution / University.

Debraj Mandal

List of Publications arising from the thesis

Journal:

1. **Adiabatic electron response and solitary wave generation by trapped particle nonlinearity in a hydrogen plasma**
   Debraj Mandal and Devendra Sharma, *Phys. of Plasmas* **21**, 102107 (2014).

2. **Nonlinearly interacting trapped particle solitons in collision-less plasmas**
   Debraj Mandal and Devendra Sharma, *Phys. of Plasmas* **23**, 022108 (2016).

3. **On the nonlinear trapping nature of undamped, coherent structures in collisionless plasmas and its impact on stability**
   H. Schamel, D. Mandal and D. Sharma, *Phys. of Plasmas* **24**, 032109 (2017).

4. **Study of trapped particle nonlinearity in ion acoustic solitary wave using Vlasov simulation**
   Debraj Mandal and Devendra Sharma, *Journal of Physics-Conference Series* **759**, 012068 (2016).

Conferences/ Schools:
International Participation:

1. "Growth of electron hole in subcritical regime of ion acoustic instability: extends the parameter regime of the conventional plasma turbulence."
   44th European Physical Society Conference on Plasma Physics (EPS-2017), 26th-30th June, 2017, Belfast, Northern Ireland, UK.

2. "Nonlinear dispersive evolution of coherent trapped particle structures in collisionless plasmas."
   58th Annual Meeting of the APS- Division of Plasma Physics (APS-DPP, 2016), 31st Oct.-4th Nov., 2016, San Jose, CA, USA.

3. "Nonlinear mode-coupling via resonant particles in small amplitude "linear" regime in collisionless plasmas."
   18th International Congress on Plasma Physics (ICPP-2016), 27th June-1st July, 2016, Kaohsiung, Taiwan.

4. "Effect of trapped particle nonlinearity in IAW solitary wave."
   10th Asia Plasma and Fusion Association Conference (APFA-2015), 14th-18th Dec., 2015, Gandhinagar, India.

5. "Study of trapped particle nonlinearity in ion acoustic solitary wave using Vlasov simulation."
   27th IUPAP Conference on Computational Physics (CCP-2015), 2nd-5th Dec., 2015, Guwahati, India.

6. "Generation of solitary wave by trapped particle nonlinearity in Vlasov plasma"
   7th International conference on the Frontiers of Plasma Physics and Technology (FPPT-7), 13th-17th April, 2015, Kochi, India.

National Participation:

1. *DST-SERC School on Tokamaks and Magnetized Plasma Fusion, 25th Feb. to 15th Mar., 2013*, IPR, Gandhinagar, Gujarat, India.

2. "Role of trapped particle nonlinearity in stabilization of a unstable IAW."
   29th National Symposium on Plasma Science and Technology & International Conference on Plasma Science and Nanotechnology (Plasma-2014), 8th-11th Dec., 2014, Kottayam, Kerala, India.

3. *Hands-on School on Nonlinear Dynamics (HSND-2015), 16th-22nd Feb., 2015*, IPR, Gandhinagar, Gujarat, India.

4. "Trapped particles nonlinearity produced solitary wave structures in kinetic plasma microinstability simulations."
   30th National Symposium on Plasma Science & technology (Plasma-2015), 1st-4th Dec., 2015, Kolkata, India.

Debraj Mandal

Dedicated to

My family

ACKNOWLEDGEMENTS

Contents

iv

List of Figures

List of Tables

SYNOPSIS

The dispersive collisionless plasma is a medium whose microscopic texture most readily manifests itself by developing macroscopic coherent structures emerging from balance between dispersion and a nonlinearity generated by particles. The first evidence that there is a coupling between the particle nature of the plasma and the routinely detectable plasma modes (of its fluid-like continuum phase) comes from the nonlinear coherence developing in the collective plasma waves well below the minimum amplitude for a nonlinearity to operate in an ideally continuous medium [1]. Underlying this small amplitude nonlinearity is the inevitable feature of a finite resonant charged particle population being trapped in collective potential nonuniformity of waves. While for the cold laboratory plasmas the conventional instability thresholds based on small amplitude linear waves [2] may be appropriate, for hot stellar and interstellar plasmas, and for the plasma in fusion devices that keeps getting ever-hotter, the instability thresholds based on small amplitude linear waves need to be obtained by revisiting the kinetic theory of collective modes that duly accommodates the particle trapping in the collective waves. Finding a general nonlinear kinetic description of collective structures defines the central idea of the modern plasma theory of collective waves and instability. Apart from a few landmark and noteworthy analytic approaches [3–7], the computer simulations remain strongest means of exploring this interesting physics and validating few existing analytic approaches to stable nonlinear kinetic structures. This constitutes the central motivation for studies done in the present thesis. The high resolution, multiscale, multispecies, fully kinetic, exact mass simulations of essentially nonlinear, collective kinetic plasma response to phase-space perturbations are done in the present study, describing: mechanism, mutual interaction, and unstable evolution of such coherent phase-space structures. In the present thesis, the nonlinear collective structures are addressed by means of computer simulations done over a wide regime of collective dynamics, covering ion acoustic [8], electron acoustic [9] and electron plasma wave regimes of trapped particle structures. The study analyzes their, development [8], mutual interaction [9] and the unstable behavior [10] resulting from such interactions. Issues addressed include the comparison of fundamentally nonlinear structures with their linear counterparts based on the advanced nonlinear kinetic formulations and the linear formulations of Landau [11] and van-Kampen [12]. The results of linear simulations are presented to highlight

the missing effects of particle trapping in essentially nonlinear structures [10].

Provided below is a more systematic chapter-wise analysis of the topics in study of the collective plasma structures governed by kinetic trapped particle nonlinearity addressed in the present thesis.

Chapter-1: Introduction

This chapter introduces the trapped particle generated nonlinear structures and motivates the study by discussing the important formulations and main existing results related to the plasma collective structures with particle trapping [1]. Observations of such structures in laboratory [13–15] and natural plasma conditions, for example in space and magnetospheric plasmas [16–20], are discussed along with their numerical simulations and corresponding results [21–24]. Standard analytic and numerical methods to formulate and analyze the physics of coherent structures are discussed with the challenges when trapped particle nonlinearity is present. Various classes of solutions proposed under existing theory [25] are discussed with regimes of their accessibility. Open problems related to collisionless structures with coherence generated by the kinetic nonlinearity are highlighted. The organization of the thesis work is described with capacity and limitations of the present approach. Introduction to numerical approach and a road map of present study is provided with a brief summary of the main results from each part of the analysis.

Chapter-2: Phase-fluid continuity of the collisionless Vlasov-Poisson system: The numerical model

The collective dynamics of collisionless plasma in an electrostatic approximation is governed by the Vlasov-Poisson system [26]. The fundamental properties of the Vlasov systems and associated continuity of the plasma treated as a phase fluid is described in this chapter and properties of its solutions are discussed. The numerical scheme for implementing phase-fluid conservation [27] is described schematically and results for standard cases are presented and benchmaked against various alternate approaches. The scheme for parallelization of the numerical technique is described and net achievable numerical efficiency is characterized with respect to the scale of computing architecture as well as the computing strength of the supercomputing system available at the IPR computer center [9]. Normalizations used for the results are described and the issue of optimum resolution of the phase-space for generating solutions with desired accuracy is discussed. Boundary conditions

for the distribution function along both x and v dimensions are described and their implementation in the numerical scheme is discussed. Various results showing confirmation with multiple time scales resolved by the code and interaction between processes on distinct time scales are examined. Dispersion properties of propagating structures are verified against their standard analytic forms [28]. The challenges associated with resolution of multiple time scales are highlighted for the simulations performed with exact electron to ion mass ratio. Standard fluid results like parametric coupling between two collective processes at different time scales [29] and the standard kinetic results, like Landau damping [11] of collective plasma perturbation are quantitatively verified.

Chapter-3: Adiabatic electron response and solitary wave generation by trapped particle nonlinearity

In collisionless regime, the kinetic effects modify the fast electron response, influencing many collective linear and nonlinear processes that are otherwise well described by the equilibrium hydrodynamic formulation of a collisional plasma [30–32]. Electron distribution in the collisionless regime shows structures like phase space vortex which can be strong enough to produce the spatial nonuniformities in the electron density associated with them [1, 3, 33]. An electron phase space distribution featuring such structures shows electron trapping with a robust total energy conservation in a collisionless equilibrium set up. The species' phase-space distribution functions, therefore, are purely a function of total energy and thus valid solutions of the corresponding Vlasov equations. With electron adiabaticity resulting in modulation of the population of particles trapped in the resonance region, these modifications in the particle distribution functions begin to affect the collective processes, most effectively by generating additional nonlinear effects [34]. The results of fully nonlinear simulation presented in this chapter show a self-consistent development of such structures, and a resulting coherence, in a situation where the linear theory prescribes that a small amplitude ion acoustic wave must grow to large enough amplitudes before showing any sign of conventional fluid nonlinearity $u \cdot \nabla u$ in the form of growing coherence [28, 35].

The rest of the chapter presents interpretation of these results based on the analytic formulation of trapped electron equilibria and electron phase-space holes by H. Schamel [4]. A detailed validation of the recovered coherent structure as collisionless trapped particle equilibria is done based on multiple cases in the simu-

lations over a range of parameters of the analytic formulation. Multiple scenarios with and without a perturbing potential produced by a coexisting electron plasma wave, capable of ergodizing the separatrix region, are explored. The evolved solutions are quantitatively compared with the analytic results of the electron hole formulations in each case. The phase space distributions of electrons and ions, spatial distributions of density and potential corresponding to evolved solitary wave structures, and associated Sagdeev potential are presented systematically. The central observations and conclusions include that the nonlinear coherent solitary wave structures developed in the simulation follow the analytical solutions of an m-KdV equation that accounts for the stronger nonlinearity produced by the electron trapping in the structure [8]. In the low k regime, where the structures coexist and interact with the undamped high frequency electron plasma waves, the nonlinear solitary structures retain their nearly analytic form as long as the trapped electron distribution stays in an independent (unperturbed) thermodynamic equilibrium. In the conditions where the developing ion acoustic structures are free from time dependent perturbations, the numerically simulated coherent structure could be characterized analytically. Such validation involved finding, from them, the necessary parameters to construct the corresponding analytic solutions and to carry out the comparison of the simulation results with the theoretical formulation that has a modified KdV equation with a stronger trapping nonlinearity [36]. Relatively small amplitude coherent structures coexisting with a periodic self-consistent potential perturbation are found to be most affected by the nonadiabatic response of the electrons. Presence of a self-consistent time dependent perturbing potential, in the form of a coexisting EPW, prevents the trapped electrons from reaching an equilibrium and forming stable trapped particle modes that are time independent stable solutions of the Vlasov equation. It is observed that although a coherent solitary structures has a sizable transient fraction of trapped particle population in the separatrix region, it remains reasonably stable as long as a finite adiabatic fraction of the trapped population existed. Finally, the time asymptotic evolution of the trapped particle mode structure associated with solitary structure generated by the trapped particle nonlinearity shows a residual growth originating from the associated trapped particle instability [37] which produces modulations in the soliton amplitude with electron bounce frequency and causes a net growth in present cases simulated using a finite current.

viii

Chapter-4: Nonlinearly interacting trapped particle solitons in collision-less plasmas

This chapter deals with the issue of mutual interaction between the structures nearly confirming with propagating solitary electron holes (SEH) solutions. The static or time independent limit of propagating trapped particle structures considered analytically by Schamel [1], showed that the nonlinearity introduced by the amplitude dependent density of trapped particles influencing the local potential can substitute the more conventional sources of nonlinearities in plasmas to produce an alternate range of interesting nonlinear solutions. Their mathematical forms include a potential hump or solitary electron hole (SEH), a cnoidal electron hole wavelet (CEHWL), and a solitary potential dip (SPD) [36]. The interaction between these time independent solutions though has received only limited attention and requires a systematic analysis since such an interaction essentially subject the structures to the effectively time varying field of each other. While an exact analytic treatment of interaction between the SEHs involves a time dependent nonlinear treatment of trapping nonlinearity, at present it is a qualitative understanding based on the approximate models [38, 39] that two colliding SEHs preserve their identity if their velocity separation is large enough ($\Delta v^2 > \psi$, where ψ is the amplitude of the soliton electrostatic potential in electron thermal units T_e/e). The effect of such interactions on the thermalized trapped particle distribution in the SEH is still unexplored in sufficient detail. The simulations of two nearly analytic interacting SEH structures presented in this chapter allow one to additionally explore their adiabatic and nonadiabatic responses to a time varying field or temporal impulse.

The simulations in this chapter explores a distinct limit of propagation and examines interaction between the faster SEH structure in regime of electron-acoustic structures. The results from this part of the work exhibit the coexistence of linear electron plasma mode and nonlinear electron acoustic mode with a comparable amplitude. The additional linear fast electron plasma modes are generated in the simulation, as a result of analytic approximations entering the SEH solutions used as initial conditions. This EPW activity consists of a set of noninteracting linear modes. Their contribution to potential evolution is therefore found separable from the potential data by their Fourier decomposition into constituent modes and following their analytic time evolution [9]. However, the modes constituting slow

coherent solitons couple nonlinearly via the strong response of the trapped electrons in the SEH structures. The strongly electron trapping equilibrium SEH structures are observed to interact adiabatically and preserve their identity across multiple events of interaction, or collision, between two SEHs. The phase-space evolution of the SEH is illustrated where a shift, mutually separating the interacting holes along the velocity coordinates, during the interaction, is noted. This consolidated shift of complete trapped population results in preservation of identities of the SEH and restoration of the pre-interaction forms of the SEH following the inter-action. The soliton velocity shows variation during the interaction such that a slight phase-shift is visible in the soliton motion for the cases where the time of interaction is longer. The phase-shift is larger for smaller soliton in the case of two non-identical interacting solitons. The interacting states of the SEH are also compared with infrequent transients observed in the magnetospheric data usually featuring frequent SEH like bipolar electric field structures [18, 19]. Properties of these interacting stages in simulation are found to confirm with the tripolar and inverse tripolar pulses observed having relatively low rate of detection in the mag-netospheric data [20].

Chapter-5: Evolving trapped particle structures with implications on plasma stability

This chapter explores the concept of stability for small amplitude nonlinear modes using a current-driven, 1D, collisionless plasma as a paradigm of driven intermit-tent plasma turbulence and anomalous transport with the focus on undamped coherent electrostatic structures. The simulation results are treated as central mo-tivating factor to make progress along the pure nonlinear branch of the plasma dispersion which is analytically developed and provides a general framework that accommodates the standard linear dispersive formulation as its special case [10]. The high resolution computer simulation results presented in this chapter illustrate an evolution of realizable phase-space perturbations, which evolve into the stable coherent structures traveling at phase velocities far from their linear prescription in addition to the familiar linear plasma modes located at a variety of time and spatial scales. Analysis presented in this chapter begins with the inspection of the plasma response in terms of a valid evolution of the Vlasov-Poisson system to a non-topological, eddy-like, initial perturbation (a locally scarce electron population

about any velocity, preferably on the rising side of a drifting $f_e(v)$). The simulated response is employed to draw the general picture in the following order: we first revisit linear fluid theory and then consider the linear Vlasov theory of Landau and van-Kampen [11, 12]. The interpretation of the overall picture that emerged from our simulation results is finally completed where we systematically include this nonlinearity and develop a general Nonlinear Dispersion Relation (NDR), capable of displaying all the observed familiar and unfamiliar responses in their corresponding limits. In order to complete the analysis by simulation, we show that a stationary hole appeared to be undamped within a full Vlasov dynamics, but dies out completely within a linear Vlasov evolution [10]. The set of simulations presented therefore has the consequence that in the case of coherency, the onset of instability as described by linear theory (e.g., Landau) is generally absent when seen realistically from the standpoint of the complete Vlasov-Poisson system. It is replaced instead by a more complex, highly unknown destabilization process in phase space, in which this manifold of trapped particle equilibria with their attracting negative energy property together with the explicit initial perturbation will play an important role. This renders plasma destabilization multifaceted and, as a rule, no longer one-dimensional in terms of the parameter-space.

Chapter-6: Electron hole instability of subcritical plasma phase-space perturbations

Turbulence in collisionless stellar and high energy space plasmas is expected to be essentially dominated by large scale potential variations, capable of trapping large density of charge particles. While being in equilibrium with potential of trapped charges these structures must interact mutually as well as with the conventional plasma modes and must get destabilized in order to be active part of the turbulent energy cascade, transferring the large scale field energy to the heat. While the ergodization of separatrix witnessed in Chaper 2 represents a nearly nonthermal decay of these structures and a direct passage of energy to the heat (or smallest accountable scale), an opposite process, where finite gain in energy of these structures results from larger scale, constitutes a sufficient condition for ensuring their place into the spectral chain of the energy cascade [40]. Interestingly, though, for sufficiently ergodized separatrix any such growth might additionally involve de-ergodization of the separatrix and an associated local increase of the entropy.

This subject therefore also opens a new dimension in the known thermodynamic aspects of the plasma turbulence where a thermalization (or possibly reversible ergodization) takes place at multiple stages of turbulent spectrum rather than at the terminally smaller scales produced by the viscous dissipation [41]. Existence and clarity of the mechanism of growth or instability of these coherent structures, via their interaction, with each other or with conventional waves, presently remains an open question. In this final chapter we focus on this mechanism by means of our simulations. Seed like perturbations in the electron distribution function [1] are analyzed below the linearly subcritical limit [2] of a current driven ion acoustic instability. Detailed analysis of the development of the nonlinear structures is carried out and their evolution is examined for the cases where they are show a multi-parameter evolution while undergoing a *nonlinear electron hole instability*. Unlike the linear instability where amplitude remains the sole growth parameter, the growth of an electron hole is characterized by the strengthening response of the trapped particle population that reflects into transformation of an initial hole in a multidimensional space of parameters. These dimensions in the presently considered Schamel formulation, include: the propagation velocity v_0, peak potential ψ and the inverse trapped electron temperature β of the structures, and are mutually coupled to each other by the Nonlinear Dispersion Relation (NDR), describing a continuum of collective nonlinear modes [1]. The parametric growth mechanism for the electron hole instability is identified involving an extended interaction between the electron hole and a background large scale ion acoustic structure. The mechanism is illustrated quantitatively using the simulation data from multiple cases which show strong to weak, or nearly vanishing, growth in specific limits of the parameters.

Chapter-7: Conclusion and future scope

This chapter provides, brief summary of the complete study presented in the thesis, summarizes the major conclusions from the present thesis work and consolidates these conclusions to provide the updated status of the knowledge on the issues addressed. The major results are also discussed in the perspective of existing experimental results and a limited number of theoretical formulations of the present problem [3–6]. Key areas are identified where the present results and conclusion can help in introducing quantitative revisions in the existing theoretical formula-

tions. The discussion is included on a more generalized structure of the nonlinear stability analysis of the collective plasma response, involving kinetic trapped particle nonlinearity. The ways to address several outstanding issues requiring kinetic inputs, e.g., plasma heating in collisionless nonthermal conditions via the generalized formulations [42] and parallel heat conduction in collisional cases [43] are considered with respect to present approaches to the issue [3–5]. The extension of the present simulation approach to more diverse phase-space equilibria [3] and naturally recovered nonlinear kinetic structures [13–20] is discussed and the possible stages involved in making progress towards addressing them are described. Possible scenarios leading to unstable phase-space perturbations and their analogue in other physical setups supporting collective processes [44, 45] are considered highlighting relevance of conclusion from the present simulation results to such alternate setups.

1

Introduction

1.1 Motivation

The physics of collective structures in plasma assumes different dimensions in various regimes of its existence. Most accessible and familiar are the dispersive modes of the collisional plasmas, validated, almost routinely, to a high degree of accuracy in the laboratory plasma experiments. In hot collisionless plasma regime, however, the collective behaviour is highly indeterministic or rather stochastic, such that the statistical measures are better means to describe its highly turbulent dynamical state. The evolution and setup of turbulent states are associated with a parameter space of a very high dimensionality. Such states indicate a rather continuous mode spectrum where nonlinear excitations populate scales that are otherwise forbidden by a fundamentally discrete mode structure of the linear plasma formulation. The nonlinearity, if exclusively tied to larger amplitudes, does not enter the operating mechanism of the turbulence since latter must progress by growing newer scales, essentially from small amplitude noise/fluctuations, hence purely linear and discrete in their spectrum. More specifically, the microinstabilities originating from interaction between collective structures and resonant particles are prescribed, at such low amplitudes, to destabilize only the discrete spectrum of linear modes, undamped under the linear Vlasov formulation.

In these terms, a host of small amplitude nonlinear structures that are also undamped, evolve deterministically, and grow by means of mechanisms other than linear wave-particle interaction, remain unaccounted for under the linear plasma stability paradigm. Analyzing their physics by means of extensive, fully kinetic,
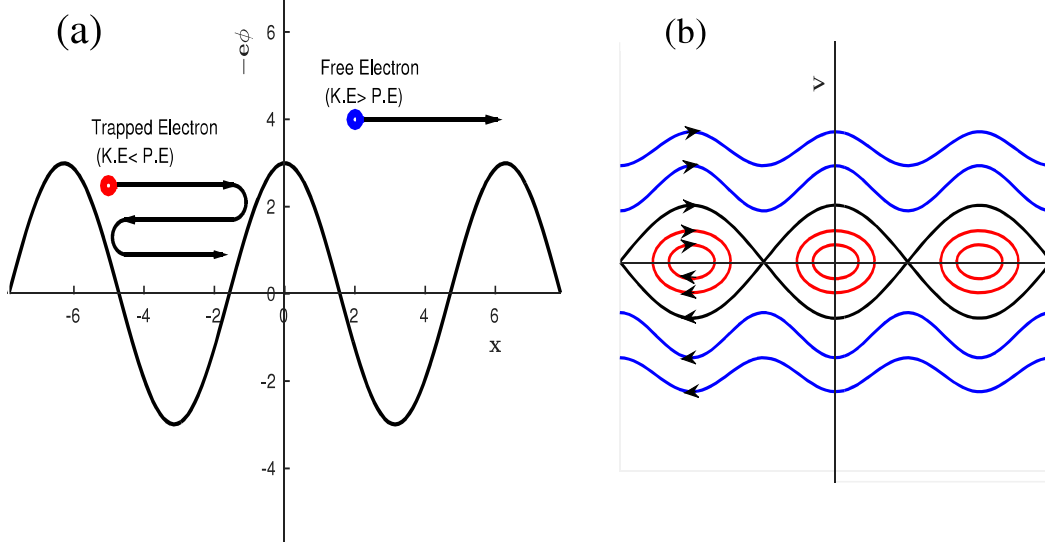
Figure 1.1: (a) Particle denoted by red dot is trapped in the wave and the particle denoted by the blue dot is a free particle. (b) Phase space of trapped and free particles denoted by red and blue lines correspondingly.

computer simulations and attempting to find a general nonlinear description of collective structures, perhaps defines a large part of the idea of the modern plasma theory of collective waves and instability. Progress on this branch of the fundamental plasma physics is mainly concerned with the underlying physics of coherence often observed at low amplitudes, having its origin in microscopic particle based kinetic structure of the plasmas rather than a fluid-like continuum.

The dispersive collisionless plasma is a medium whose microscopic texture most readily manifests itself by developing macroscopic coherent structures [24]. Underlying this is the inevitable feature of a finite resonant particle population being trapped in collective potential nonuniformity of waves (see the schematic Fig. 1.1). The fast electron response to electrostatic perturbations is inhibited, for example, by the kinetic effects where resonant electrons are either reflected or get trapped by even small potential nonuniformities. The oscillations of trapped particles add to the degrees of freedom [32] and result into phase-space vortices [24] that can modify the spatial nonuniformities associated with the vortex depending up on the trapped particle density as well as the amplitude of nonuniformity. The analytic structure of trapped particle equilibria is extensively analyzed in various limits,

2

e.g., where trapped particles can be maintained in isolated non-thermal states and the exact nonlinear solutions are obtained as Bernstein-Greene-Kruskal (BGK) modes [3], and for the cases where the trapped particles are well approximated as having an equilibrium distribution with finite *temperature* [1, 25, 46]. In the later limit, considered analytically in great detail by H. Schamel, it was shown [1] that the nonlinearity introduced by the amplitude dependent density of trapped particles influencing the local potential, can substitute the more conventional sources of nonlinearities in plasmas to produce an alternate range of interesting nonlinear solutions. Their mathematical forms include a potential hump or solitary electron hole (SEH), a cnoidal electron hole wavelet (CEHWL), and a solitary potential dip (SPD) [1]. A large class of structures in laboratory and natural plasmas perhaps follow this description which admits a far restricted entropy production rate and hence displays a wider agreement with a range of structures recovered both in experiments and in computer simulations.

The Vlasov equation, describing the plasmas in their ideal collisionless limit, admits infinite solutions since all the functions of total energy at any phase space location satisfy the Vlasov equation. While all of these solutions enjoy a mathematical equivalence, most appealing are often those that are most robust and would satisfy also the formulations that apply to regimes of maximum contrast with respect to the Vlasov theory. It is hence not surprising that these most successful solutions are natural starting point for all the efforts to make progress in the direction of other relevant solutions that are required when the horizons of usually familiar part of the sphere of the subject are to be crossed. In this respect, even the alternatives adopted in more general rigorous approaches to the plasma stability theory make only a modest excursion from the conventional sphere of knowledge, but they, fortunately, open a window to an ocean of possibilities of new and challenging explorations in this area.

The studies in this thesis address the issues of plasma stability rather passively but explore the kinetic nonlinearity driven structures that defy the characteristics of linear plasma modes and therefore offer an extended set of solutions for a more general theory of plasma stability to cover. The kinetic trapped particle equilibria are a dominant category of full nonlinear solutions of Vlasov equation. They are often encountered in laboratory and space plasmas and therefore indicate that they are likely to be a dominant missing element from the puzzle of the plasma

turbulence and its operating mechanism [10]. In order to further introduce the subject of this thesis, we discuss important existing approaches to this subject in Sec. 1.2. The contribution of the studies presented in this thesis is then briefly described in Sec. 1.2.2. In Sec. 1.3 and Sec. 1.4 we revisit various approaches to collective structures in plasma, beginning from the conventional linear fluid theory which is discussed so as to point out limitation of linear approaches and their eigenmodes in representing the *coherence* of the collective structures. We also provide essential introduction to existing rigorous solutions of trapped-particle equilibria by H. Schamel that are mainly followed in most part of the present simulations. In its overall structures, this thesis presents simulations of development, propagation and interaction of undamped trapped particle equilibria in two separate slow and fast regimes in Chapter 3 and Chapter 4, respectively. This is followed by exploring, in Chapter 5, their activity and possibility of their destabilization by non-conventional means in the regime where the linear theory prescribes their stability. In Chapter 6, they, finally, are shown to be indeed destabilized in terms of growth in parameters other than the amplitude, which remains the sole growth parameter for the conventional eigenmodes of the linear formulations.

1.2 Existing studies on phase-space coherence and stability

The fundamental kinetic approach to plasma instability was given by Landau by recovering a microinstability in linear dispersive plasma eigenmodes introduced by their interaction with resonant particles. In contrast to this, van-Kampen [47] acknowledged existence of trapped particles in a linearized form and recovered a continuum, or *off-dispersion* range, of modes. The first two motivating factors for the newer version of plasma stability theory involving nonlinear coherent structures were (i) the identification of coherence in its ideal mathematical form by Zabuski and Kruskal [48] as solutions of Kortweg-de Vries equation [49] and (ii) the prescription for exact non-perturbative approach to plasma oscillation by Bernstein, Greene and Kruskal introducing the idea of well known Bernstein-Greene-Kruskal (BGK) modes [3]. The limitation on the stability of all classes of BGK solutions motivated studies by H. Schamel [25] to explore more stable subclasses of BGK modes. Schamel adopted a pseudo-potential approach to achieve more realistic

trapped particle distributions by using additional constraints on them to satisfy the Vlasov-Poisson system, these aspects are also reviewed recently in sufficient detail by I. Hutchinson [7].

First analytic exploration of electron hole-like solutions was started by H. Schamel [25] over four decades ago. Subsequently, Schamel and coworkers also derived the stability criteria for the holes [36, 50]. Schamel importantly introduced, in 1972 [4] (see also [51]), a method to partly replace the more general BGK method [3] for obtaining mainly the stable physical solutions. This has been an effective method which allows to discard or avoid physically inadequate solutions. Its applicability has been proven in numerous studies dealing with solitary wave propagation, cnoidal electron and ion holes, double layers, holes of negative energy, group velocity of periodic structures or longitudinal structures superimposed on coasting and bunched beams in circular accelerators, to mention a few. Reviews on this alternative method can be found in [1, 36, 52–54] as well as in [55, 56]. The growth of these nonlinear equilibria, possible in a subcritical plasma, was addressed analytically in the past by Dupree [5] who concluded that the amplitude of these structures must grow due to scattering of particles for propagation velocities in the range where ion and electron distribution function have opposite signs of velocity derivatives. Solution for coherent phase space density hole using the Sagdeev's pseudo-potential technique were also prescribed by T. H. Dupree [5]. Dupree provided a thermodynamic basis for the Schamel-like trapped particle distribution function. T. H. Dupree also characterized the turbulent state of plasma by random small scale phase space granulation or formation of *clumps* [46], where clumps are defined as structures originating from particle orbits that become random and stochastic due to the presence of fluctuating electric field in a turbulent plasma. This leads to the distribution function differing from its average value as the regions of phase space with different density are mixed to produce such finite granulation. A quasi-linear approach to nonlinear Landau damping was made by Thomas O'Neil [32]. Thomas O'Neil showed that the resonant particles are trapped in a wave after time, $\tau_B = \sqrt{m/eEk}$, equivalent to inverse of bounce frequency of the particle in the wave. After time $\tau_B = \omega_{be}^{-1}$ the linear Landau damping theory fails due to failure of linear limit $\partial f_0/\partial v \sim \partial f_1/\partial v$. In his quasi-linear theory, O'Neil incorporated modifications of the background distribution f_0 arising from particle trapping to derive the nonlinear growth rate for $t > \tau_B$.

O'Neil used a *quasi-linear* approximation for the resonant region and defined a new distribution by coarse-grain averaging the actual distribution. As $t/\tau_B \to \infty$, the size of the mesh used in the coarse-grain averaging approaches zero and the coarse-grained distribution becomes constant along the phase-space trajectories. Therefore the distribution function becomes a constant function of time. The growth rate $\gamma(t) \propto \partial_v f_0|_{\omega/k}$ therefore becomes zero as $t/\tau_B \to \infty$. The quasi-linear treatment, however, does not recover the formation of coherent structures that requires finite mode coupling.

1.2.1   Important experimental and simulation studies

The existence of the electron hole has been demonstrated in laboratory experiments as well as space plasma observations in Earth's ionosphere and magnetosphere. Saeki *et al.* detected electron holes in a Q-machine experiment [13] in 1979. Petraconi *et al.* [14] recovered strong-electron holes and double layers in a low pressure mercury plasma column with evidence that electron-hole formation is driven by an ion beam, hence is not possible in isolation since its formation requires a nearby ion accelerating potential structure. Recently many studies have detected the existence of electron holes in various experiments. Electrostatic solitary structures were generated in a quasineutral plasma in LAPD by applying an electron beam parallel to magnetic field line [57]. Generation of phase space electron hole has been observed during magnetic reconnection in a toroidal device [58]. Experiments with non-neutral plasmas [59] in Penning-Malmberg traps have also shown the existence of trapped particle modes and their contribution to anomalous transport of the plasma particles in a perpendicular direction to magnetic field lines. Solitary electron hole was also generated from a high voltage initial potential pulse in unmagnetized plasma [15] at IPR, India. Generation of ion acoustic soliton from a compressional pulse and their growth or decay in a inhomogeneous plasma density was studied in 1976 by P. I. John and Y. C. Saxena [60]. An excitation of holes below linear threshold was reported in the laboratory experiments by Moody and Driscoll [61].

Among many areas of applications are particle accelerators where observations relate to coasting and bunched beams in synchrotrons and storage rings, representing further Vlasov-Poisson systems. In the Fermi Main Ring, for example, while operating near the stability limit [52], sharp gaps or notches have been wit-

nessed in the response function [62], which correspond to depletion zones in the momentum distribution function. This is seen at the lowest measurable signal level and sheds light on the spectrum of small amplitude perturbations, discussed above, as the alternate modes supplementing the linear discrete eigenmodes. A similar phenomenon, of stable, coherent, longitudinal structures superimposed on bunched beams [63], has been observed during "rf activity" in stochastic cooling studies [64, 65].

In 1974 detection of Broadband Electrostatic Noise (BEN), having frequency extended up to plasma frequency, in the geomagnetic tail across the neutral sheet was reported [66]. This was an early observation of the signature of existence of electron hole in space plasma which was confirmed in 1994 by Matsumoto *et al.* from GEOTAIL spacecraft data [16]. They reported that most of the BEN in the plasma sheet boundary layer (PSBL) was not a continuous broadband noise but was composed of a series of bipolar pulsed electric fields, corresponding to Electrostatic Solitary Waves (ESW). Observations by subsequent spacecraft missions [17–19] provide evidence of a strong electron hole activity in magnetospheric plasma routinely attributed to these solitary structures. There are many observations in different regions by various satellites which show the existence of solitary electron holes, e.g., in the Earth's auroral region (FAST) [17], bow shock (Wind) [67], magnetopause (GEOTAIL) [68], magnetosheath (Cluster) [69, 70], (MMS) [71], plasma sheet (THEMIS) [72], (Cluster) [73], outer radiation belt (Van Allen Probes) [74, 75] and also in the free solar wind, at interplanetary shocks, and current sheets (Wind) [76–79]. One recent study by A. Osmane *et al.* [80] discovers long-lived electrostatic coherent structures with large-amplitude electric fields in planetary radiation belts by the Van Allen Probes. It reveals alternative routes for nonlinear subcritical growth of electron phase space hole through which planetary radiation belt's acceleration can take place.

Among considerable simulation based studies, the electron holes were observed in a kinetic computational simulation of two stream instability in 1D electrostatic plasmas by K. V. Robert and H. L. Berk [81]. They followed the motion of the phase space boundaries of an incompressible and constant density phase space fluid and observed the formation phase space and condensation of electron holes. H. L. Berk, C. E. Nielson and K. V. Robert [39] studied the formation of electron holes and collisions between such two structures with large and small relative velocity.

They had used water bag like distribution function in the kinetic simulation and also compared their results with stable proton clusters which develop from the negative-mass instability in the mirror experiment DCX-1. Formation and comparison of phase space eddies or electron hole in 1D, 2D and 3D simulation of two beam plasma were studied by R. L. Morse and C. W. Neilson [82]. The reported phase space eddies were formed in 1D, but in 2D and 3D they starts to form and finally they disappeared. Effect of ion motion on an electron phase space hole having phase velocity smaller than or equals to ion acoustic wave was studied by K. Saeki and H. Genma [38] through computer simulation. They found that due to ion motion the electron hole disrupted into two holes and formed coupled states of electron holes and ion acoustic solitons which were explained by using Sagdeev's potential for a water bag like distribution function. Shakanaka [83] performed numerical simulation of formation and interaction of ion acoustic solitary wave with Vlasov equation for ions and Boltzmann distribution for electron. V. L. Krasovsky, H. Matsumoto and Y. Omura [84] showed theoretically and by computer simulation that electron holes perform inelastic collision due to a specific irreversibility caused by the nonadiabatic modification of the internal structure of the holes which is related with the phase mixing of trapped electron.

Simulations by Berk *et al.* [21] recovered spontaneous hole-clump pair creation close to the linear threshold for instability. A well documented excitation of holes below linear threshold could be seen also in numerical simulations of pair plasmas [85]. Lesur *et al.* [22, 23, 86] in their numerical simulations of these structures also recovered growth in subcritical regime resulting from exchange of momentum with other species or with the wave pseudo-momentum. Similarly, the growth of ion phase-space structures was recovered by Petkaki *et al.* [87] in a Vlasov simulation generating anomalous resistivity that exceeds the quasilinear estimates driving the reconnection. Another mechanism of subcritical hole excitation was recently proposed by Lesur *et al.* [88], augmenting the Berk-Breizman model [89], by wave coupling with a linearly unstable (supercritical) mode. In another work, P. H. Diamond *et al.* [22, 90, 91] had defined a new quantity *phasestrophy* to determine the growth of unstable coherent structures in presence of dissipative wave. B. Eliassson and P. K. Shukla [92] had studied the formation, acceleration and interaction of phase space holes in both nonrelativistic and relativistic limit through Vlasov simulation. Simulating SEH like structures in large amplitude

regime ($\psi > 1$) that admits other nonlinearities, Eliasson *et al.* [93] showed that colliding electron holes coalesce and get trapped by the ion density nonuniformities produced by their stationary phase.

1.2.2 Contribution of the present study

The studies in this thesis explored the kinetic particle trapping driven coherence and its impact on stability using high resolution Vlasov simulations. In the simulations of driven ion acoustic instability, we have (D. Mandal *et al.* [8]) presented early signs of coherence in growing ion acoustic wave structures where electron trapping nonlinearity begins to introduce solitary attributes in the potential profiles. There we have showed increasing agreement with solutions of a modified Kd-V equation obtained by H. Schamel for the cases with stronger trapping and less modification in the phase-space separatrix by perturbation from a coexisting trapped particle structures on the electron plasma wave branch. The stable propagation and identity preserving mutual interactions of phase-space structures proposed by H. Schamel [1] were simulated by us (Mandal *et al.* [9]). In this study we showed activity of solitary solutions of the modified Kd-V incorporating electron trapping nonlinearity on the faster electron acoustic branch. We showed that modes with smaller spatial scales couple by means of trapped particles to produce coherence and defy the linear dispersive propagation as followed by rest of the coexisting linear modes of equivalent amplitude at larger spatial scale. We also interpreted the bipolar and, somewhat less frequent, tripolar pulsed electric field variations measured in magnetosphere by a cluster of four spacecraft [18, 19], as electron-hole waveforms with similar proportion of probability of their detection in an ensemble of interacting coherent structures with a localized source. In a dual set of high resolution simulations performed to illustrate the distinct evolution of undamped plasma modes predicted by linear and nonlinear stability models, respectively, both linear and nonlinear versions of Vlasov simulations were performed using non-conventional phase-space perturbations as presented by us (Schamel, Mandal and Sharma [10]). Adopting a pseudo-potential approach, this study elaborated that the coherence is inaccessible under the linear model as a result of failure in achieving a pseudo-potential to construct a potential structure with time-stationary phase velocity. As a direct consequence of this, the coherent structures are absent from the linear version of simulations as well. The

linear simulation additionally validates absence of any fluid nonlinearity at this small amplitude in nonlinear simulations. The linear eigenmodes thus cease to represent solutions of the full Vlasov-Poisson system and intrinsically nonlinear solutions emerge. Construction of phase-space perturbation with limited entropy production then allows construction of valid pseudo-potential that leads to highly stable nonlinear solutions representing a newer level of coherent mode structures recovered in the nonlinear simulations. This work highlighted, in turn, the nonlinear modes that participate in small amplitude noise like activity must grow by mechanisms independent of those driving the linear instabilities (linear or Landau growth and damping). These processes which might involve their growth in terms of parameters other than amplitude, such as phase velocities that are no longer fixed during the growth unlike those of the eigenmodes of linearized Vlasov Poisson system.

In the final part of this thesis, the full nonlinear simulations, once again performed in the regime where linear theory predicts no growth, show evidence of initial perturbations that produce undamped modes of both the classes, namely, the conventional linear eigenmodes and coherent trapped particle structures closely described by electron hole formulations. In the cases of localized phase space perturbations, seeded at small phase velocity, the initially developed nonlinear structures are shown to accelerate and *mode-convert*. The destabilization is shown both by an intrinsic hole instability as well as a parametric-like instability of the holes where holes transform by interacting with background plasma nonuniformities generated from linear structures.

1.3   Useful notions and formulations

We now introduce some useful notions which were discussed qualitatively in the motivation in the view of their more quantitative forms frequently applied in the interpretation of the simulation results.

1.3.1   Coherence and linear (fluid) description

A mutually exclusive relationship between coherence and linearity can be illustrated by means of a 1D linearized fluid treatment of the collisional plasmas. As derived in sufficient detail in Appendix A, linearized version of plasma fluid equa-

tions, apart from yielding the linear dispersion relation can be rearranged to obtain the variable Φ (potential) which executes a simple harmonic motion with amplitude ψ in a pseudo potential,

$$-\mathcal{V}(\Phi) = \frac{k^2}{2}\Phi(\psi - \Phi),\qquad(1.1)$$

thus representing the standard expression of a single harmonic wave of wave number k,

$$\Phi_\pm(x,t) = \frac{\psi}{2}\left(cos[kx \mp \omega_L t] + 1\right),\qquad(1.2)$$

which is essentially an expression for two Langmuir waves propagating in opposite direction, where $\omega_L = \sqrt{1+3k^2} \equiv \omega_L(k)$ is the k-dependent Langmuir wave frequency.

Note that when we attempt to construct *coherent composite* solutions by superposition of distinct eigenmodes, the time dependence cannot be contained in the phase part of the propagating waveform, as required, and instead a time dependent amplitude emerges. Existence of a characteristic time independent $\mathcal{V}(\Phi)$ is therefore ruled out. In the case, for example, of two superimposed counterpropagating modes, $\Phi(x,t) = \frac{\psi}{2}[\cos(\omega_L t)\cos(kx)+1]$, and the $\mathcal{V}(\Phi)$ is

$$-\mathcal{V}(\Phi) = \frac{k^2}{2}\Phi(\psi - \Phi) - \frac{1}{2}\left[\frac{k\psi}{2}\sin(\omega_L t)\right]^2,\qquad(1.3)$$

i.e., no time-independence in the frame of the propagating structure $\Phi(x,t)$, which itself is oscillatory, is possible. This gives us the opportunity to postulate an intimate relationship between the physical phenomenon "coherency" and its mathematical analogue "$\mathcal{V}(\Phi)$". In rest of this chapter we shall denote, by $\Phi(x)$, the solutions for which a consistent, i.e., valid $\mathcal{V}(\Phi)$ exists and call them "coherent" structures, whereas we term solutions for which such a property is missing "incoherent" and denote them by $\phi(x)$. However in rest of the thesis Φ is used as argument of $\mathcal{V}$, i.e., $\mathcal{V}(\Phi)$ for representing the pseudo potential corresponding to coherent structures only.

1.3.2 Coherence from dispersion and nonlinearity

In the plasma waves represented by (1.2), the propagation velocity ω/k of each mode depends on its wave number k, these waves are therefore called the linear dispersive waves. During propagation of a group of waves (wave packet) with different k_i, the modes disperse or spread and therefore the wave packet diminishes over distance. If the dependence of frequency ω_L on the amplitude (i.e, $\omega_L = \omega(k,a)$, where a is the amplitude of the wave), neglected in the linear formulation (Appendix A), is retained, the plasma equations no longer remain linear. However, the change in the phase velocity with changing k, present in linear approach, can be compensated by appropriate change in the amplitude such that modes with different k can propagate coherently. The essential form of an equation that allows introduction of such a co-operative nonlinearity can be obtained by allowing, in a simple wave equation

$$\frac{\partial \phi}{\partial t} + c_0 \frac{\partial \phi}{\partial x} = 0 \tag{1.4}$$

satisfying $\phi = \cos(x - c_0 t)$, a nonlinear dispersion $\omega = c_0 k + c_1 k^3$ and an amplitude nonlinearity $c_2 \phi \partial_x \phi$, that preserve the nondissipative character of the wave equation, yielding,

$$\partial_t \phi + c_0 \partial_x \phi + c_2 \phi \partial_x \phi + c_1 \partial_x^3 \phi = 0. \tag{1.5}$$

In a more refined form, (1.5) is the well known wave equation for nonlinear dispersive waves, namely, the Korteweg-de Vries (Kd-V) equation,

$$\partial_t \phi + \phi \partial_x \phi + \frac{1}{2} \partial_x^3 \phi = 0. \tag{1.6}$$

Transforming plasma fluid equations, (A.1)-(A.3) in the from of (1.6) under relevant approximations successfully provides the explanation of large amplitude nonlinear coherent structures [94] in plasmas where the nonlinearity $u\partial_x u$, of the Eq. (A.2) is significantly large. Due to this nonlinear term in a wave equation, higher harmonics $(2\omega, 2k)$ couple to the original wave (ω, k). The appearance of shorter wavelengths means *steepening*. If the higher harmonics travel at the same velocity as the fundamental the coupling becomes stronger. But if the higher harmonics travel with a different velocity than the fundamental, the coupling be-

comes weaker and steepening stops. Due to the dispersive property of the medium, the higher harmonics with higher wave numbers $(2k, 3k, ...)$ have different phase velocities than the fundamentals. Therefore there is a competition between the steepening and dispersion. Solitary wave solution is a special type of nonlinear solution in which these two terms balance with each other. Hence the solitary wave solution is a remarkably stable nonlinear solution. Therefore in the formation of any coherent stable structure in plasma, both the nonlinearity and dispersive property plays an important role.

In this thesis however the coherence is explored for the regime where an alternate nonlinearity, arising from particle trapping, replaces the nonlinearity in a set of kinetic equations of hot collisionless plasma at much lower amplitudes.
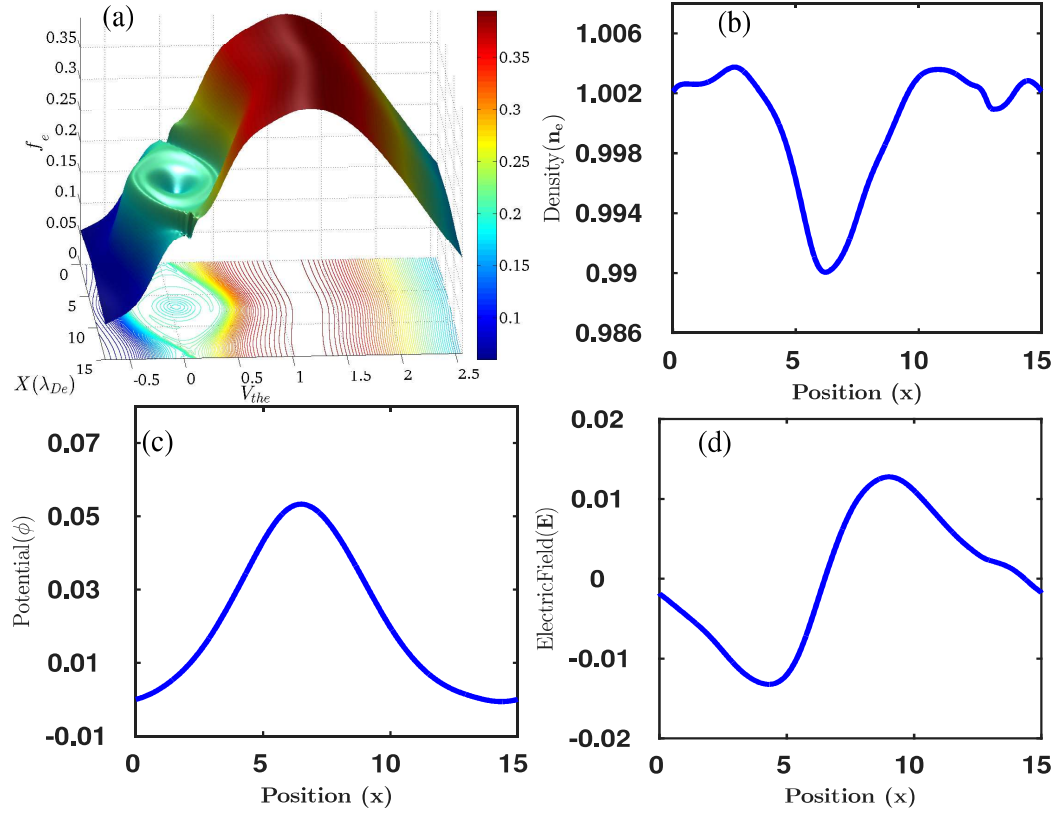
Figure 1.2: (a) Electron distribution function, (b) electron density, (c) electrostatic potential and (d) electric field corresponding to a coherent phase-space electron hole is generated by kinetic trapped particle nonlinearity during study of the current driven ion acoustic instability.

1.3.3 Fluid and trapped particle nonlinearities

In a macroscopic fluid picture of plasmas, the nonlinearity is incorporated by the nonzero value of the $\mathbf{v} \cdot \nabla \mathbf{v}$ term, which is applicable at large amplitude limit. However, in microscopic kinetic picture nonlinearity is introduced by wave particle interaction and the particle trapping in the wave potential. Particle trapping is a nonlinear phenomenon. The background distributions of the particles are essentially modified by the particle trapping such that the trapped particle distribution can satisfy both the Vlasov equation and the Poisson equation. An example of an electron distribution function modified by a hole as simulated in this work is presented in Fig. 1.2(a). The corresponding electron density, potential ϕ and electric field E are plotted in Figs. 1.2(b), (c) and (d) respectively. Such equilibrium cannot be recovered by disallowing the modification in the background distribution function, hence, the nonlinear term $E\partial_v f$ in the electrostatic Vlasov equation,

$$\frac{\partial f}{\partial t} + v_x \frac{\partial f}{\partial x} + \frac{q}{m} E \frac{\partial f}{\partial v_x} = 0, \tag{1.7}$$

must be accounted for. The linear Vlasov theory that must use a linear form, $E\partial_v f_0$, of this term, must therefore ignore the trapped particle density and cannot find an equilibrium with respect to the change in the trapped particle density. This fundamentally kinetic nonlinearity involves a small resonant region of the phase space and therefore begins to act from very small level of amplitude, rather than the fluid effects that involve mobilization of entire distribution.

1.4 Kinetic descriptions of the collective plasma phenomena

The microscopic kinetic description of plasmas is obtained using the Vlasov equation. The response of a plasma to an initial perturbation is treated both under the linear and nonlinear formulation of Vlasov theory. In the following, we first introduce the existing linear approaches following Landau and van-Kampen. The nonlinear or approaches prescribed by Bernstein, Greene and Kruskal and that given by H. Schamel are discussed subsequently.

1.4.1 Linear Landau approach

The linearized form of the Vlasov equation (1.7) is rather easy to solve and has been basis of most of the plasma kinetic theory. The solutions of this linearized Vlasov equation were presented by L. D. Landau [11] in 1946. The theory investigates evolution of the perturbation in the equilibrium distribution function f_α and the electric field **E**, as

$$
\begin{aligned}
f_\alpha(x,v,t) &= f_{\alpha 0}(x,v,t) + \epsilon_1 \, f_{\alpha 1}(x,v,t), \\
\mathbf{E}(x,t) &= \mathbf{E}_0(x,t) + \epsilon_1 \, \mathbf{E}_1(x,t)
\end{aligned}
\tag{1.8}
$$

obtaining the linearized form of Vlasov equation,

$$
\partial_t f_{\alpha 1} + v_x \partial_x f_{\alpha 1} + \frac{q_\alpha}{m_\alpha} \mathbf{E}_1 \partial_v f_{\alpha 0} = 0.
\tag{1.9}
$$

Here, ϵ_1 is amplitude of the perturbation and $\epsilon_1 << 1$. E_1 can be calculated from the linearized Poisson's equation

$$
\partial_x E_1 = 4\pi \sum_\alpha q_\alpha \int f_{\alpha 1} \, dv.
\tag{1.10}
$$

Eq. (1.9) is a linear partial differential equation. The validity of the linearized Vlasov approach demands the smallness of the velocity gradient of f_1: $|\partial_v f_1| << |\partial_v f_0|$. Treating (1.8)-(1.10) as an initial value problem it was solved by the Fourier-Laplace transform and a complex integral along the Landau contour to obtain time-asymptotic linear dispersion relation (LDR),

$$
1 - \sum_\alpha \frac{\omega_{p\alpha}^2}{k^2} \int \frac{\mathbf{k}.\partial_v f_{\alpha 0}}{\omega - \mathbf{k}.\mathbf{v}} \, dv = 0.
\tag{1.11}
$$

Considering the unperturbed distribution f_0 as Maxwellian, and by defining the plasma dispersion function $Z(\zeta)$ as,

$$
Z(\zeta) = \frac{1}{\pi^{1/2}} \int_\infty^\infty \frac{e^{s^2}}{s - \zeta} \, ds,
$$

the dispersion relation (1.11) can be written as,

$$k^2 - \frac{1}{2} Z' \left(\frac{\omega - k v_D}{\sqrt{2} k} \right) = 0. \tag{1.12}$$

The real part of the dispersion relation (1.12) gives the normal modes of plasma and the imaginary part gives the growth rate or damping rate of the amplitude of the wave. The growth rate or damping rate is proportional to $\partial_v f_0$. Due to the wave-particle interaction, the resonant particles having lower velocity than the wave, gain energy from the wave and the particles having higher velocity lose energy to the wave. If the number of resonance particles having higher velocity is more compared to the particles having lower velocity, then the wave grows.

In Landau approach f_0 always remains fixed, which is also used in fluid description of plasma (where f_0 is additionally Maxwellian obtained in the maximum entropy limit, although Landau's f_1 evolves conserving entropy [28]). Therefore, the number density of the resonant particles does not change with time. Further, the growth/damping rates are evaluated at the poles of the integrand that essentially represent the discrete linear modes of the plasma, hence displaying no coherence, as discussed in Sec. 1.3.2. This theoretical model does not account for trapped particles and an equilibrium with respect to them. It can, therefore not, explain the existence of continuum plasma modes.

1.4.2 Linear van-Kampen approach

Under the van-Kampen approach [47], the solutions of linearized Vlasov equation can be derived, after making Fourier transformation of the linearized Vlasov equation (1.9) in both space and time, as,

$$f_1(v) = \frac{8\pi^2 q^2}{mk} n_0 \left[\mathbf{P} \frac{v f_0(v)}{\omega - kv} + \lambda \delta(\omega - kv) \right]. \tag{1.13}$$

Here, $\mathbf{P}$ indicates that the first term within the square bracket is to be interpreted as a principal value, λ is an arbitrary function of ω and k and δ denotes the Dirac delta function at $v = v_0 = \omega/k$, where v_0 is the phase velocity of a wave. Therefore, for each value of v_0 there is a different solution for f_1. These are called van-Kampen modes. The van-Kampen modes are singular functions that do

not represent a physically meaningful perturbation. Therefore, to study the time dependence of a physical initial perturbation, one should consider a superposition of infinitely many van-Kampen modes. Although each mode is undamped, the total perturbation will show Landau damping because the various modes get out of phase with one another.

Here the arbitrary function λ is used to introduce the trapping phenomena. Only the particles with $v = v_0$ are trapped. The van-Kampen approach can explain the existence of continuum plasma modes, which are not be explainable by linear Landau approach. More detailed comparison of Landau and van-Kampen approaches is discussed in chapter-5.

1.4.3 Nonlinear BGK waves

In linear Landau description of plasma by neglecting the term $\partial_v f_1$ and considering $\partial_v f_0 = 0$ at $v = v_0$, both, the amplitude dependent macroscopic fluid nonlinearity and the microscopic trapped particle nonlinearity are not considered. The nonlinear collective coherent stable structures can be explained only by complete nonlinear solutions of the Vlasov equation (1.7). A steady state solution of nonlinear Vlasov equation is found by considering $\partial f_\alpha / \partial t = 0$ in Eq. (1.7) written for species α. In one dimension, the equation for f_α is,

$$v_x \frac{\partial f_\alpha}{\partial x} - \frac{q_\alpha}{m_\alpha} \frac{\partial \phi}{\partial x} \frac{\partial f_\alpha}{\partial v_x} = 0. \tag{1.14}$$

The total energy, $\epsilon = \frac{1}{2} v^2 - \phi$, remains constant on particle orbits. The general solution can be represented as,

$$f_\alpha = f_\alpha \left(v_x^2 + \frac{2 q_\alpha \phi}{m_\alpha} \right) \equiv f(\epsilon). \tag{1.15}$$

These types of stable solutions having trapped and free particles were first given by I. B. Bernstein, J. M. Greene and M. D. Kruskal in 1957 [3]. According to their names these types of solutions are called BGK modes. There are two different ways to obtain these types of coherent structures as defined by Bernstein, Greene and Kruskal. One is the *integral equation* and another is *differential equation* technique. The integral approach is well known as BGK approach and the differential approach is well known as Sagdeev or Schamel approach [7].

In integral or BGK approach, from the knowledge of potential $\phi(x)$ and the background distribution $f(v, x = \infty)$, the trapped particle distribution f_t and the free particle distribution f_f at any point x can be derived. The only constraint is that f_t can not be negative. One noticeable thing in this technique is that, any monotonic potential $(\phi(x))$ structure can be constructed. There is no restriction on the shape of trapped particle distribution function. That is why all the solutions of BGK theory are not stable physical solutions. For an example, the trapped particle distribution function for a linear Langmuir wave is a delta function which also has been introduced previously in van-Kampen approach. Another example is phase-space electron holes. Phase-space electron hole of any length can be constructed according to BGK theory. But after a maximum length, the slope singularity of the trapped particle distribution function $(\partial f/\partial v \rightarrow \infty)$ appears [7] at the separatrix $(v = \sqrt{\psi})$.

1.4.4 Schamel's nonlinear model

After Bernstein, Greene and Kruskal's (BGK) formulation, H. Schamel in 1971 [25] provided a formulation to explore more stable subclasses of BGK modes. Schamel used in the formulation for trapped particle distribution function the *differential equation* technique [25]. In this technique, the total distribution function is written by joining trapped and free particle distribution functions in corresponding regions,

$$f(x, v) = \frac{1 + k_0^2 \psi/2}{\sqrt{2\pi}} \left(\theta(\epsilon) \exp[-\frac{1}{2}(\sigma\sqrt{2\epsilon} - v_0)^2] + \right.$$
$$\left. \theta(-\epsilon) \exp(-\frac{v_0^2}{2}) \exp(-\beta\epsilon) \right). \qquad (1.16)$$

Function (1.16) is a formal solutions of the Vlasov equation since it is function only of total energy ϵ. Here, β is the trapping parameter. The first exponential term within the bracket represents the free particle expression which is valid for $\epsilon > 0$ and the second exponential terms together represent the trapped particle distribution which is valid for $\epsilon \leq 0$ where $\epsilon = v^2/2 - \phi(x)$.

The density obtained from the distribution function (1.16) is used to derive potential $\phi(x)$ by solving the Poisson equation using the Sagdeev potential or pseudopotential $\mathcal{V}(\phi)$ technique. The boundary conditions applied on values of $\mathcal{V}(\phi)$ at two extreme values of ϕ ($\phi = 0$ and $\phi = \psi$, where ψ is the maximum

value of ϕ) determine a Nonlinear Dispersion Relation (NDR) Eq. (5.13) and the choice of value k produces various classes of coherent nonlinear solutions, apart from producing linear eigenmodes in a limiting case. These classes of nonlinear
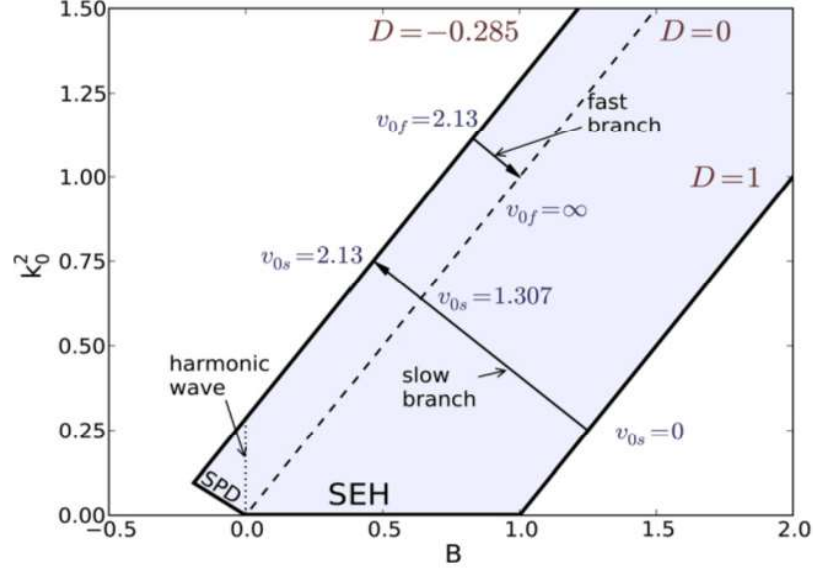
Figure 1.3: Phase diagram of the trapped particle nonlinear structures in the parameter space k_0^2-B, presented by Schamel [1] as obtained from the nonlinear dispersion relation (NDR). Here, $D = B - k_0^2$ and the velocities v_{0s} and v_{0f} are the velocities of slow and fast branches, respectively. More detailed description about B is given in Chapter-5.

mathematical forms include a potential hump or solitary electron hole (SEH), a cnoidal electron hole wavelet (CEHWL), and a solitary potential dip (SPD) [1]. The velocity v_0 of the structures are determined by a nonlinear dispersion relation (NDR) Eq. (5.13). The potential expression for the case of a stable solitary electron hole (SEH), according to this model is, $\phi(x) = \psi \, \mathrm{sech}^4(x/4)$. Schamel [1] identified a parameter B whose value demarcates harmonic waves and the coherent solutions in the formulation. A phase diagram as produced by schamel in the parameter space k_0^2-B, reproduced here in Fig. 1.3, describes regimes of existence of the above branches of solutions. As seen from the phase-diagram, the solutions with $B = 0$ are harmonic waves while solutions with finite B correspond to coherent structures. Similarly identifiable in the phase-diagram are the solitary structures

or SEH having $k_0^2 = 0$. One most important characteristic of this solution is that the shape of the potential $\phi(x)$ approximately follows the Debye shielding property $n_e \propto \exp(\phi) \to 1 + \phi$ [7]. A more detailed discussion about the Schamel's model and NDR is given in Chapters 4-6.

1.4.5   Entropy of hole equilibria: Dupree and Lynden-Bell approaches

T. H. Dupree gave solutions for coherent phase space density hole [5] using, once again, the *Sagdeev potential* or pseudo-potential technique. In respect to entropy, both Schamel's and Dupree's model consider entropy maximization for constructing the trapped particle distribution function. They have used Maxwell-Boltzmann statistics to calculate the entropy, therefore this hole velocity distribution function is addressed by Dupree as Maxwell-Boltzmann hole. The entropy is defined quantitatively by Dupree as,

$$- \sigma = -n \int dx \int dv f \ln f, \qquad (1.17)$$

where n is the average number density and f contains an average over microstates, while mentioning that the proper choice of σ for the Vlasov system is not a well understood problem. Highlighting its relevance to the collisionless Vlasov plasmas, for example, D. Lynden-Bell in 1967 [6] found the equilibrium distribution in an encounterless relaxation by use of a fourth type of statistics related to both Fermi-Dirac statistics and equipartition of energy per unit mass. In the limit of distinguishable micro-particles and no exclusion of micro-cells by them, this statistics becomes Maxwell's distribution but with temperature proportional to mass.

1.5   Content of the thesis and major results

The studies presented in this thesis analyze the issues discussed in the above section mainly by the means of kinetic Vlasov simulation. Here we highlight the contents and important results from the chapters of this thesis.

Chapter 2 presents a numerical technique for solving the Vlasov-Poisson equation in 1D case for electrostatic plasmas. The fundamental properties of the Vlasov systems and associated continuity of the plasma treated as a phase fluid is described

in this chapter and properties of its solutions are discussed. The numerical scheme for implementing phase-fluid conservation is described schematically and results for Landau damping of electrostatic Langmuir waves are presented and benchmarked. The scheme for parallelization of the numerical technique is described and net achievable numerical efficiency is characterized with respect to the scale of computing architecture as well as the computing strength of the supercomputing system available at IPR. Boundary conditions for the distribution function along both x and v dimensions are described and their implementation in the numerical scheme is discussed. Various results showing confirmation with multiple time scales resolved by the code and interaction between processes on distinct time scales are examined. Dispersion properties of propagating structures are verified against their standard analytic forms. The challenges associated with resolution of multiple time scales are highlighted for the simulations performed with exact electron to ion mass ratio. Standard fluid results like parametric coupling between two collective processes at different time scales and the standard kinetic results, like Landau damping of collective plasma perturbation and particle trapping in electron plasma wave and ion acoustic wave are quantitatively verified. Conservation of different norms, total energy, entropy and momentum are also verified during the simulation.

Chapter 3 presents shelf consistent generation of solitary ion acoustic wave due to electron trapping in a current driven electrostatic plasma through kinetic Vlasov simulation. The results of fully nonlinear simulation presented in this chapter show a self-consistent development of electron trapping in waves, and a resulting coherence, in a situation where the linear theory prescribes that a small amplitude ion acoustic wave must grow to large enough amplitudes before showing any sign of conventional fluid nonlinearity $u \cdot \nabla u$ in the form of growing coherence [28, 35].

The rest of the chapter presents interpretation of these results based on the analytic formulation of trapped electron equilibria and electron phase-space holes by H. Schamel [4]. A detailed validation of the recovered coherent structure as collisionless trapped particle equilibria is done based on multiple cases in the simulations over a range of parameters of the analytic formulation. Multiple scenarios with and without a perturbing potential produced by a coexisting electron plasma wave, capable of ergodizing the separatrix region, are explored. The evolved solutions are quantitatively compared with the analytic results of the electron hole

formulations in each case. The phase space distributions of electrons and ions, spatial distributions of density and potential corresponding to evolved solitary wave structures, and associated Sagdeev potential are presented systematically. The central observations and conclusions include that the nonlinear coherent solitary wave structures developed in the simulation follow the analytic solutions of an m-KdV equation that accounts for the stronger nonlinearity produced by the electron trapping in the structure [8]. In the low k regime, where the structures coexist and interact with the undamped high frequency electron plasma waves, the nonlinear solitary structures retain their nearly analytic form as long as the trapped electron distribution stays in an independent (unperturbed) thermodynamic equilibrium. In the conditions where the developing ion acoustic structures are free from time dependent perturbations, the numerically simulated coherent structure could be characterized analytically. Such validation involved finding, from them, the necessary parameters to construct the corresponding analytic solutions and to carry out the comparison of the simulation results with the theoretical formulation that has a modified KdV equation with a stronger trapping nonlinearity. Relatively small amplitude coherent structures coexisting with a periodic self-consistent potential perturbation are found to be most affected by the nonadiabatic response of the electrons. Presence of a self-consistent time dependent perturbing potential, in the form of a coexisting EPW, prevents the trapped electrons from reaching an equilibrium and forming stable trapped particle modes that are time independent stable solutions of the Vlasov equation. It is observed that although a coherent solitary structures has a sizable transient fraction of trapped particle population in the separatrix region, it remains reasonably stable as long as a finite adiabatic fraction of the trapped population existed. Finally, the time asymptotic evolution of the trapped particle mode structure associated with solitary structure generated by the trapped particle nonlinearity shows a residual growth originating from the associated trapped particle instability [37] which produces modulations in the soliton amplitude with electron bounce frequency and causes a net growth in present cases simulated using a finite current.

Chapter 4 deals with the issue of mutual interaction between the structures nearly confirming with propagating solitary electron holes (SEH) solutions. The simulations in this chapter explores a distinct limit of propagation and examines interaction between the faster analytic SEH solutions [1] in regime of electron-

acoustic structures [9]. The results from this part of the work exhibit the coexistence of linear electron plasma mode and nonlinear electron acoustic mode with a comparable amplitude. The additional linear fast electron plasma modes are generated in the simulation, as a result of analytic approximations entering the SEH solutions used as initial conditions. This EPW activity consists of a set of noninteracting linear modes. Their contribution to potential evolution is therefore found separable from the potential data by their Fourier decomposition into constituent modes and following their analytic time evolution [9]. However, the modes constituting slow coherent solitons couple nonlinearly via the strong response of the trapped electrons in the SEH structures. The strongly electron trapping equilibrium SEH structures are observed to interact adiabatically and preserve their identity across multiple events of interaction, or collision, between two SEHs. The phase-space evolution of the SEH is illustrated where a shift, mutually separating the interacting holes along the velocity coordinates, during the interaction, is noted. This consolidated shift of complete trapped population results in preservation of identities of the SEH and restoration of the pre-interaction forms of the SEH following the interaction. The soliton velocity shows variation during the interaction such that a slight phase-shift is visible in the soliton motion for the cases where the time of interaction is longer. The phase-shift is larger for smaller soliton in the case of two non-identical interacting solitons. It is observed that in the limit of larger relative velocity between the SEH structures (Δv, compared to square root of their amplitude, $\sqrt{\psi}$) the solutions show identity preserving interaction, however in the cases of $\Delta v \sim \sqrt{\psi}$ the structures undergo a strong modification and coalesce after a few events of interaction. The interacting states of the SEH are also compared with infrequent transients observed in the magnetospheric data usually featuring frequent SEH like bipolar electric field structures [18, 19]. Properties of these interacting stages in simulation are found to confirm with the tripolar and inverse tripolar pulses observed having relatively low rate of detection in the magnetospheric data [20].

Chapter 5 explores the concept of stability for small amplitude nonlinear modes using a current-driven, 1D, collisionless plasma as a paradigm of driven intermittent plasma turbulence and anomalous transport with the focus on undamped coherent electrostatic structures. The simulation results in this chapter are treated as central motivating factor to make progress along the pure nonlinear

branch of the plasma dispersion which is analytically developed and provides a general framework that accommodates the standard linear dispersive formulation as its special case [10]. The high resolution computer simulation results presented in this chapter illustrate an evolution of realizable phase-space perturbations, which evolve into the stable coherent structures traveling at phase velocities far from their linear prescription in addition to the familiar linear plasma modes located at a variety of time and spatial scales. Analysis presented in this chapter begins with the inspection of the plasma response in terms of a valid evolution of the Vlasov-Poisson system to a non-topological, eddy-like, initial perturbation (a locally scarce electron population about any velocity, preferably on the rising side of a drifting $f_e(v)$. The simulated response is employed to draw the general picture in the following order: we first revisit linear fluid theory and then consider the linear Vlasov theory of Landau and van-Kampen [11, 12]. The interpretation of the overall picture that emerged from our simulation results is finally completed where we systematically include this nonlinearity and develop a general Nonlinear Dispersion Relation (NDR), capable of displaying all the observed familiar and unfamiliar responses in their corresponding limits. In order to complete the analysis by simulation, we show that a stationary hole appeared to be undamped within a full Vlasov dynamics, but dies out completely within a linear Vlasov evolution [10]. The set of simulations presented therefore has the implications that in the case of coherency, the onset of instability as described by linear theory (e.g., Landau) is generally absent when seen realistically from the standpoint of the complete Vlasov-Poisson system. It is replaced instead by a more complex, and general destabilization process in phase space, in which this manifold of trapped particle equilibria with their attracting negative energy property together with the explicit initial perturbation will play an important role. This renders plasma destabilization multifaceted and, as a rule, no longer one-dimensional in terms of the parameter-space.

Chapter 6 Turbulence in collisionless stellar and high energy space plasmas is expected to be essentially dominated by large scale potential variations, capable of trapping large density of charge particles. While being in equilibrium with potential of trapped charges these structures must interact mutually as well as with the conventional plasma modes and must get destabilized in order to be active part of the turbulent energy cascade, transferring the large scale field energy to the heat.

While the ergodization of separatrix witnessed in Chapter 3 represents a nearly nonthermal decay of these structures and a direct passage of energy to the heat (or smallest accountable scale), an opposite process, where finite gain in energy of these structures results from larger scale, constitutes a sufficient condition for ensuring their place into the spectral chain of the energy cascade [40]. Existence and clarity of the mechanism of growth or instability of these coherent structures, via their interaction, with each other or with conventional waves, presently remains an open question. In this final chapter we focus on this mechanism by means of our simulations. Seed like perturbations in the electron distribution function [1] are analyzed below the linearly subcritical limit [2] of a current driven ion acoustic instability. Detailed analysis of the development of the nonlinear structures is carried out and their evolution is examined for the cases where they are show a multi-parameter evolution while undergoing a *nonlinear electron hole instability*. Unlike the linear instability where amplitude remains the sole growth parameter, the growth of an electron hole is characterized by the strengthening response of the trapped particle population that reflects into transformation of an initial hole in a multidimensional space of parameters. These dimensions in the presently considered Schamel formulation, include: the propagation velocity v_0, peak potential ψ and the inverse trapped electron temperature β of the structures, and are mutually coupled to each other by the Nonlinear Dispersion Relation (NDR), describing a continuum of collective nonlinear modes [1]. The parametric growth mechanism for the electron hole instability is identified involving an extended interaction between the electron hole and a background large scale ion acoustic structure. The mechanism is illustrated quantitatively using the simulation data from multiple cases which show strong to weak, or nearly vanishing, growth in specific limits of the parameters.

Chapter 7 provides, brief summary of the complete study presented in the thesis, summarizes the major conclusions from the present thesis work and consolidates these conclusions to provide the updated status of the knowledge on the issues addressed. The major results are also discussed in the perspective of existing experimental results and a limited number of theoretical formulations of the present problem [3–6]. Key areas are identified where the present results and conclusion can help in introducing quantitative revisions in the existing theoretical formulations. The discussion is included on a more generalized structure of

the nonlinear stability analysis of the collective plasma response, involving kinetic trapped particle nonlinearity. The ways to address several outstanding issues requiring kinetic inputs, e.g., plasma heating in collisionless nonthermal conditions via the generalized formulations [42] and parallel heat conduction in collisional cases [43] are considered with respect to present approaches to the issue [3–5]. The extension of the present simulation approach to more diverse phase-space equilibria [3] and naturally recovered nonlinear kinetic structures [13–20] is discussed and the possible stages involved in making progress towards addressing them are described. Possible scenarios leading to unstable phase-space perturbations and their analogue in other physical setups supporting collective processes [44, 45] are considered highlighting relevance of conclusion from the present simulation results to such alternate setups.

2

Phase-fluid continuity of the collisionless Vlasov-Poisson system: The numerical model

2.1   Introduction

In the essential kinetic description of plasmas in their collisionless regime, the evolution of collective processes are governed by the Vlasov equation [26, 28]. The linearized Vlasov theory, which addresses the small amplitude regime of potential perturbations, is obtained by linearization of Vlasov equation. The linear theory successfully recovers the standard linear dispersive wave that, under the kinetic theory, additionally interact with resonant particles and result in damping or growth of the perturbations. The majority of collective processes in hot collisionless plasmas however involve finite and large amplitude plasma structures. The analytic approach to growth/damping of presents the complex analytic challenge and an area of active research as introduced in detail in Chapter 1. The presently active efforts for develop more general nonlinear version of plasma theory of waves and turbulence is greatly aided by the numerical simulations with pure nonlinear and fully kinetic approach. In order to perform the kinetic simulations customized for exploring fundamental physics of the subject of nonlinear plasma stability, a high resolution Vlasov simulation procedure is first developed in these studies. This simulation procedure is systematically described and validated in this chapter.

The exact nonlinear solutions desired in in this study of kinetic equations

governing collisionless plasmas include those finite amplitude where particles are trapped by the perturbations. The linear results, that neglect trapping, are, in turn, recovered as their limiting cases of this general evolution. The various numerical methods [95, 96] underlying the simulation procedure therefore essentially implement the fundamental conservation properties described by the collisionless Vlasov equations, without using any linear approximation, in order to simulate the realistic evolution of distributions in the species phase-space.

In the present studies, the fundamental "Flux Balance" [27] method is applied to simulate the evolution of both electrons and ion phase-space distributions governed by the 1-D Vlasov equation in an electrostatic case using the numerical procedure as presented in Sec. 2.2 of this chapter. The full set of electrostatic effects observable in these limits are recovered, as analyzed in Sec. 2.4, including the well known effects identified under the conventional linear theory, for example, the high-frequency electrostatic Langmuir waves, ion acoustic waves, and their corresponding collisionless Landau damping or growth. In addition to these readily identifiable processes, a host of nonlinear effects and structures, as originally intended, emerge allowing their in depth analysis in rest of this thesis. The simulation results are compared to the analytic value and also have the signature of existence of trapped particle modes, while limiting the study to the small amplitude limit where the conventional fluid nonlinearities have a negligible role.

2.2 Evolution of a collisionless phase-fluid: The numerical scheme

The Vlasov equation signifies the fundamental conservation of the flux of the probability density in the phase-space. The components of its characteristics are canonical conjugates, coupled to each other by means of Hamilton's equations of motion. The transport of probability density f of species α having charge q and mass m in the phase-space (x, v) is hence purely deterministic and the Vlasov equation takes the form of a continuity equation for the net probability flux. In the Eularian representation of phase-space coordinates, for example, its total time derivative of f must vanish in absence of any source (or sink) of the probability density,

$$\frac{\partial f}{\partial t} + \mathbf{u} \cdot \nabla f = 0. \tag{2.1}$$

where **u** is a hyper-velocity field in the phase-space (x, v), having the components,

$$\mathbf{u} = \hat{x}\dot{x} + \hat{v}\dot{v} = \hat{x}v + \hat{v}(F/m) \tag{2.2}$$

such that the component along $\hat{v}$ is the acceleration F/m in the configuration space. For electrically charged fluids, F is the Lorentz force, or the electric field force qE acting in the electrostatic limit, that appropriately yields the Vlasov equation,

$$\frac{\partial f}{\partial t} + v\frac{\partial f}{\partial x} + \frac{qE}{m}\,\frac{\partial f}{\partial v} = 0. \tag{2.3}$$

With the above interpretation, all the usual methods for solving PDE's apply to Eq. (2.1). The numerical procedure adopted here to solve Eq. (2.1), by splitting it in two ODEs, is described in the following section.

2.2.1   Split time evolution

The transformation (spectral) schemes [97] and the splitting scheme [27, 95, 96] are commonly used in Vlasov simulations. The splitting scheme is widely used because of the simplicity of its algorithms. Under the splitting scheme, the integration of distribution functions reduces to a numerical interpolation. However, to maintain the energy and mass conservation and to suppress numerical diffusion a large number of grid points are needed in both configuration and velocity dimensions. The flux balance method is used in the present simulations based on splitting the analytic form of the Vlasov equation along the configuration and velocity dimensions in the phase space and applying a flux corrected time evolution to both of them as discuss bellow:

When the lengths, time and potential are normalized to electron Debye length λ_{D}, inverse electron plasma frequency ω_{pe}, and the electron thermal energy, $k_B T_e / e$, respectively, the Vlasov equation (2.3) for the species under consideration can be written as,

$$\frac{\partial f}{\partial t} + v\frac{\partial f}{\partial x} + \eta E(x, t)\frac{\partial f}{\partial v} = 0 \tag{2.4}$$

where, the dimensionless factor η scales the electrostatic force produced by the electric field $E(x, t)$ on the species depending up on the ratios of its charge and mass with the electron. The electric field $E(x, t)$ can be calculated using the

Poisson equation for a single ion species plasma,

$$\frac{\partial E}{\partial x} = q_i \int_{-\infty}^{+\infty} f_i(x,v)dv - q_e \int_{-\infty}^{+\infty} f_e(x,v)dv \qquad (2.5)$$

Using time splitting method the Vlasov equation Eq. (2.4) for each species can be split into two similar linear advection equations as:

$$\frac{\partial f^*}{\partial t} + v\frac{\partial f^*}{\partial x} = 0; \qquad (2.6)$$

which is evolved to obtain $f^*(x, v, t = n\Delta t)$ using $f^* = f^{**}(x, v, t = (n-1)\Delta t)$, and

$$\frac{\partial f^{**}}{\partial t} + \eta E(x, t = n\Delta t)\frac{\partial f^{**}}{\partial v} = 0; \qquad (2.7)$$

which is evolved to obtain $f^{**}(x, v, t = n\Delta t)$ using $f^{**} = f^*(x, v, t = n\Delta t)$. Eqs. (2.6) and (2.7) are solved simultaneously. As indicated, in each time step the time evolved f from one of the equations is being used as the initial condition for the other. Electric field is calculated by solving the Poisson Eq. (2.5) once when f for all species become available. We have used a leap-frog type scheme for splitting the time, which is second order and symmetric in time [27].

2.2.2   The flux balance scheme

Fig. 2.1 schematically explains the flux balance technique using a model of three adjacent cells, $(i-1)^{\text{th}}$, i^{th} and $(i+1)^{\text{th}}$ having width Δx each, with X as the corresponding position. Assuming that the distribution function f is smooth in each elementary cell and velocity is positive, in the Fig. 2.1 the upper grid represents f at time t and the lower grid at time $t + \Delta t$, where Δt is the time step. For Δt sufficiently small, the fluid or the distribution function $f(t)$ within the length $v\Delta t$ from one cell moves to the next cell at time $t + \Delta t$. In the Fig. 2.1 the region shaded with horizontal lines represents fluid loss, F_{loss}^i, from i^{th} cell to $(i+1)^{\text{th}}$ cell and the region shaded with vertical lines represents fluid gain, F_{gain}^i, from $(i-1)^{th}$ cell to i^{th} cell. The new value of f at the ith cell at time $t + \Delta t$ is therefore,

$$f^i(t + \Delta t) = f^i(t) + F_{gain}^i - F_{loss}^i. \qquad (2.8)$$

Values of F_{loss}^i and F_{gain}^i can be obtained from the Eq. (2.6) as,
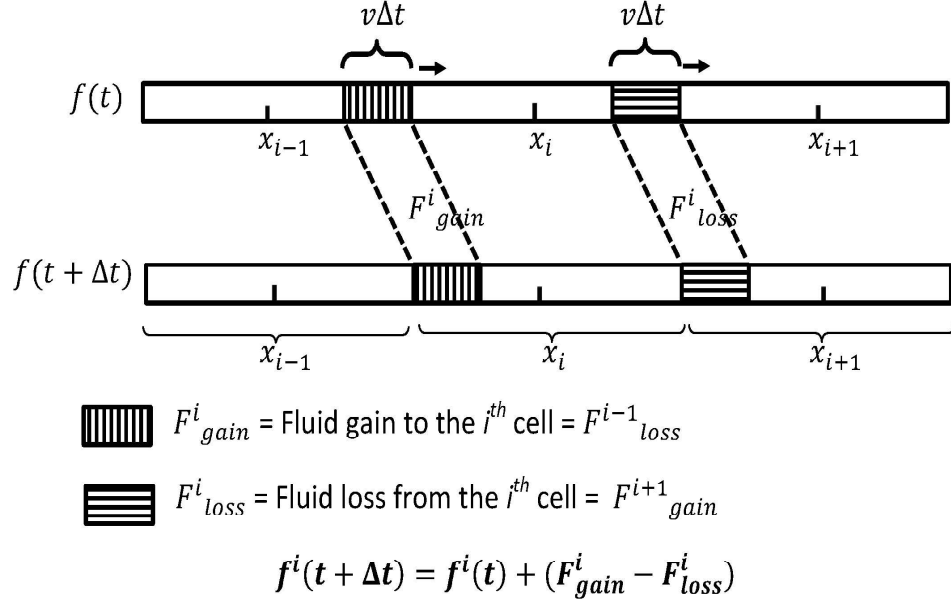
Figure 2.1: Block diagram of the Flux Balance Technique. The fluid element of length $v\Delta t$ from x_{i-1}th cell of $f(t)$ (vertical shaded region) moves to the x_ith cell of $f(t + \Delta t)$, is denoted by gain of fluid flux to i^{th} cell. Similarly, fluid element of length $v\Delta t$ from x_ith cell of $f(t)$ (horizontal shaded region) moves to the x_{i+1}th cell of $f(t + \Delta t)$, is denoted by loss of fluid flux from i^{th} cell.

$$
\begin{aligned}
F_{loss}^i &= \frac{1}{\Delta x} \int_{x_i + \Delta x/2 - v\Delta t}^{x_i + \Delta x/2} f(h - x_i) \, dh; \\
F_{gain}^i &= \frac{1}{\Delta x} \int_{x_{i-1} + \Delta x/2 - v\Delta t}^{x_{i-1} + \Delta x/2} f(h - x_{i-1}) \, dh;
\end{aligned}
$$

where h is an integration variable. Similar expressions of F_{loss}^i and F_{gain}^i are obtainable for negative velocities and are applicable to both parts of the splitted equations.

2.2.3   Characterization of the numerical procedure

In order to preserve the positivity of the distribution function, the velocity range of the species phase space needs to be chosen carefully in combination of the time step.

The required temporal and spatial resolutions thus determine the limiting values of the species velocity space. The variations or fluctuations of many conserved quantities are monitored during the evolution for the validation of the numerical procedure using an exact mass ratio of electrons and ions, $m_e/m_i = 1836$ for hydrogen plasma. These quantities include, total electrostatic field energy $\mathcal{E}_f$, total kinetic energy $\mathcal{E}_k$, total energy $\mathcal{E}_T$, momentum $\mathcal{M}$, entropy $\mathcal{S}$, volume or L1 norm $\mathcal{L}_1$, L2 norm $\mathcal{L}_2$, maximum value of distribution function $\mathcal{F}_{\max}$ and minimum value of distribution function $\mathcal{F}_{\min}$. Table 2.1 represents the name of these quantities, their expressions and values of their fluctuation/variation from their corresponding initial values in a simulation for excitation of electrostatic modes from a small amplitude cosine density perturbation to both electrons and ions in a hydrogen plasma (described in Sec.2.4.1.1). The difference of these quantities from their initial ($t = 0$) values are denoted by Δ.

Fig. 2.2 presents the time histories of difference of these quantities from their corresponding initial values. The variation in quantities $\mathcal{E}_k$, $\mathcal{E}_T$, $\mathcal{S}$, $\mathcal{L}_1$, $\mathcal{L}_2$ and $\mathcal{F}_{max}$ are normalized by their initial values, while that in $\mathcal{M}$ and $\mathcal{E}_f$ are normalized to the thermal velocity and thermal energy of the electrons, respectively. As seen from Fig. 2.2(a), the electrostatic energy corresponding to electron plasma wave is Landau damped due to high damping rate (estimated in Sec. 2.4.1.1) and the residual oscillations seen are due to excitation of multiple ion acoustic modes. The Fig. 2.2(b) presents the total energy, denoted by red solid line, that is seen to show a residual oscillation, within the tolerance, because of finite dimensions of the velocity space covered. The frequency of the two counter-propagating structures to cover the box length agrees with the frequency of the wave because of the wave length of the standing mode is chosen equal to box length. The total energy fluctuation is only in the form of kinetic energy of ions because of uncovered part of distribution due to rather limited velocity boundary values for ions. This frequency appears in rest of the norms presented which are well within the desired tolerance.

The Fig. 2.2(c) presents the normalized volume of electron and ion phase space that oscillates about a constant value because of finite velocity space boundaries for both distributions. Note that the exact magnitude of fluctuation with the same frequency for both electrons and ions may differ because of independent choice of the velocity space boundaries for both. Figs. 2.2(d)-(e) present the fluctuation of $L2$ norm of electron and ion distribution functions which are limited within a

Table 2.1: Variation/fluctuation of different quantities in simulation.

Name of quantities	Expressions	Value of fluctuation/variation
Potential Energy ($\mathcal{E}_f$)	$\int |E_x|^2 dx$	$\mathcal{E}_f + \mathcal{E}_k \sim \mathcal{E}_T \pm 10^{-6}$
Kinetic energy ($\mathcal{E}_k$)	$\sum_j \int \int v^2 f_j \; dvdx$	$\mathcal{E}_f + \mathcal{E}_k \sim \mathcal{E}_T \pm 10^{-6}$
Total Energy ($\mathcal{E}_T$)	$\mathcal{E}_T = \mathcal{E}_f + \mathcal{E}_k$	$\dfrac{\Delta \mathcal{E}_T(t)}{\mathcal{E}_T(t=0)} \sim 10^{-6}$
Momentum ($\mathcal{M}$)	$\int \int v f_j \; dvdx$	$\Delta \mathcal{M}(t) \sim 10^{-6}$
Entropy ($\mathcal{S}$)	$\int \int |f_j| \; \ln(|f_j|) \; dvdx$	$\dfrac{\Delta \mathcal{S}(t)}{\mathcal{S}(t=0)} \sim 10^{-6}$
Volume or L1 norm ($\mathcal{L}_1$)	$\int \int f_j \; dvdx$	$\dfrac{\Delta \mathcal{L}_1(t)}{\mathcal{L}_1(t=0)} \sim 10^{-6}$
L2 norm ($\mathcal{L}_2$)	$\int \int |f_j|^2 \; dvdx$	$\dfrac{\Delta \mathcal{L}_2(t)}{\mathcal{L}_2(t=0)} \sim 10^{-6}$
Maximum value of distribution function	$\mathcal{F}_{\max} = \max[f_{e,i}]$	$\dfrac{\Delta \mathcal{F}_{\max}(t)}{\mathcal{F}_{\max}(t=0)} \sim 10^{-3}$
Minimum value of distribution function	$\mathcal{F}_{\min} = \min[f_{e,i}]$	$\mathcal{F}_{\min} \geq 0$

fraction $\sim 10^{-6}$ of its initial value. In Fig. 2.2(f) the electron entropy is denoted by blue line and that of ion distribution by red line. Remarkably, the entropy
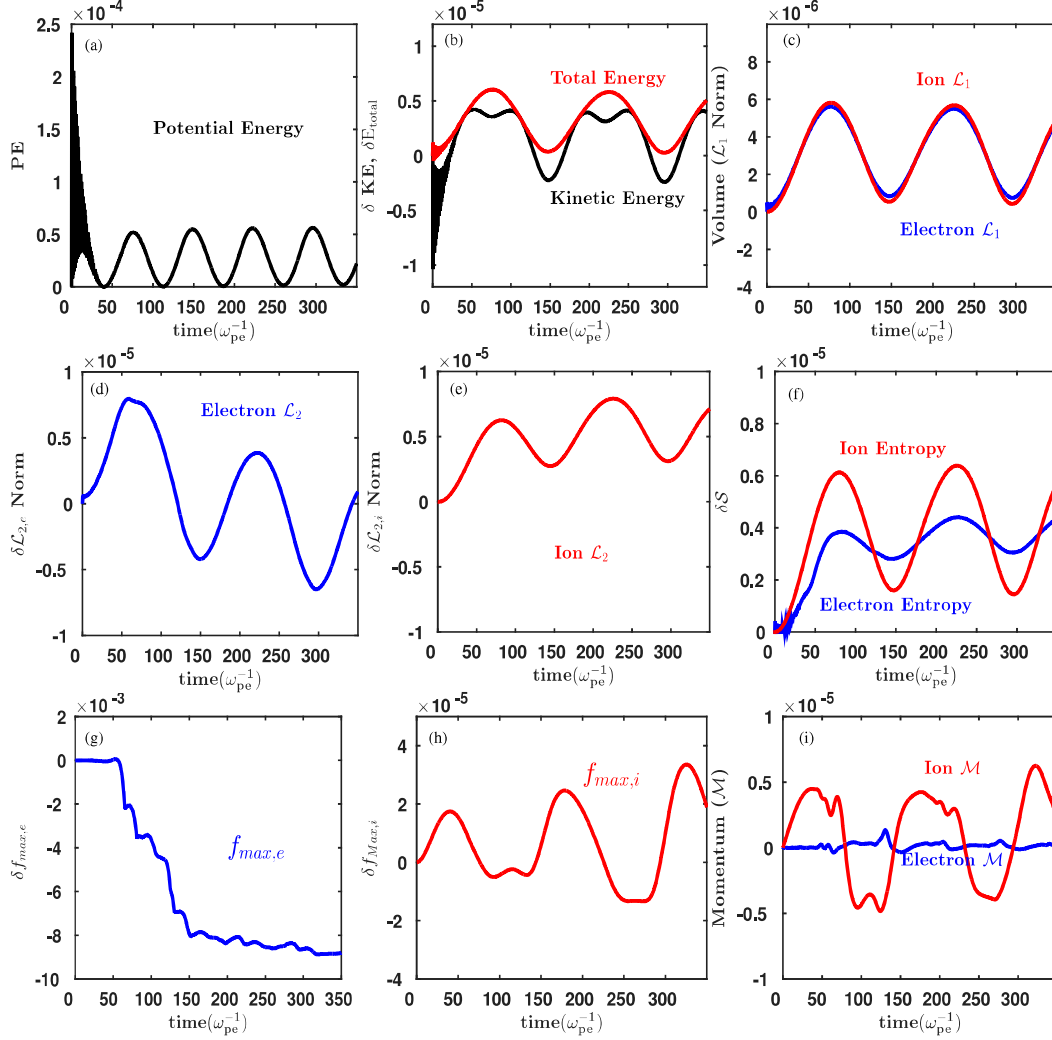
Figure 2.2: Time evolution of fluctuation of (a) potential energy, (b) sum of kinetic energy of electron and ion (black line) total energy (red line), (c) L1 norm of electron (blue solid line) and ion (red solid line), (d) L2 norm of electron, (e) L2 norm of ion, (f) ion entropy (red solid line) and electron entropy (solid blue line), (g) maximum value of electron distribution function, (h) maximum value of ion distribution function and (i) electron momentum (solid blue line) and ion momentum (solid red line). All the quantities are plotted as deviation from their initial values. The quantities $KE = \mathcal{E}_k$, $E_{total} = \mathcal{E}_T$, $\mathcal{S}$, $\mathcal{L}_1$, $\mathcal{L}_2$ and $f_{max} = \mathcal{F}_{max}$ are normalized by their initial values and $\mathcal{M}$ and PE are normalized to thermal velocity and thermal energy of electron.

34

has no significant change during the initial Landau damping phase of the electron plasma wave in agreement with the theory. The entropy subsequently increases signifying the slow numerical diffusion of poorly resolved fine structures created in the electron phase-space by the process of Landau damping of the wave due to presence of highly oscillating ballistic term ($\sim \exp(-i\mathbf{k}.\mathbf{v}t)$) [28] in velocity space, which can not be resolved with finite grid size. It is however conserved and oscillates about a constant value with transit frequency ion acoustic structures once macroscopic structures (significantly larger compared to grid size) are formed and are studies in the evolution. In the regime where Landau damping is not significant we however recover an undamped trapped particle structure in the simulation which is not predicted by the linear Landau theory that ignores particle trapping. Example of such small k evolution is presented and discussed in Sec. 2.4.

The Figs. 2.2(g)-(h) present maximum value of electron and ion distribution functions respectively Which also stay in required tolerance limit. The maximum of ion distribution function shows increasing magnitude of variation signifying slow evolution of structures propagating with slightly different phase velocities. Fig. 2.2(i) presents variation of momentum of electrons and ions, denoted by solid blue and red line, respectively, which also remain bounded for both species through out the simulation. We have additionally monitored the minimum value of electron and ion distribution function which remain positive everywhere in their respective phase-spaces.

2.3 Parallelization using MPI and Open-MP

The numerical operation Fig. 2.1 constitutes a standard procedure to be performed over a large number of phase-space cells and for each of the species in the simulations. It is therefore possible under the present scheme to efficiently distribute these large number of identical operations to be performed parallely by a large number of computational achieving a greater numerical efficiency and speed up. This parallelization of computational procedure is achieved systematically by implementing the standards of the Message Passing Interface library and those of the Open-MP parallelization scheme for the numerical procedures. The General parallelization scheme implemented in present computations is presented schematically in Fig. 2.3(a) and the effective speedup generated by these schemes as a function

of increasing number of computing nodes is characterized in Fig. 2.3(b). The in-
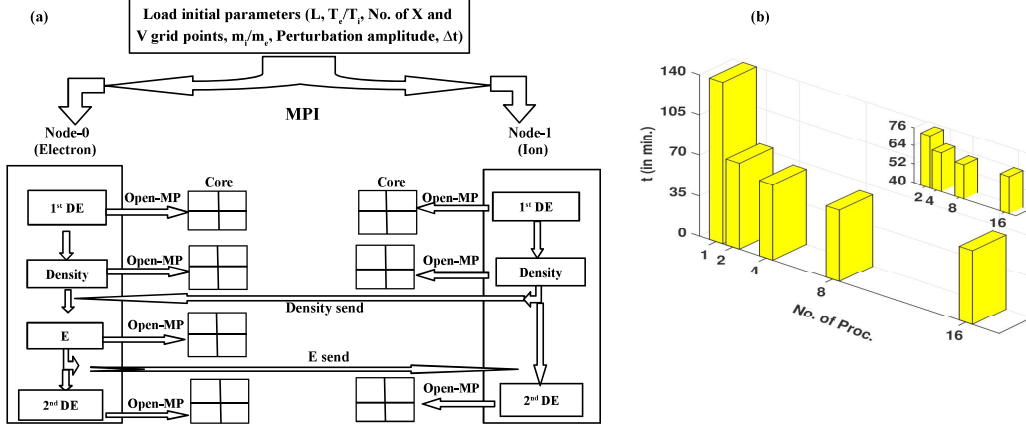
Figure 2.3: (a) Block diagram of the parallelization scheme. (b) Variation of time taken for 1000 time steps in (4096×8192) grid with different no. of Processors. Number of processor 1 for the serial code and 2 for only 2 MPI nodes, 4 (2×2) for 2 MPI nodes and 2 Open-MP cores in each MPI node, 8 (2×4) for 2 MPI nodes and 4 OpenMP cores in each MPI node. The subplot shows the time taken for 2,4,8 and 16 processors.

ternal computations associated with both the species are distributed on four cores using the OpenMP scheme. Fig. 2.3(b) presents the computation time for the 1000 time step in a (4096×8192) dual mesh grid with increasing number of processor showing that a computational speed up of about 2 times was achievable up on an optimization and implementation of MPI to use minimum two MPI nodes as compared to the time taken for a single processor (serial) execution represented by the bar at number of processors = 1. The bars at even larger number of processors (4 and more) represent only the effect of adding more OpenMP cores while using only two MPI nodes. This parallelization scheme also helped in generating a considerable speed up for rather small number of grid points. The efficiency of the parallel scheme compared to a serial one increases with the increase of number of grid points. The characterization presented in Figs. 2.4 and 2.2 are for studying the Landau damping and generation of trapped particle nonlinearity generated coherent structures with sufficiently long spatial scales that are well resolved by a minimum grid resolution of 512×512. Higher grid resolutions are required for studying time evolution of spatially smaller structures.

36

2.4   Benchmark using standard analytic results

The numerical procedure developed and presented in Sec. 2.2 is validated by simulating the standard results for plasmas involving both electron and ion response to desired accuracy before its application to exploring more fundamental physics of trapped particle structures and the associated nonlinearity [7, 53].

2.4.1   Recovery of electrostatic plasma modes

The Vlasov theory of plasma waves prescribes two most dominant electrostatic eigenmodes of plasma, namely, electron plasma waves (EPW) and ion acoustic waves (IAW) [28]. The phase velocity of the waves can be calculated using the corresponding linear dispersion relations. According to linear Vlasov theory the dispersion relation for electron plasma waves having phase velocity $\omega/k >> v_{the}$ is,

$$\omega_r^2 = \omega_{pe}^2(1 + 3k^2\lambda_{De}^2).$$

(2.9)

where, ω_r is real part of the frequency, k is wave number, $\lambda_{De} = \sqrt{\frac{kT_e}{\epsilon_0 n e^2}}$ is the Debye length and $\omega_{pe} = \sqrt{\frac{ne^2}{\epsilon_0 m_e}}$ is the electron plasma frequency. In the warm, finite species temperature plasmas, however, the resonance particles additionally exchange energy with the wave and therefore wave has a finite damping or growth rate ω_i [28]. If there are more resonant particles moving slightly slower than the wave than those moving slightly faster than the wave, then the slower particles take energy away from the wave hence cause the wave energy to damp. Conversely, a growth must be recovered if the number of faster moving particles are larger than the slower moving particles. According to linear Landau theory the linear damping rate $\omega_i \propto \partial f_{e0}/\partial v$ and the damping rate under the approximation of a Maxwellian electron equilibrium distribution is obtained from the imaginary part of the dispersion relation as,

$$\omega_i = -\sqrt{\frac{\pi}{8}} \frac{\omega_{pe}}{\mid k^3\lambda_{De}^3 \mid} \exp-\left(\frac{1}{2k^2\lambda_{De}^2} + \frac{3}{2}\right).$$

(2.10)

Similarly, the dispersion relation for ion acoustic wave in terms of real part of

its frequency, ω_r, is given by,

$$\omega_r^2 = \frac{T_e}{m_i} \left(\frac{k^2}{1 + k^2 \lambda_{De}^2} + \gamma_i k^2 \frac{T_i}{T_e} \right) \tag{2.11}$$

Here, $\gamma_i = 3$. m_i is mass of ion. In the following analysis we have present recovery of these analytic results in our numerical simulations.

2.4.1.1   Numerical Results: dispersion and collisionless Landau damping

In order to study of Langmuir wave in a collision-less plasma in 1D electrostatic simulations a stationary Maxwellian velocity distribution function is used for both electrons and ions.

$$f_j(x, v_j, t = 0) = f_{0j}(x) \exp \left[-\frac{m_j (v_j)^2}{2 T_j} \right] \tag{2.12}$$

where the subscript $j = e$ and i correspond to electron and ion, m_j, T_j, and v_j are the mass, temperature, and velocity co-ordinate of the species j respectively. The quantity f_{0j} is the normalization constant.

The other standard normalization used here are given in the Table 2.2, where λ_{De}, v_{the} and ω_{pe} are the plasma Debye length, electron thermal velocity and electron plasma oscillation frequency, respectively. In rest of this thesis the symbols with sign $\sim$ for the normalized quantities are replaced by normal symbols for the simplicity. Initially, a cosine density perturbation is applied to both electron and ion such that total density can be written as, $n_i = n_e = n_0 + n_1 \cos(2\pi x / L)$, where n_1 and n_0 are the amplitude of the density perturbation and the background density, respectively. In present simulation a 512×512 dual-mesh grid in phase-space and periodic boundary condition at the end of simulation zone L in x is used for both electron and ion for solving Vlasov equation for the initial parameter n_1=0.01, T_i =0.05 and the exact species mass ratio $m_i / m_e = 1836$. The distributions $f_{i,e}$ are evolved in time according to Vlasov equation for two different k values of initial perturbation, Case-I: $k = 0.209$ (L=30 λ_{De}) and Case-II: $k = 0.314$ (L=18 λ_{De}). This density perturbation generates high frequency electron plasma wave and slow frequency ion acoustic wave in both the cases. The frequency of the EPW and the IAW follow corresponding dispersion relations given by Eqs. (2.9) and (2.11), re-

Table 2.2: List of normalized quantities.

Name of quantities	Expressions
Potential ($\tilde{\phi}$)	$\tilde{\phi} = e\phi/T_e$
Length ($\tilde{x}$)	$\tilde{x} = x/\lambda_{De}$
Time ($\tilde{t}$)	$\tilde{t} = t\omega_{pe}$
Velocity ($\tilde{v}$)	$\tilde{v} = v/v_{the}$
Temperature ($\tilde{T}_j$)	$\tilde{T}_j = T_j/Te$
Mass ($\tilde{m}_j$)	$\tilde{m}_j = m_j/m_e$
Charge ($\tilde{q}_j$)	$\tilde{q}_j = q_j/q_e$

spectively. In case-II with $L = 20\lambda_{De}$, the Landau damping rate is higher compare to the case-I with $L = 30\lambda_{De}$. Fig. 2.4(a) presents temporal evolution of potential at middle of the simulation box for case-I. The subplot shows the evolution up to 15 ω_{pe}. The frequency of the high-frequency wave structure agrees well with EPW frequency Eq. (2.9) ($\omega_r = 1.032\omega_{pe}$ and $\omega_i = -1.7 \times 10^{-4}$). For case-II we estimate $\omega_i = -0.0284$ that also agrees well with simulation result as shown in the subplot of Fig. 2.4(b), where time average of potential fluctuation is removed from the original data to bring the potential fluctuation about zero.

In both the Figs. 2.4(a) and (b), the low frequency waves are the IAW. The Figs. 2.4(c) and (d) additionally present the ion and electron phase-space distributions in the region of the ion acoustic phase velocity and electron plasma wave phase velocity. For the set of parameters used, the phase velocity of electron plasma wave $\omega/k \approx 5v_{the}$ and that of ion acoustic wave $\omega/k \approx 0.023v_{the}$. Since, bounce
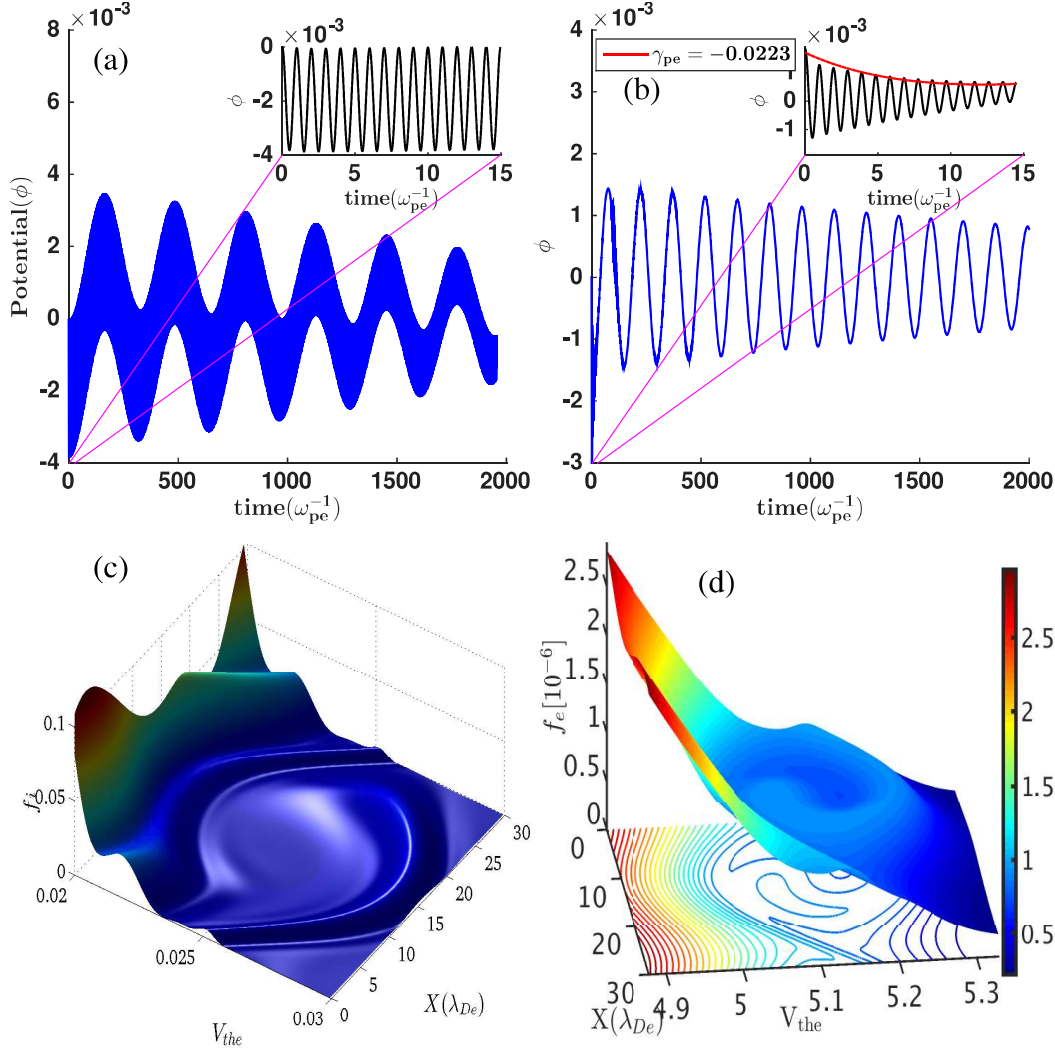
Figure 2.4: (a)-(b) Temporal evolution of potential at the middle point of the simulation box for a perturbation for two different box length $L = 30$ and $L = 20\lambda_{De}$ respectively. The subplot shows the evolution up to $t = 15\omega_{pe}$. (c)-(d) Ion and electron distribution functions near phase velocity of ion acoustic wave and electron plasma wave respectively. Ions are trapped in ion acoustic wave and electrons are trapped in electron plasma wave.

frequency of particles is greater than the damping frequency $\left(\omega_b = \sqrt{\frac{e\phi k^2}{2m}} >> \omega_i\right)$, they are trapped in the corresponding potential structures. The Fig. 2.5 presents Fast Fourier Transformation (FFT) of the potential fluctuations in the simulation. Observable in Fig. 2.5 are two fundamental modes, the one at the higher frequency
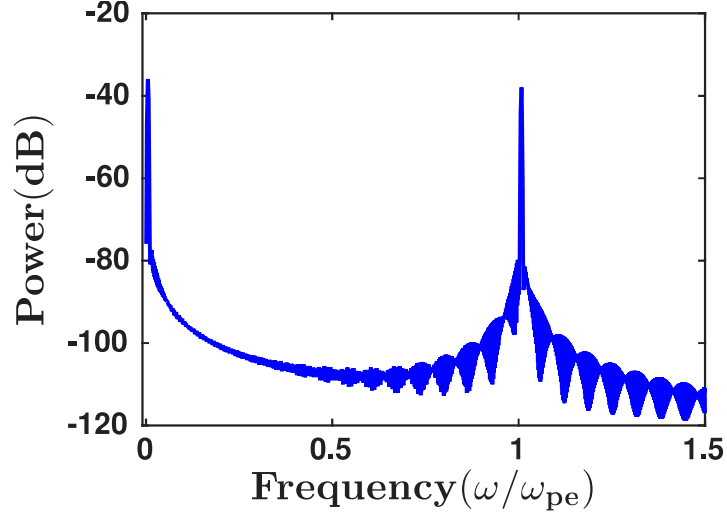
Figure 2.5: Fast Fourier transformation (FFT) of potential fluctuation.

corresponds to the electron plasma wave of frequency $\omega/\omega_{pe} = 1$ while the other one, corresponding to ion acoustic wave of frequency $0.023\omega_{pe}$. Other small amplitude peaks are seen generated due to the parametric coupling between EPW and IAW resulting into multiple side-bands about these fundamental frequencies [29].

2.5   Summary and Conclusion

We have described the basic structure of the dynamics of the Vlasov plasmas where they are treatable as an incompressible phase-fluid that fallows an associated phase-space flux conservation. An algorithm based on the flux balance of this phase-fluid in a localized, Eularian, phase-space volume element, undergoing the time evolution, is described. The numerical procedure involving splitting of the Vlasov equation along the configuration and velocity dimensions is presented and its implementation to a multispecies plasma is described. The characterization of the numerical procedure is done by computing a series of conserved quantities and norms for the distribution defined under the framework of the Vlasov theory. For typical phase-space grid resolutions and plasma parameters, the time evolution of conserved quantities are characterized describing their observed variation with respect to the tolerance specified for the set of parameters. Standard electrostatic plasma modes and their dispersion properties are shown to be successfully recov-

ered by performing test runs of the simulation with typical plasma parameters and system size. The adopted numerical procedures is additionally shown to have high potential for an efficient parallelization and the detailed scheme for the parallelization based on the MPI and Open-MP standards is described with the achieved effective speed up as a function of increasing number of computing nodes.

The numerical characterization and physical validation of the procedure using electrostatic plasma mode simulations are resulted in the following conclusions. For the cases where the electrostatic energy corresponding to the electron plasma waves damps with a faster Landau damping rate, the residual oscillations in the conserved quantities correspond to the periodic displacement of the distribution function in the phase-space, arising from the periodic interaction of counter-propagating collective ion acoustic wave structures. The displaced distribution function yield displacement dependent values of velocity integral performed with limited velocity space boundaries as opposed to those ideally located at infinity. For physically acceptable numerical solutions, the oscillations in the conserved quantities and norms are suitably ensured within a tolerable limit by choice of the velocity space boundaries for the individual species.

The agreement of simulation results with standard analytic physical results is successfully recovered for typical plasmas for which standard sinusoidal perturbation was used to excite 1D electrostatic modes in a finite electron and ion temperature Maxwellian distribution of both the species. Apart from recovering the real frequencies of the electrostatic electron plasma and ion acoustic modes to a sufficient accuracy, the implemented simulation procedure also recovered the fundamental kinetic characteristics like collisionless Landau damping of these electrostatic modes. In the low k regime of weak Landau damping, the examination of regions of ions and electron phase-space close to the phase velocity of the respective modes reveals the existence of highly stable trapped particle equilibrium structures arising from trapping of charged species resonant with the phase velocities of the recovered electrostatic modes. These trapped particle equilibria and the nonlinearity associated with them are further analyzed in sufficient detail by means of the developed simulation procedure in rest of this thesis.

We have used the general flux balance technique for solving Vlasov equation numerically including both electrons and ions are mobile. Standard fluid results like parametric coupling between two collective processes at different time scales and

42

the standard kinetic results, like Landau damping of collective plasma perturbation are quantitatively verified. All the norms, total energy, entropy and momentum remain conserved through out the simulation. Their fluctuation are in required tolerance limit. The presented simulations resolve a large range of time scales including fast electron plasma waves, an intermediate electron bounce frequency and a much smaller ion acoustic frequency with exact mass ratio between electrons and ions, highlighting nonlinear effects produced by trapping of resonant electrons in slower ion acoustic waves at very small amplitudes.

3

Adiabatic electron response and solitary wave generation by trapped particle nonlinearity

3.1 Introduction

A variety of effects emerge in collisionless plasmas when the fast electron response is impeded by trapping in potential structures, influencing many collective linear and nonlinear processes otherwise well described by the equilibrium hydrodynamic formulation of a collisional plasma [3, 30–32]. The phase-space distributions of trapped species in such collisionless cases show structures like phase-space vortex which can be strong enough to produce the spatial non-uniformities in density profiles obtained from their velocity integration [1, 33]. In equilibrium with macroscopic potential structures, the species distributions featuring such trapped zones display a robust total energy conservation where they are purely functions of total energy and therefore valid solutions of the corresponding Vlasov equations that couple to each other via macroscopic fields. For stronger trapping the modifications in the particle distribution functions begin to affect the collective processes, most effectively by generating additional nonlinear effects [1, 36] since the trapping strength is intrinsic function of the amplitude, unlike the amplitude independent results of the linear theory.

The coherent structures serve as very effective first signature of the nonlinearity in collective modes as discussed in Chapter 1. Among the electrostatic plasma

modes the ion acoustic response shows most visible signature of nonlinearity by readily producing ion acoustic solitons and solitary waves for finite amplitudes. The ion acoustic structures therefore serve as an ideal paradigm for nonlinearity produced coherence in the plasma theory. Finite amplitude ion acoustic waves (IAW) are known for many decades to posses multiple regimes and origins of the underlying nonlinearity [4]. They enter into the nonlinear regime by a combined effect of the nonlinearities that originate from multiple sources and are often dominated by the strongest of them at the onset of their nonlinear regime, as well as various stages of its evolution. In case of ion acoustic waves, the set of these nonlinear effects includes the one that has a pure hydrodynamical origin and the another one which is somewhat less discussed in the available literature on coherent structures and has its origin in the vortex like phase-space structures discussed above [1], and in preceding chapters. The nonlinearity of the latter class in an ion waves appears in the regime of collisionless adiabatic response of the electron species whose *pressure* must provide the necessary restoring force for the perturbed ion fluid density. This picture acquires additional complexity in the regimes where ion response is also adiabatic [34].

Displaying its underlying correlation with emergence of coherence, the nonlinearity, in an exact non-perturbative treatment, causes the effective wave potential $\phi(x)$ to have a spatial variation governed by a Sagdeev's pseudo potential $\mathcal{V}(\Phi)$ [98], consistent with the solitary solutions that correspond to the familiar notion of the motion along its separatrix for a Hamiltonian system $H(\phi, \dot{\phi})$ with the nonlinear potential $\mathcal{V}(\Phi)$. The solitary solutions vary accordingly in their shape, velocity and width, depending on the type and strength of the effective nonlinearity and its multiple underlying sources. In the cases where a source of free energy, capable of driving a microinstability [99], is available, it is of interest to investigate that (i) whether a nonlinear saturation occurs due to resonant processes modifying the particle distribution leading to the formation of undamped coherent structures, and (ii) to which regime of nonlinearity such saturation is likely to be reached, in case, for example, of an ion acoustic instability. Given the complexity of combined effect of these nonlinearities, such a time evolution is best analyzed by means of numerical simulations as done in the present study. The simulations adopted by us also allow examining the impact of other self-consistently excited multiple timescale plasma modes on the electron-ion trapped particle equilibrium forming

46

in such saturated states. The time evolution of the species distribution function is analyzed by means of a multiple scale numerical simulation procedure, covering a range of time scales from electron to ion response times with an exact mass ratio ($m_i/m_e = 1836$). The simulations results presented here additionally allow analysis of the nonlinear regimes of collective ion waves with an adiabatic electron response. Similar to the effect of a sufficiently higher electron collisionality which can prevent particle trapping in a wave and consequently the development of undamped BGK structures [30], for a collisionless Vlasov plasma our simulations indicate that the presence of a high frequency undamped electron plasma mode can be one of the factors that affect the process of electron trapping in the solitary structures, reducing the effect of a stronger, particle trapping generated nonlinearity.

In an approximate analytic approach addressing the saturated stationary structures in the limit of cold ions, H. Schamel [4] discussed that the ion acoustic solitons [100] are generally governed by the Kortweg-de Vries (KdV) equation [48, 94] which gets modified by the presence of trapped electrons as [4],

$$\frac{\partial \phi}{\partial t} + \left(1 + \frac{1 - \beta}{\sqrt{\pi}} \phi^{1/2} + \phi \right) \frac{\partial \phi}{\partial x} + \frac{1}{2} \frac{\partial^3 \phi}{\partial x^3} = 0, \tag{3.1}$$

where ϕ is the wave amplitude and β a measure of inverse temperature of the trapped electrons. Note that the nature of the nonlinearity in Eq. (3.1) is sensitive to the variation in the inverse temperature β from 1, which effectively results in appearance of a stronger nonlinearity. In the limit $\beta \to 1$, however, the equation with its usual nonlinearity produces the Sagdeev's original soliton solutions. Effects of the stronger nonlinearity thus appear in the stable soliton structures and modify their form from the standard solitary solutions obtained in the limit $\beta \to 1$. Results form the present simulation enable us to analyze the structure of self-consistently generated stable solitons in the nonlinearly saturated state of a current driven microinstability [99] and study the stronger trapping nonlinearity. The solitons, and the electron response associated with them modify the distribution at the wave phase velocity and lead the microinstability to a nonlinear saturation. In the saturated states recovered in our simulations they exist in equilibrium with a drifting electron distribution and therefore effectively in a setup with a finite current. The stable saturated solutions are analyzed further as the BGK-like equilibrium struc-

tures in the electron phase-space, thereby obtaining from them a set of parameters necessary to benchmark them against the special solutions of the existing analytical formulation, essentially in the presence of a finite current. In the final part of the study we present a useful analysis where we compare the relative strengths of the kinetic nonlinearity generated by the trapped particles with the conventional fluid nonlinearity by means of the solutions of the m-KdV equation (3.1) for the recovered solitary electron hole parameters. This analysis concludes that at small amplitude regime the trapped particle nonlinearity does dominate over the fluid nonlinearity.

The present simulations take into account the adiabatic response of both electrons and ions by considering both the species to be hot and collisionless. The analysis presented is however, limited to the response of a current carrying plasma to small sinusoidal density perturbations in short systems ($L \leq 30\lambda_\mathrm{D}$) and excludes more complex initial conditions representing adiabatically generated ion phase-space holes that develop into stationary negative potential solitary-wave structures [101], and in presence of a finite current, reflect the drifting electrons, leading to the formation of ion acoustic double layers [53, 102].

In this chapter, in Sec. 3.2 we introduce methodology adopted for exploring the characteristics of kinetic nonlinearity using the Vlasov simulations and main results recovered. In Sec. 3.2.1 the multispecies computational setup is described as applied in order to simulate the evolution of the current driven ion acoustic microinstability in above conditions. The self-consistent generation of stable solitons in the regime of stronger nonlinearity, produced by a large trapped electron population, is studied and characterized using the corresponding analytical formulation in Sec. 3.3. A comparison between the strength of kinetic and hydrodynamic nonlinearity for the investigated regime of parameters is presented based on the solitary solutions of the m-KdV equation (3.1) in Sec. 3.4. The results are summarized and conclusions are presented in Sec. 3.5.

3.2   Vlasov simulations of the current driven IAW

In the following sections we present the simulation results showing that in a current carrying hydrogen plasma the microinstability associated with the resonant electrons drives the ion acoustic mode unstable. In small k regime the high fre-

quency electron plasma waves (EPW) also form undamped BGK-like equilibrium and can coexist with the ion acoustic waves. Cases with such a combination are additionally included in the analysis. The EPW is however, heavily damped in the regime of large k and the evolution of ion acoustic mode is free from its effects. In both these cases, the soliton structures appear following a nonlinear saturation of the resonant microinstability. The saturation approaches following the entry of the wave into a nonlinear regime governed predominantly by a stronger nonlinearity, having its origin in the kinetic effects. The observed stable solitary structures are characterized using the solutions of the modified KdV equation, showing that the structures follow the analytical solutions in cases where the electrons trapped in them are in a local thermodynamic equilibrium. In absence of effects like electron collisionality or high frequency fluctuations, the trapped electrons have a largely unperturbed distribution. Consequently, all the observed coherent structures obey this condition and are therefore comparable to the nonlinear solutions of the mKdV equation.

3.2.1   Simulation setup, normalizations and phase-space perturbation

In order to represent a current carrying plasma in the 1D electrostatic simulation setup, an initial stationary Maxwellian velocity distribution is used for the ions while the initial electron distribution is a shifted Maxwellian. This is consistent with a drift in the average velocity of electrons with respect to ions. Accordingly, the initial electron and ion distribution functions are chosen of the following form:

$$f_j(x, v, t = 0) = f_{0j}(x) \exp\left[-\frac{m_j(v_j - u_j)^2}{2kT_j} \right],$$ (3.2)

where the subscript $j = e$ and i correspond to electrons and ions, m_j is the mass, v_j is the velocity coordinate and u_j is the drift velocity of the species j. The quantity $f_{0j}(x)$ is a constant that normalizes the value of velocity integration of (3.2) to the density value $n_j(x)$ at $t = 0$. The present simulations are performed in the frame of ions and therefore a zero ion drift velocity, $u_i = 0$, is used. In order to consider a current carrying plasma, the electron drift velocity u_e may be set to a finite value. The time evolution of the distribution is done following a flux-balance algorithm [27], as developed in Chapter 2, in the phase-spaces of electrons and

hydrogen ions with $m_i/m_e = 1836$ and using a periodic boundary condition as the ends of the simulation zone of length L. Setting the ion temperature $T_i = \Theta T_e$ determines the choice of normalization for the species temperature in the system as electron temperature T_e, the other normalized quantities used for the purpose of numerical simulations are as given in the Table 2.2, i.e., the potential $\tilde{\phi} = e\phi/T_e$, the length along $\hat{x}$, $\tilde{x} = x/\lambda_{\mathrm{D}}$, time $\tilde{t} = t\omega_{pe}$, velocity $\tilde{v} = v/(v_{th} = \sqrt{T_e/m_e})$ and the electric field $\tilde{E} = eE/T_e\lambda_{\mathrm{D}}$, where $\lambda_{\mathrm{D}} = \sqrt{T_e/4\pi n_0 e^2}$ is the plasma Debye length and $\omega_e = \sqrt{4\pi n_0 e^2/m_e}$ is the electron plasma frequency. In order to explore the ion wave growth by the current driven microinstability, a finite electron drift $u_e > u_i = 0$ is used in combination with a cosine initial perturbation in the density distribution of both the species in the space, $n_j(x)$, such that,

$$n_i = n_e = n_0 + n_1 \cos\left(2\pi x/L\right), \tag{3.3}$$

where L is the length of the simulation zone and n_0 is the unperturbed average density of the background plasma. Various cases with finite range of the electron drift velocity u_e and simulation zone dimension L are explored by simulating the time evolution of an initial perturbation in the electron and ion distribution functions on a 512×512 node dual-mesh in the phase-spaces of both electrons and ions.

3.2.2   Ion acoustic instability of the collisionless plasma

The time evolution of the electron distribution and the potential profile in one of these cases, case-I with $(u_e, L) = (0.8v_{th}, 15\lambda_{\mathrm{D}})$ is presented in Fig. 3.1, where $\Theta = 20$ and $n_1 = 0.008$ are used. The region of the electron phase-space is zoomed about the phase-velocity c_s of the ion acoustic wave where the effects of electrons resonant with the ion acoustic wave appear prominently. The distribution in rest of the phase-space remains nearly Maxwellian, except the presence of modulations in average values due to the collective plasma modes. The initial and a late time $(t > 2.5 \times 10^2\omega_{pe}^{-1})$ electron distributions are discussed in greater detail in Sec. 3.3 for various cases examined, including a case with $(u_e, L) = (0.8v_{th}, 30\lambda_{\mathrm{D}})$ where multiple solitons are generated. Note that with a finite initial drift velocity $u_e = 0.8v_{th}$ for case-I, the electron distribution function f_e at the value of the ion acoustic velocity $c_s \sim 0.02v_{th}$ has a finite gradient and, as a result, the perturbation at ion

acoustic velocity experiences a Landau growth from the resonant electrons.

For the case-I with $(u_e, L) = (0.8v_{th}, 15\lambda_D)$, the potential profiles at various times during the evolution are plotted in the Figs. 3.1(b), (d), (f), (h) and (j), along with the contours of electron phase-space distribution function at the corresponding time steps during the various stages of the evolution, plotted in Figs. 3.1(a), (c), (e), (g) and (i). The time evolution of the ion acoustic wave amplitude in this case is plotted in Fig. 3.2 where the data from two additional cases, case-II with $(u_e, L) = (0.8v_{th}, 30\lambda_D)$ and case-III with $(u_e, L) = (1.2v_{th}, 15\lambda_D)$ is also included. In case-II the ion acoustic wave grows and coexists, additionally, with an EPW, identified by the presence of a high frequency temporal fluctuation whose impact is discussed later in the analysis. As seen from Fig. 3.2, in the case-I, $(u_e, L) = (0.8v_{th}, 15\lambda_D)$, following a very brief interval that scales with the inverse linear Landau damping rate γ_L^{-1} [28] and lasts a few electron plasma periods, an initially excited EPW is completely damped and a linear ion acoustic wave is excited whose growth confirms with the linear Landau growth rate ω_I [28]. The excited IAW maintains a nearly sinusoidal form (Fig. 3.1(d)) for a period scaling with the electron bounce frequency $\omega_{be}^{-1} \sim \sqrt{m_e/k^2\psi}$ [32], beyond which it begins to steepen and deviate from its sinusoidal potential profile as seen in the profiles from and beyond $t = 31\omega_{pe}^{-1}$ plotted in Fig. 3.1(f).

3.2.3   Development of nonlinear ion acoustic wave

The next phase of the evolution of the IAW indicates the entry of wave into a strong nonlinear regime where it begins to develop coherent potential structures. The corresponding electron distribution function shows presence of vortex like structures developing at the ion acoustic velocity in the electron phase space, as visible in contour plots presented in Fig. 3.1(e) and beyond. A remarkable modification in the distribution function is visible at the ion acoustic velocity. Since generation of vortex like structures in electron phase space distribution results in the diminishing gradient of the electron distribution function $\partial f_e/\partial v_e$ at the resonant velocity which must be nonzero for the linear growth in the ion acoustic wave, the evolution and the observed saturation in wave growth indicates a nonlinear saturation of the growth where the resonant particles act to flatten the zero order electron distribution, allowing $\partial f_e/\partial v_e \to 0$ at the phase velocity of the wave. Note that at an amplitude quite comparable to its initial sinusoidal stage at $t = 10\omega_{pe}^{-1}$
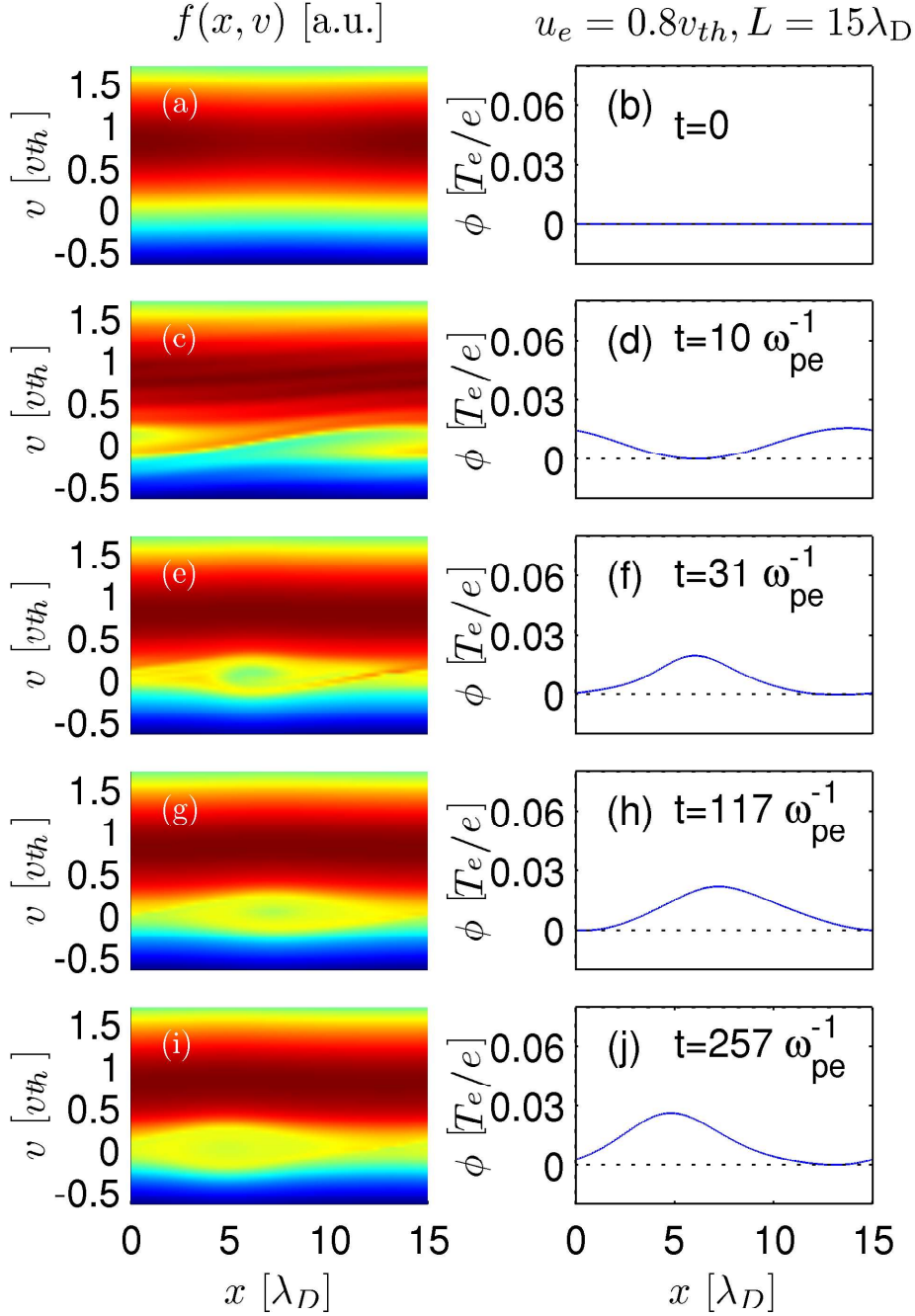
Figure 3.1: Temporal evolution of the electron distribution function $f_e(x, v, t)$ (left) and the wave potential $\phi(x, t)$ (right) for the simulation box size $L = 15\lambda_{\mathrm{D}}$ (wavelength of the initial linear IAW $\sim k\lambda_{\mathrm{D}} = 2\pi/15$) and the electron drift velocity, $u_e = 0.8v_{th}$.
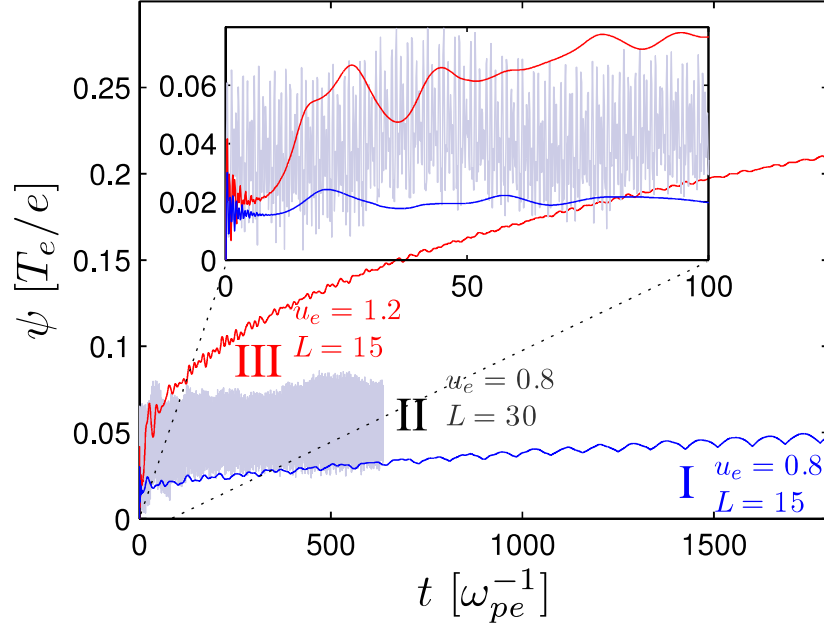
Figure 3.2: Temporal evolution of the wave amplitude ψ for the case-I, II and III corresponding to, $(u_e, L) = (0.8v_{th}, 15\lambda_\mathrm{D})$, $(u_e, L) = (0.8v_{th}, 30\lambda_\mathrm{D})$ and $(u_e, L) = (1.2v_{th}, 15\lambda_\mathrm{D})$, respectively. The subplot shows evolution up to $t = 100\omega_{pe}^{-1}$ in detail.

(Fig. 3.1(d)), the strong nonlinear effects begin to appear in the IAW at $t = 31\omega_{pe}^{-1}$ (Fig. 3.1(f)) and beyond. We explore this dominant nonlinearity in IAW more quantitatively in Sec. 3.3.

3.2.4 Coherent structures formation by electron trapping in IAW

Analyzing further the amplitude evolution presented in Fig. 3.2, in the cases where the EPW is absent or quickly damped following an initial short phase, an intermediate phase ($15 < t\omega_{pe} < 25$) follows where the ion acoustic wave experiences an exponential growth from the resonant electrons since $\partial f_e / \partial v_e$ is finite at the ion acoustic velocity c_s. It is in this secondary phase that the growing nonlinear wave, depending on the allowable k values in the simulation, either develops into a train of solitons of various heights and speeds, or produces a single soliton structure.

The parametric growth rate of ion acoustic wave (IAW) from coupling to EPW in case II

$$\gamma_p = \left(\frac{k^4 e^2 \phi_{EPW}^2}{m_e m_i \omega_{pe}} \right)^{1/3} \tag{3.4}$$

has a negligible value, $\sim 1.5 \times 10^{-3} \omega_{pe}$ isolating the constant EPW energy from the energy balance.

The amplitude evolution at longer times shows that the growth of this nonlinear wave or structures is arrested as the structures begin to trap the resonant electrons and, in turn, their amplitudes begin to approach corresponding saturation values. The nonlinear growth in this saturation phase remains considerably smaller for the cases with smaller drift in the electrons ($u_e < v_{th}$). In this saturated phase a trapped particles (electrons) instability [37] is the mechanism responsible for the observable residual growth in the nearly saturated soliton amplitude that shows a modulation with the frequency equivalent to the electron bounce frequency ω_{be}, as visible in the evolution at longer time for the case-I with $(u_e, L) = (0.8v_{th}, 15\lambda_{\mathrm{D}})$ presented in Fig. 3.2. Note that in current-free cases the trapped particle instability must result in a nonlinear Landau damping of the wave, unlike the present current driven cases where it produces a residual nonlinear growth of the nonlinear solitary ion acoustic structures. The process in the latter case results in gradual strengthening of the structure amplitude and should enable them to trap (or expel) larger population of resonant electrons with time. However, the capability of structures to trap particles is affected by the growing modulation associated with the instability.

3.2.5   Electron trapping structure of EPW

For case-II the undamped EPW is well resolved in our simulations and visible as a well developed undamped BGK-like structure at the electron phase velocity v_{phase} in the electron distribution function plotted in Fig. 3.3(a) in the region around v_{phase} at a long time $t = 2.52 \times 10^2 \omega_{pe}^{-1}$. The EPW is verified to be standing in nature whose Doppler shifted frequency is given by

$$\omega + u_e k = \omega_{pe}(1 + \frac{3}{2}k^2\lambda_D^2) + u_e k, \tag{3.5}$$
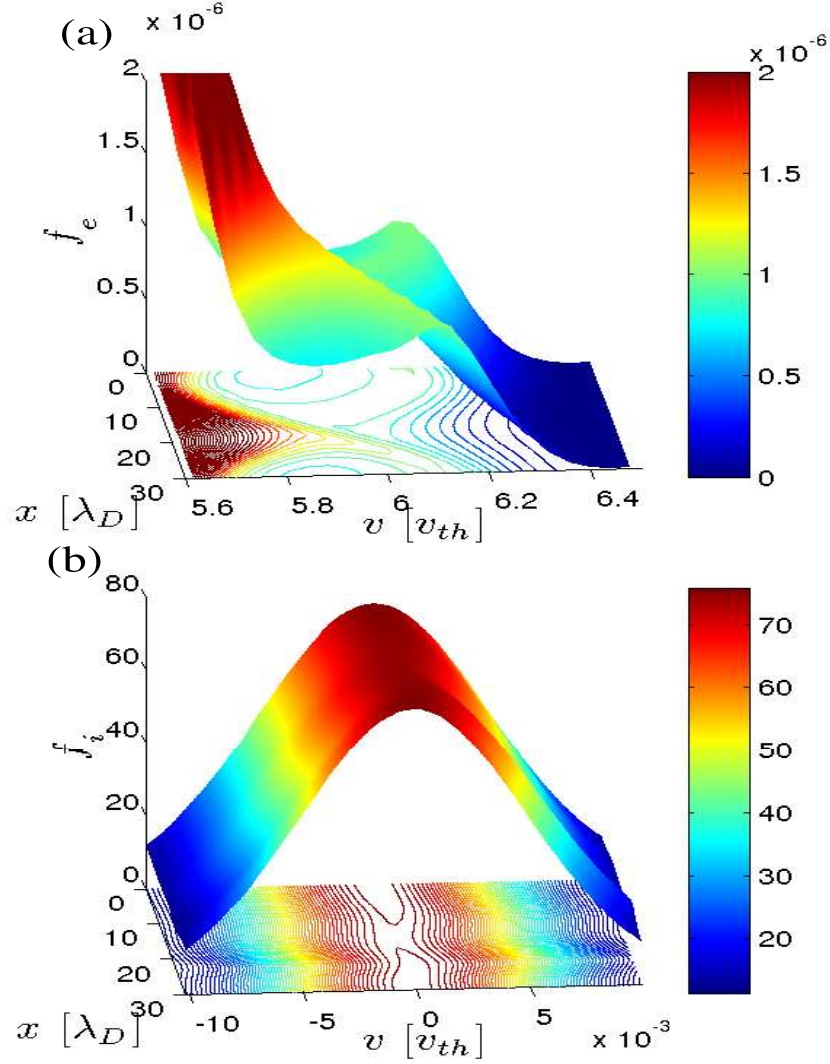
Figure 3.3: (a) Electron phase-space distribution at EPW phase velocity $v_{\mathrm{phase}} = 5.87\ v_{the}$ for case-II and $t = 2.52 \times 10^2 \omega_{pe}^{-1}$. Here, the phase velocity of the EPW is Doppler shifted. (b) Ion phase-space distribution at ion acoustic velocity c_s for case-II and $t = 2.52 \times 10^2 \omega_{pe}^{-1}$.

hence $v_{phase} = 5.87 v_{th}$ [28] in very good agreement with our simulations, where $k\lambda_D = 2\pi/30$, $\omega_{pe} = 1$ and the drift value $u_e = 0.8 v_{th}$ are used in accordance with case-II. The formation of a trapped particle mode in EPW indicates that for case-II where the electron bounce frequency exceeds the Landau damping rate of

the EPW, $\omega_{be} > \gamma_{\mathrm{L}}$, a stable BGK mode develops and arrests the linear Landau damping of the EPW, unlike the cases I and III where $\omega_{be} < \gamma_{\mathrm{L}}$ and a linear landau damping of EPW must result. Note that the electron distribution function at this velocity location however has a vanishingly low magnitude and effect of this marginal trapped electron population is unlikely to affect the ion waves. The ion phase-space distribution function $f_i(x, v)$ is also plotted in Fig. 3.3(b) in the region of ion acoustic velocity c_s that shows the effect of the presence of solitons at $t = 2.52 \times 10^2 \omega_{pe}^{-1}$. The ion distribution function however appears as a sharp delta-function like structure on the scales of electron thermal velocity, as visible in Fig. 3.7(c).

3.2.6   Effect of EPW potential on electron trapping in IAW

The further analysis shows that despite the presence of two major destabilizing factors (i) a fast EPW and (ii) a large current, most of the features of nonlinear ion acoustic wave may be preserved, including the formation of ion acoustic solitons due to a stronger nonlinearity that originates from the particle trapping in the finite amplitude ion waves rather than purely due to the conventional hydrodynamical nonlinearity in the dynamics of relatively less warmer ions. Among the noticeable effects of the additionally present EPW, it can strongly perturb the trapped particle population by subjecting it to a fast adiabatic process due to its periodically time varying large perturbing potential, effectively driving the trapped electrons away from their thermodynamical equilibrium state. Since the trapped particles no longer have an equilibrium phase-space distribution, the structures with such a transient trapped particle population are likely to show deviation from the results of the analytic kinetic model which assumes trapped particle in a thermodynamical equilibrium. The nonlinear structures with sufficiently large amplitude, satisfying $\psi > \psi_{\mathrm{EPW}}$, (or with a possibility of being in a phase-locked state with the EPW) however show a good agreement with the analytical results in the same case, as discussed in Sec. 3.3 in further detail.

3.2.7   Charge density associated with coherent structures

We conclude this section by presenting the profiles for the density difference $\Delta n = (n_e - n_i)$ from the cases I and II and their relation with the analytical classification
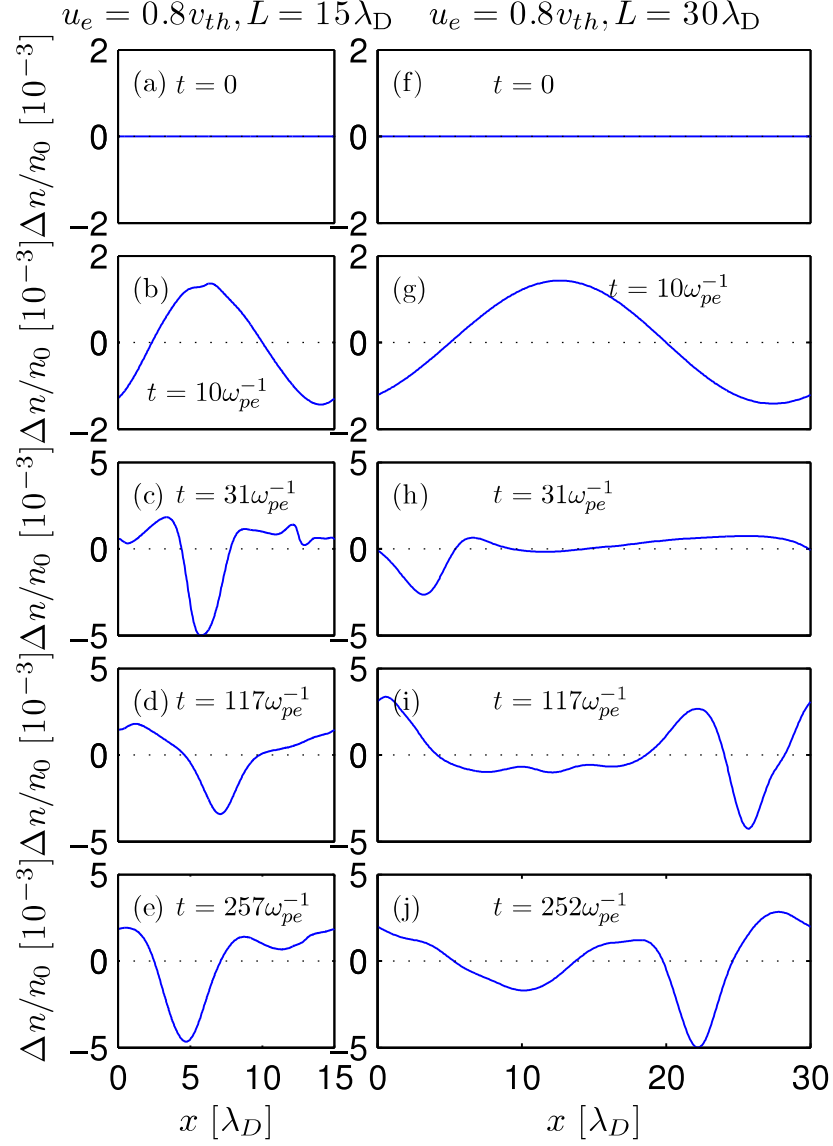
Figure 3.4: Temporal evolution of the profile for the density difference, $\Delta n = n_e - n_i$, for case-I (left) and case-II (right).

of the solutions [4] in Fig. 3.4. The potential profiles at time $t = 10\omega_{pe}^{-1}$ for both the cases (e.g., for the case-I plotted in Fig. 3.1(d)) appear almost sinusoidal however the nonlinear effects already begin to appear in the density profiles in the case-I at this early stage as clear from the evolution of the density difference $\Delta n = (n_e - n_i)$

plotted in Fig. 3.4(b) where the wave clearly shows signs of deviation from the sinusoidal form due to the particle trapping at the potential maximum which is free from any potential perturbation. The Δn profiles show that for sinusoidal wave like profiles the ideal background plasma parameters correspond to the locations where $\phi'' = -\Delta n \to 0$ and the ϕ'' oscillates periodically about this mean value in the space. The maximum value of Δn (i.e., minimum ϕ'') is also much larger than 0 and equal to its minimum value in magnitude. However, for the long time soliton like profiles, Δn no longer oscillates periodically in space about a mean value. The maximum Δn value for long time structures approaches a background value of about zero that corresponds to a value for the unperturbed plasma parameters. This essentially implies that in comparison to the small time profiles, for the long time profiles the parameter k_0, defined as the difference between the minimum value of ϕ'' and the value of ϕ'' corresponding to the background plasma parameters, approaches zero. This is as required, analytically, for the pure soliton solutions [4] and is discussed further in Sec. 3.3.

3.3   Soliton generation by trapping nonlinearity

The coherent structures form at relatively smaller amplitudes as compared to the soliton formation with isothermal electron response with Boltzmann distributed electrons and where the trapped particle effects are ignored. Whether the observed solitons are governed by the stronger nonlinearity originating from the large trapped particle density rather than the nonlinearity present in the conventional hydrodynamic model, needs to be determined by analysis of the simulation results by benchmarking them against the well-known fully kinetic analytical formulation by Schamel [4] as described in the following sections.

3.3.1   A pseudo-potential based approach to trapped particle generated coherence

Note that in the presence of trapped electrons the density of electrons is function of wave potential additionally via the trapped particle density $n_t(\phi)$. Therefore, by introducing the appropriate corrections in the electron distribution function in order to accommodate also the trapped particles, the integration of this modi-

fied distribution can be made to produce a net density that includes the effect of trapped particles. The net density, in turn, is a more complex function of the potential than the conventional Boltzmann relationship in absence of trapping. When this modified density expression is substituted in the Poisson's equation instead of Boltzmann electrons, a nonlinear relationship between potential and trapped particle parameters is obtained. The resulting equation can be cast in the form prescribed by Sagdeev where the potential variation in the space is determined by a modified Sagdeev potential $\mathcal{V}(\Phi)$. When the amplitude of the potential variation $\phi(x)$ is large and it explores the region where $\mathcal{V}(\Phi)$ is no longer parabolic, the wave must show a deviation from the usual sinusoidal waveform, indicating its entry to the nonlinear regime. When the variation of $\phi(x)$ extends up to the boundary of the barrier created by $\mathcal{V}(\Phi)$, the potential $\phi(x)$ varies along the separatrix of the system,

$$\frac{\partial^2 \phi}{\partial x^2} = -\frac{\partial \mathcal{V}}{\partial \Phi}. \tag{3.6}$$

Since the right hand side is a known function of ϕ considering the Poisson's equation,

$$\frac{\partial^2 \phi}{\partial x^2} = \int f_i(x,v) - f_e(x,v) dv, \tag{3.7}$$

where the ϕ dependence enters the right hand side via the trapped particle distribution function, the Sagdeev potential $\mathcal{V}(\Phi)$ can be derived and the analytical form of $\phi(x)$ is obtainable, in terms of plasma and trapped particle parameters entering $\mathcal{V}(\Phi)$, by integrating (3.6). Note that the normalized variables are used in Eqs. (3.6) and (3.7) as well as in the analysis that follows.

Following the above methodology, the electron distribution function obtained from the saturated stages of the present simulation, where the stable solitonic structures are recovered, is compared and fitted with the following form of the distribution function parameterized at the location of the trapping potential [4],

$$f_{\text{fit}}(x,v) = \frac{1 + k_0^2 \psi/2}{\sqrt{2\pi}} \left[\theta(\epsilon) \exp\left\{ -\frac{1}{2}(\sigma\sqrt{2\epsilon} - v_{\text{eff}})^2 \right\} \right.$$
$$\left. + \theta(-\epsilon) \exp\left(-\frac{v_{\text{eff}}^2}{2} \right) \exp\left(-\beta\epsilon \right) \right], \tag{3.8}$$

where $\theta(\epsilon)$ represents the Heaviside step function, $\sigma = sg(v)$ is the sign of velocity, $v_{\text{eff}} := v_D - v_0$, where $v_D = u_e$ is the drift velocity between electrons and ions existing in unperturbed state and v_0 is the phase velocity of the wave/hole with respect to ion distribution function and ψ is the wave amplitude in terms of potential. k_0 is the parameter determining the character of the potential variation such that $k_0^2 > 0$ and $k_0^2 = 0$ correspond to a sinusoidal wave and a soliton solution, respectively. The solution (3.8) satisfies the Vlasov equation,

$$v\frac{\partial f}{\partial x} + \frac{\mathrm{d}\phi}{\mathrm{d}x}\frac{\partial f}{\partial v} = 0, \tag{3.9}$$

given that the variable ϵ is constant of motion for collisionless electrons and therefore most suitably $\epsilon = \frac{v^2}{2} - \phi(x)$.

3.3.2   Characterizing coherent structures as trapped particle equilibria

Table 3.1: The parameters obtained from best fit of the simulated distribution function to the analytical function (3.8).

Cases (u_e, L)	β	ψ	$v_{\text{eff}} = u_e - c_s$
I (0.8, 15)	-7.5	0.02137	0.78
II (0.8, 30)	-6.1	0.02988	0.78
III (1.2, 15)	-1.62	0.09720	1.18

The values of parameters ψ, β, and the effective velocity $v_{\text{eff}} = u_e - c_s$ were obtained by making a best fit of the function (3.8) to the simulated electron distribution function at the trapping location such that $(v_{\text{phase}} - v_{\text{sep}})^2 = 2\psi$, where v_{sep} is the location of the separatrix on the velocity axis. For the cases I, II and III, we have compared the simulated electron distribution function at soliton locations, in the nonlinearly saturated phase of the microinstability where strong vortex like structures appear in the phase-space, with the expression (3.8), obtaining a best fit of (3.8) to the simulation results with respect to variation in the parameters β, ψ and v_{eff}. This exercise, in turn, produces the optimum values of the fit parameters in the each of the cases presented in Fig. 3.2. While the results of this optimization are presented graphically in Figs. 3.5(a), (c) and (e) for the cases I,

II and III, respectively, the corresponding values of parameters recovered from the simulation data using the best fit to the analytical results for all the three cases plotted in Fig. 3.5 are provided in Table 3.1. A more detailed graphical analysis of
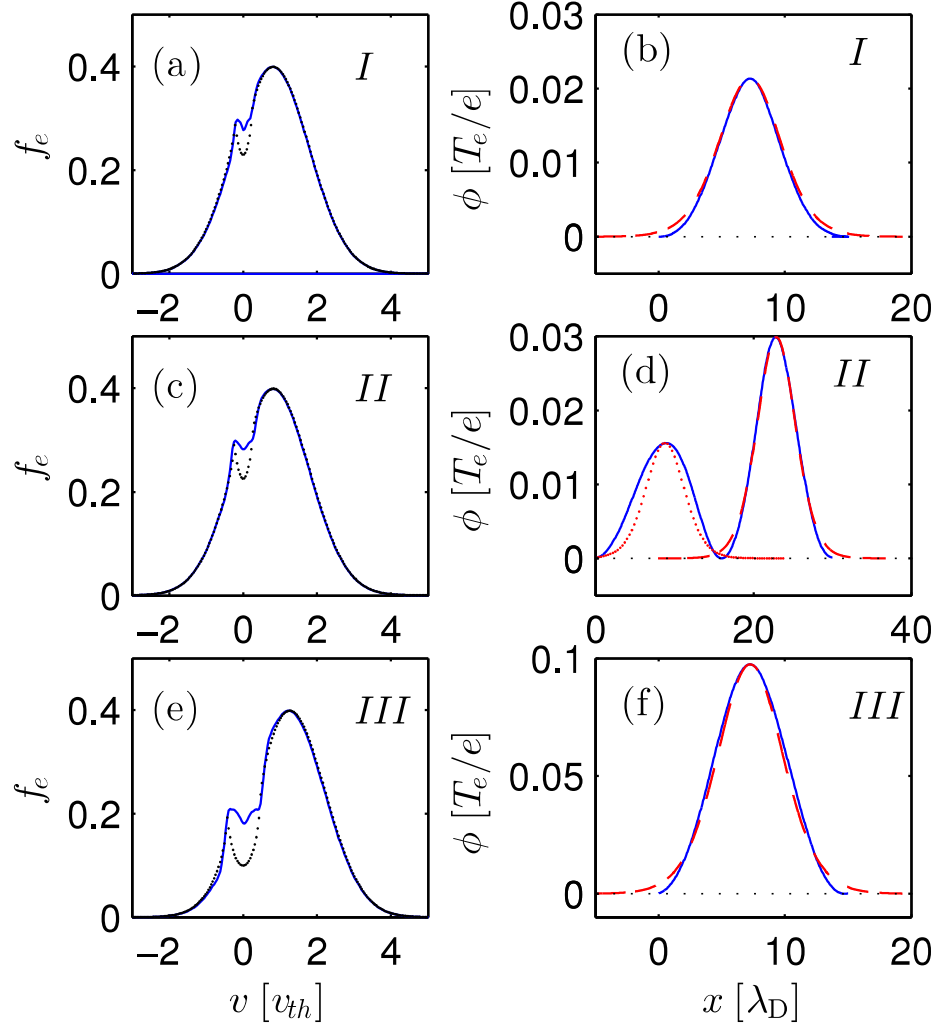
Figure 3.5: (Left) Best fit of the simulated electron distribution function $f_e(v)$ to the analytical function (3.8). Subplots (a), (c) and (d) correspond to the cases-I, II and III, respectively. (Right) Comparison of the simulated potential profile $\phi(x)$ with the soliton solution (3.11) with the parameters obtained from the simulated distribution function with trapped electrons. Subplots (b), (d) and (f) correspond to the cases-I, II and III, respectively.

the simulation result using the best fit for an example case, case-II with $L = 30\lambda_{\mathrm{D}}$

and $u_e = 0.8 v_{the}$, is done and presented using Figs. 3.7(a)-(d). With the parameters β, ψ and v_{eff} determined from the parametric fit of the simulation data to (3.8), the soliton like spatial variation of the potential of the structures recovered in the simulation can be verified against the analytical results. In order to do this, imposing the necessary condition that $n_i(\psi)u_i - n_e(0)u_e = j/e$ (where j is the saturated current density) and seeking the bounded solutions for the potential such that $\phi(x_{\min}) = 0$ and $\phi(x_{\max}) = \psi$ (where $x_{\max}$ and $x_{\min}$ are the locations of the minimum and maximum of the potential profile forming the structure), the modified Sagdeev potential $\mathcal{V}(\Phi)$ is obtained in the form [4],

$$
-\mathcal{V}(\Phi) = \frac{k_0^2}{2}\Phi(\psi - \Phi) + \frac{8}{15}\frac{(1-\beta)}{\sqrt{\pi}}\Phi^2(\sqrt{\psi} - \sqrt{\Phi})
$$
$$
+ \frac{(1 + k_0^2)^2 - 1/3}{2}\Phi(\psi - \Phi). \tag{3.10}
$$

Substituting (3.10) in Eq. (3.6) and a subsequent integration in the limit $k_0^2 \to 0$, applicable to the existence of the solitary solution, leads to the following solutions for the potential structure $\Phi(x)$ in terms of the parameters obtainable from the fit,

$$
\Phi(x) = \psi \, \text{sech}^4 \left[\sqrt{\left(\frac{(1-\beta)}{15} \sqrt{\frac{\psi}{\pi}} \right) x} \right]. \tag{3.11}
$$

The simulated soliton potential profiles from three different cases are plotted in Figs. 3.5(b), (d) and (f) at nonlinearly saturated state of the ion acoustic resonant microinstability superimposed by the corresponding analytical profiles of trapping nonlinearity generated solitons drawn using (3.11) and the parameter values resulting from the fit. With inclusion of case-II in the analysis the presented data includes the cases of trapping nonlinearity generated solitons both with and without the presence of a high frequency EPW. The presence of an EPW in case-II does not show any noticeable impact on the accuracy of agreement with the analytical solutions at the soliton location, provided that the structures with $\psi > \psi_{\text{EPW}}$ are considered.
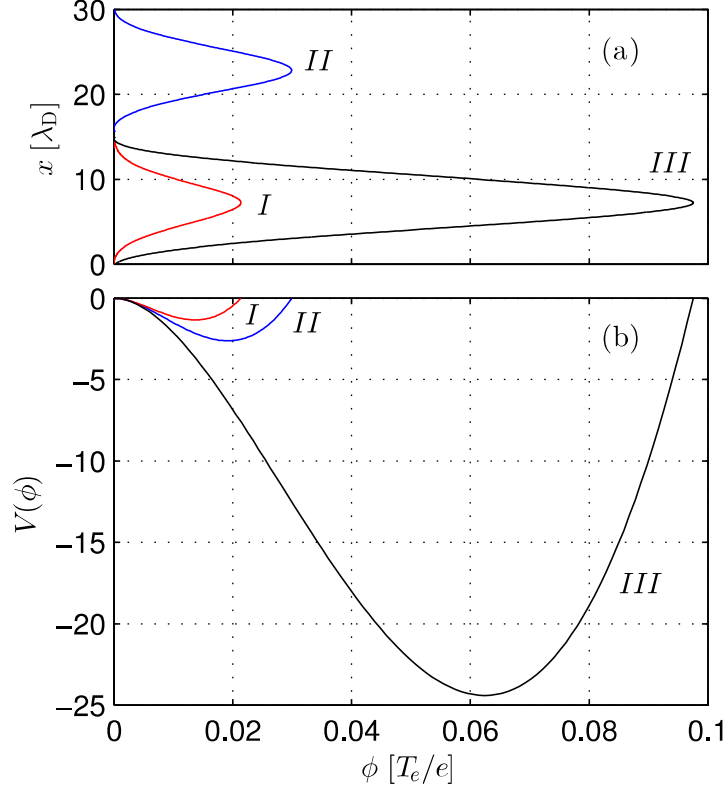
Figure 3.6: (a) Profiles for the simulated wave potential $\phi(x)$ for the cases-I, II, and III, at $t = 257, 252$ and $199\ \omega_{pe}^{-1}$. (b) Modified Sagdeev potential (3.10) for the corresponding cases plotted using trapping parameters obtained from the simulations.

3.3.3   Pseudo-potential $\mathcal{V}(\Phi)$ associated with solitary electron holes

The modified Sagdeev potential $\mathcal{V}(\Phi)$ for all the three cases are plotted in Fig. 3.6(b) using the expression (3.10). It can be noted from the corresponding plots of $\phi(x)$ in Fig. 3.6(a) that in agreement with Eq. (3.6) the potential $\phi(x)$ has a vanishing second derivative at its minimum value, $\phi = 0$, which also coincides with the vanishing derivative of the modified Sagdeev potential, $\partial \mathcal{V}/\partial \Phi = 0$. This is the analytical requirement for the soliton solution according to the definition $k_0^2 = 0$ [4], where k_0^2 is defined as the difference between the potential at the point where $\partial \mathcal{V}/\partial \Phi = 0$ (ϕ turning point in Fig. 3.6(a)) and the value of the unperturbed potential (set

to be zero in Fig. 3.6). Note that the additional peak in the profile of the case II does not satisfy $\psi > \psi_{\mathrm{EPW}}$ and therefore the potential profile corresponding to this structure is difficult to be verified against the expression (3.11) since an accurate value of β could not be determined in absence of a well-defined concave shape of the distribution about c_s. However, the taller structure that obeys $\psi > \psi_{\mathrm{EPW}}$ is in a very good agreement with (3.11) highlighting that the presence of an EPW in case-II does not show any noticeable impact on the accuracy of agreement with the analytical solutions (3.11) as long as the trapped particles are in an isolated (micro-canonical) equilibrium as a result of the fact that the condition $\psi > \psi_{\mathrm{EPW}}$ is well satisfied and the minimum of the trapping potential is largely time independent.

3.3.4   Impact of EPW perturbation on trapped distribution adiabaticity

As described above, the electron plasma wave in the case-II has smaller Landau damping and a high frequency potential fluctuations persist due to its presence in the background. This fast potential variation, if larger than ψ, can subject the density of the trapped particles to an adiabatic variation, preventing the population of the trapped electrons form reaching a thermal equilibrium and a stable β value to develop, as essential for characterizing the equilibrium using (3.1). Existence of strong EPW affects the agreement of observed variation of $\phi(x)$ from the analytical results unless $\psi > \psi_{\mathrm{EPW}}$. Applying this to the case-II (presented in more detail in Fig. 3.7), among the two solitary structures present at $x = 9.57\lambda_{\mathrm{D}}$ and $x = 22.7\lambda_{\mathrm{D}}$, the conditions applicable to (3.1) are well satisfied for the relatively stronger second solitary structure located at $x = 22.7\lambda_{\mathrm{D}}$ making it to be a suitable choice for the comparison with analytical results. The simulated electron distributions corresponding to locations of both these solitons is plotted in Fig. 3.7(d) where the f_e for the second soliton at $x = 22.7\lambda_{\mathrm{D}}$ (dark blue line) is clearly seen to have a thermalized trapped particle distribution with $\beta = -6.1$ while the f_e for the first soliton at $x = 9.57\lambda_{\mathrm{D}}$ (light gray line) has a transient nonequilibrium population of trapped particles which is partly renewed in every cycle of the EPW due to stochastic nature of trajectories in the separatrix region and therefore fails to attain an equilibrium temperature, or a time independent β value. Furthermore, for the second soliton in case-II and those in each of the cases-I and III, $k\lambda_{\mathrm{D}} \gg 1$, such that a strong Landau damping of EPW is present the EPW excited

initially damps away in the period of few ω_{pe}^{-1}, therefore the agreement of simulated structures in these cases with the analytical results remain much more robust and unambiguous as presented above.
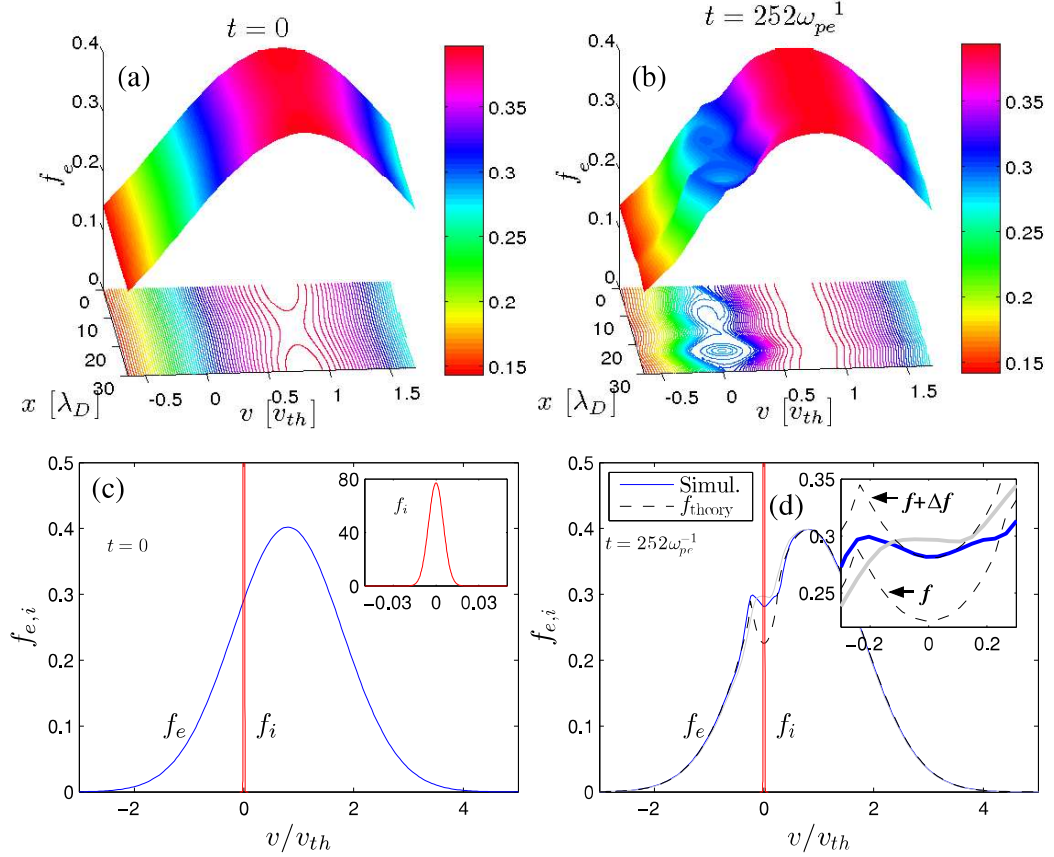
Figure 3.7: (a) Electron distribution function $f(x,t)$ at time $t = 0$. (b) Electron distribution function at time $t = 2.52 \times 10^2 \omega_{pe}^{-1}$. (d) The electron distribution featuring the electron trapping in the ion acoustic solitons located at $x = 8.9$ and $22.7 \lambda_{\mathrm{D}}$. (c) Electron and ion distribution $f(v)$ at $t = 0$ at the first soliton location $x = 22.7 \lambda_{\mathrm{D}}$. (d) Electron and ion distribution $f(v)$ at $t = 2.52 \times 10^2 \omega_{pe}^{-1}$. The electron distribution is additionally plotted at first soliton location $x = 9.57 \lambda_{\mathrm{D}}$ (light gray line), at second soliton location $22.7 \lambda_{\mathrm{D}}$ (dark blue line) and using the analytical function (3.8) (dotted line) with the parameters obtained from the best fit to the simulated electron distribution function at the location of the second soliton $x = 22.7 \lambda_{\mathrm{D}}$, where $\beta = -6.1$, $\psi = 0.02988$ and $v_{\mathrm{eff}} = 0.78 v_{th}$.

The irregularity of the phase-space contours of electron distribution function corresponding to the smaller peak in comparison with those corresponding to the

taller soliton in case-II, as seen in Fig. 3.7(b), is a visibly strong sign of larger degree of ergodization of the separatrix (curve dividing trajectories of trapped and streaming electrons in the phase space) by a regular or stochastic (noise-like) perturbation. For the distribution at the location of taller soliton (plotted with darker solid line in Fig. 3.7(d)) this destruction of the separatrix is limited to the outer boundary of the vortex while the trapped particles in the vortex interior are largely unaffected by the perturbation and have stable closed phase-space trajectories. In contrast to this, the distribution at the location of smaller soliton with $\psi < \psi_{\mathrm{EPW}}$ (plotted with a lighter solid line) has a flat profile at the resonant velocity, indicating that the high frequency EPW perturbation is capable of ergodizing the separatrix such that the width of ergodic region covers the complete vortex region in the phase-space. The trajectories up to the center of the vortex are chaotic and, given the flatness of the distribution that still evolves at the finer scales, show a continuity with streaming trajectories via the ergodized separatrix. This dynamics corresponds to a transient population of resonant particles which strongly interacts with the EPW and is unable to reach its own thermodynamical equilibrium in a collisionless Vlasov plasma. The non-equilibrium distribution effectively translates into the difficulty in finding a well defined and stable β value from the present simulation results for the cases with $\psi < \psi_{\mathrm{EPW}}$.

3.3.5   Regime of stronger EPW and trapped particle interaction

We now discuss the relevance of the above analysis to the cases where the properties of the population trapped in the coherent structure are such that the associated trapped particle density modes have a finite temporal correlation with main or additional wave processes like EPW (or a rather low frequency process than the EPW [103]). This might allow the former to enter into a mutually phase-locked state with the wave processes leading to a potentially stable (undamped) perturbed BGK solutions, though with a complex collective dynamics of the trapped particle density [104, 105]. This highlights the possibility of formation of time dependent trapped particle equilibrium where an adiabatic version of the trapped particle generated nonlinear structures can arrive at an equilibrium with another periodic process by means of a mutual phase-locking. An analogous mechanism is discussed in the cases of waves that stably trap the particles in an anharmonic potential or

in presence of a low frequency applied ponderomotive field [103] in a process that has a close relationship with the mechanism of Negative Mass Instability (NMI) [106]. In the present cases of valid trapped particle solitons, however, the EPW because of its high frequency has a considerable mismatch with a rather low electron bounce frequency ω_{be} and its effect is limited to perturbing the separatrix of the BGK structures and triggering additional trapped particle modes. These modes, owing to large $\partial f/\partial v$ at resonant location, result in a residual growth of the structures as well as that of the perturbation. Finally, at sufficiently longer times ($t \sim 10^3 \omega_{pe}^{-1}$ and beyond) when the amplitude modulation due to trapped particle instability grows sufficiently large, it begins to destroy the separatrix by allowing larger fraction of the trapped particles to escape via the fluctuating potential barriers. The agreement with the model Eq. (3.1) at longer time, when the separatrix is sufficiently ergodized, is therefore found to be limited only in an increasingly narrow region about the location (peak) of the coherent structure where a small trapped electron density may still have a local equilibrium. A large bunching of the trapped particles is seen at the same time, which is responsible for the growing amplitude of modulations as observable in Fig. 3.2 at later times. In this respect we note that the frequency of the slowly growing modulations in the long time evolution of wave amplitude, observable in Fig. 3.2 for case-I and III, shows a good agreement with the electron bounce frequency for the respective cases.

3.4   Comparison between kinetic and hydrodynamic nonlinearity

Finally, it is useful to compare the relative strengths of the kinetic nonlinearity generated by the trapped particles with the conventional fluid nonlinearity by means of the solutions of m-KdV equation 3.1 for the recovered solitary electron hole parameters, as presented below. We begin by the well known solitary solution of the Kd-V equation Eq. (1.6) [49],

$$\phi(x) = A \, \text{sech}^2 \left[\sqrt{\frac{A}{6}} \, (x - vt) \right], \tag{3.12}$$
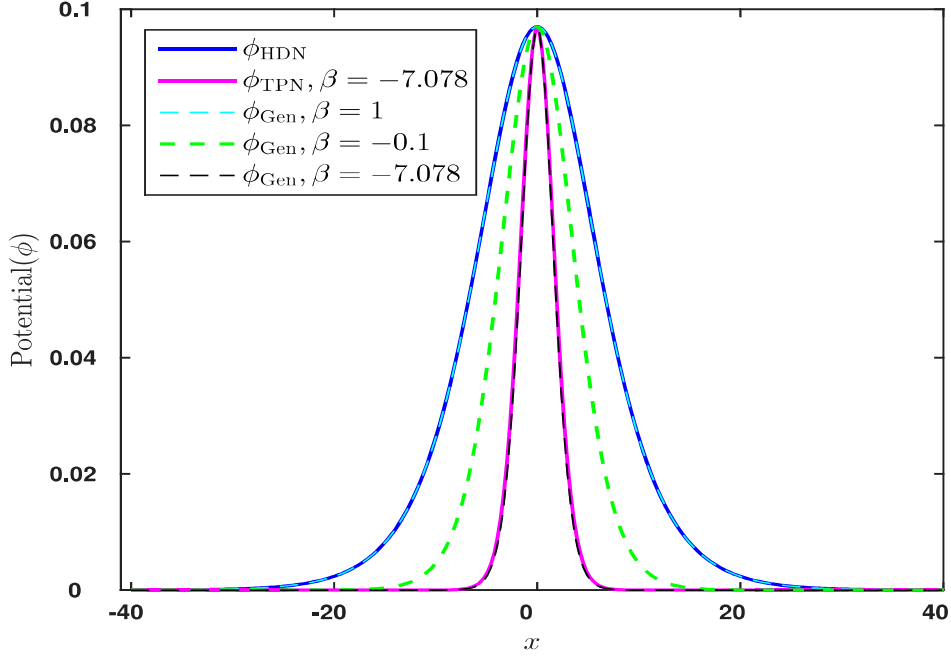
Figure 3.8: The solid blue line represent the solution for the soliton considering only the hydrodynamic nonlinearity Eq. (3.12), and the solid green line represent the soliton considering only the trapping nonlinearity Eq. (3.17) with $\beta = -7.078$ and all the dashed lines represent the soliton having both hydrodynamic and trapped particle nonlinearity Eq. (3.19) for different value of trapped particle parameter β.

where, A is the amplitude of the wave. Propagation velocity of the solitary wave is $v = A/3$. Instead of hydrodynamic nonlinearity, considering only the contribution of trapped particle nonlinearity the Kd-V equation is modified to an mKd-V equation [45].

$$\partial_t \phi + \frac{1-\beta}{\sqrt{\pi}} \sqrt{\phi} \partial_x \phi + \frac{1}{2} \partial_x^3 \phi = 0. \tag{3.13}$$

3.4.1   Solution for trapped particle solitary waves

For solving Eq. (3.13) we substitute $\frac{1-\beta}{\sqrt{\pi}} = m$ and $\phi = f(\xi) = f(x - vt)$, where $\xi = x - vt$. Therefore, $\frac{\partial}{\partial t} \equiv \frac{\partial \xi}{\partial t} \frac{\partial}{\partial \xi} \equiv -v \frac{\partial}{\partial \xi}$, and $\frac{\partial}{\partial x} = \frac{\partial \xi}{\partial x} \frac{\partial}{\partial \xi} = \frac{\partial}{\partial \xi}$. Using these values

68

and then integrating ones, the above equation can be written as,

$$-vf + \frac{2m}{3}f^{3/2} + \frac{1}{2}f'' = c,$$ (3.14)

where c is a constant of integration. Multiplying (3.14) by f' and integrating with respect to ξ once, produces,

$$\frac{-v}{2}f^2 + \frac{4m}{15}f^{5/2} + \frac{f'^2}{4} = cf + c_0.$$ (3.15)

For solitary wave like solution, the boundary conditions are $f(\xi) = f'(\xi) \to 0$ as $\xi \to \pm\infty$, which gives $c = c_0 = 0$. Substituting these values and considering only the solution with negative sign it can be written as,

$$f' = -f\sqrt{2v - \frac{16m}{15}f^{1/2}}.$$ (3.16)

The velocity of the solitary wave is obtained by applying the initial condition $f(0) = A$ and $f'(0) = 0$ as, $v = \frac{8}{15}m\sqrt{A}$, where A is amplitude of the soliton. Above first order nonlinear differential equation (3.16) can be solved by considering $f(\xi) = A\,\text{sech}^4\theta$. Hence, $f(0) = A$, $f'(0) = 0$ and $f'(\xi) \leq 0$ for $\xi \geq 0$. Additionally, $df = -4A\,\text{sech}^4\theta\tanh\theta\,d\theta$. Substituting these values in the above equation and integrating, we get, $\theta = \sqrt{\frac{m\sqrt{A}}{15}}\,\xi$. Using the value of θ, m and ξ, the final solution becomes

$$f = A\,\text{sech}^4\left[\sqrt{\frac{(1-\beta)\sqrt{A}}{15\sqrt{\pi}}}\,(x - vt)\right]$$ (3.17)

3.4.2 General solution

The general mKd-V equation, including both the hydrodynamic and trapped particle nonlinearity, is,

$$\partial_t\phi + \left[\frac{1-\beta}{\sqrt{\pi}}\sqrt{\phi} + \phi\right]\partial_x\phi + \frac{1}{2}\partial_x^3\phi = 0$$ (3.18)

Eq. (3.18) can be solved similarly as Eq. (3.13). After the essential co-ordinate transformation and integrating twice with respect to ξ, we get the first order

nonlinear differential equation equivalent to Eq. (3.16),

$$\Rightarrow f' = -f\sqrt{2v - \frac{16m}{15}f^{1/2} - \frac{2}{3}f},$$

which can be solved by substituting

$$f(\xi) = \frac{A\left(bm - 1\right)^2}{\left(bm\ \cosh^2\theta - 1\right)^2}.$$

Where b is a constant and A is the amplitude of the solution. Therefore, $f(0) = A$, $f'(0) = 0$ and $f'(\xi) \leq 0$ for $\xi \geq 0$. The final solution of Eq. (3.18) becomes,

$$f = \frac{A\left(D - 1\right)^2}{\left[D\cosh^2\left\{\frac{1}{4}\sqrt{\frac{16m\sqrt{A}}{15} + \frac{2A}{3}}\left(x - vt\right)\right\} - 1\right]^2}, \qquad (3.19)$$

where $D = \left(2 + \frac{8m}{5\sqrt{A}}\right)$, $m = \frac{1-\beta}{\sqrt{\pi}}$ and $v = \left(\frac{8}{15}m\sqrt{A} + \frac{A}{3}\right)$ is the velocity of the wave. All the three solutions, i.e., those of Eqs. (3.12), (3.17) and (3.19) are plotted at t=0 in Fig. 3.8 using the solitary wave parameters recovered in the simulations. The solid blue and green lines correspond to the solitary solutions of Eqs. (1.6) and (3.13), respectively. All the dashed lines correspond to the solitary solutions of Eq. (3.18) with different value of trapping parameter β which is varied from value 1.0 to -7.078. The value $\beta = 1$ corresponds to no trapping. This can be seen that with increase in the value of the coefficient $(1 - \beta)$ of the trapping nonlinerity in Eq. (3.18), the solution modifies from soliton having only fluid nonlinearity Eq. (3.12), to the soliton having only the trapped particle nonlinearity Eq. (3.17). The present simulation of generating of IA-solitary waves in presence of current, we have recovered the solitary soliton of amplitude $\psi = 0.097$ and $\beta = -7.078$ for drift velocity of electron distribution function $v_{De} = 1.2$. Therefore, it can be suitably concluded that at small amplitude regime the trapped particle nonlinearity dominates over the fluid nonlinearity.

3.5   Summary and conclusions

The coherent structures provide very effective first signatures of the nonlinearity in collective modes as discussed in Chapter 1. Among the electrostatic plasma

modes the ion acoustic response shows most visible signature of nonlinearity by readily producing ion acoustic solitons and solitary waves for finite amplitudes. The ion acoustic structures therefore serve as an ideal paradigm for nonlinearity produced coherence in the plasma theory and their growing phase is investigated in this chapter.

We have presented results of a two species Vlasov simulation featuring self-consistent generation of solitons produced from a stronger nonlinearity originating from the kinetic effects of trapped electron population in a finite amplitude ion acoustic wave driven unstable by a current driven microinstability. The numerical simulations presents a general time dependent evolution of the particle distribution functions that obey the collisionless Vlasov equation. The simulations are motivated by solitary structures predicted by nonlinear nonperturbative formulation based on the Vlasov-Poisson system that reduces into a m-KdV equation. In order to effectively compare the evolution usually recovered by conventional linear procedure using harmonic (cosine) density perturbations, the investigation is done by selecting this class of perturbations as initial conditions.

In the initial phase of evolution, a remarkable modification in the distribution function is visible at the ion acoustic velocity. Since generation of vortex like structures in electron phase space distribution results in the diminishing gradient of the electron distribution function $\partial f_e/\partial v_e$ at the resonant velocity which must be nonzero for the linear growth in the ion acoustic wave, the evolution and the observed saturation in wave growth indicates a nonlinear saturation of the growth where the resonant particles act to flatten the zero order electron distribution, allowing $\partial f_e/\partial v_e \to 0$ at the phase velocity of the wave. We have noted that at an amplitude quite comparable to its initial sinusoidal stage at $t = 10\omega_{pe}^{-1}$, the strong nonlinear effects begin to appear in the IAW at $t = 31\omega_{pe}^{-1}$ and beyond. In the secondary phase the growing nonlinear wave, depending on the allowable k values in the simulation, either develops into a train of solitons of various heights and speeds, or produces a single soliton structure. The amplitude evolution at longer times shows that the growth of this nonlinear wave or structures is arrested as the structures begin to trap the resonant electrons and, in turn, their amplitudes begin to approach corresponding saturation values. In this saturated phase a trapped particles (electrons) instability [37] is the mechanism responsible for the observable residual growth in the nearly saturated soliton amplitude that shows a modulation

with the frequency equivalent to the electron bounce frequency ω_{be}.

The nonlinear coherent soliton structures developed in the simulation are shown to follow the analytical solutions of mKdV equation that accounts for the stronger nonlinearity produced by the electron trapping in the structure. In the low k regime where the structures coexist and interact with the undamped high frequency electron plasma waves, the nonlinear soliton structures retain their modified nonlinear analytic structure as long as the trapped electron distribution is allowed to be in a thermodynamical equilibrium. For the the structures where associated trapped electron equilibrium is perturbed by a time dependent variation of the trapping potential, it is difficult to characterize the trapped electron distribution using the equilibrium parameters. In the conditions where the developing ion acoustic structures are free from time dependent perturbations, the numerically simulated coherent structure could be characterized analytically, by finding from them the necessary parameter to construct the corresponding analytical solutions and carry out the comparison of the simulation results with the theoretical formulation that leads to a modified KdV equation with a stronger nonlinearity. The modified Sagdeev potential, $\mathcal{V}(\Phi)$, corresponding to the numerically simulated solutions is also constructed and verified to confine the electrostatic potential $\phi(x)$ in the limits of the observed soliton structures.

Relatively small amplitude coherent structures coexisting with a periodic self-consistent potential perturbation are found to be most affected by the adiabatic response of the electrons. Presence of a self-consistent time dependent perturbing potential, present in the form of an EPW in the simulations, prevents the trapped electrons from reaching an equilibrium and forming stable BGK modes that are time independent stable solutions of the Vlasov equation. Although the coherent ion acoustic solitary structures with such a transient trapped particle population are observed and found to be reasonably stable. In the cases where EPW is undamped, it is well resolved in our simulations and visible as a well developed undamped BGK-like structure at the electron phase velocity v_{phase} in the electron distribution function. This indicates that for the cases where the electron bounce frequency exceeds the Landau damping rate of the EPW, $\omega_{be} > \gamma_{\text{L}}$, a stable BGK mode develops and arrests the linear Landau damping of the EPW, unlike the cases where $\omega_{be} < \gamma_{\text{L}}$ and a linear landau damping of EPW must result. We also compared the relative strengths of the kinetic nonlinearity generated by the

trapped particles with the conventional fluid nonlinearity by means of the solutions of m-KdV equation (3.1) for the recovered solitary electron hole parameters. It is seen that with increase in the value of the coefficient $(1 - \beta)$ of the trapping nonlinerity, the solution modifies from soliton having only fluid nonlinearity to the soliton having only the trapped particle nonlinearity. In the present simulation of generation of IA-solitary waves in presence of current, we have recovered the solitary soliton of sufficiently small amplitudes within the regime of trapped particle nonlinearity. Therefore, it can be suitably concluded that at small amplitude regime the trapped particle nonlinearity dominates over the fluid nonlinearity.

Finally, the time asymptotic evolution of the BGK structure associated with soliton generated by the trapped particle nonlinearity shows a residual growth originating from the nonlinear trapped ion instability which produces modulations in the soliton amplitude with electron bounce frequency and causes a net growth in present cases simulated using a finite current.

4

Nonlinearly interacting trapped particle solitons in collisonless plasmas

4.1   Introduction

Solitary structures indeed governed by the trapping nonlinearity were presented in Chapter 3 as recovered in the simulation of an ion acoustic microinstability. These structures were identified by their characteristic steeper analytic form, having origin in a the microinstability that saturated into a coherent state by the trapped-particle nonlineairty. The functional structure of the self-consistently generated SEH was analyzed in Chapter 3 and shown to confirm with the analytic coherent SEH solutions corresponding to ion acoustic branch [1]. These slow SEH structures also stably coexisted with high frequency electron plasma waves that showed signs of supporting another set of trapped particle structures on the electron plasma wave (EPW) branch. The SEH activity is presented in this chapter on a distinct electron acoustic branch of a drift-free stable plasma, involving their multiple identity preserving collisions or overtake. In the analysis present in this chapter, we present Vlasov simulations [8] of the interacting SEH solutions in the limit of large enough separation of their velocities $\Delta v^2 > \psi$ as well as relatively small $\Delta v^2 \sim \psi$ (where ψ is the amplitude of the soliton electrostatic potential $\phi(x)$ in electron thermal units, T_e/e), however at their smaller amplitude ($\psi \ll 1$) as compared to earlier studies [93]. The coherent evolution of analytic solutions

as initial conditions in our case therefore displays their mutual interactions free from any destabilizing ion response chaotic movement, breaking or coalescence. Exploring this regime thus offers us an opportunity to carefully investigate their interaction and interpret some experimental observations based on this process.

The identity preserving multiple interactions of SEH resulting in the cases with $\Delta v^2 > \psi$, display an adiabatic trapped particle response, and also open up many interesting physical possibilities, for example, formation and existence of a system of multiple solitons interacting weakly via exchange of trapped particle bunches or macro-particles [104, 106, 107], and perhaps a distinct statistical mechanics associated with thermodynamic limit of such a system [108]. From analytic view point, their stability might qualify them as an alternate set of nonlinear eigenmodes for such systems during their quasi-stationary equilibria [109, 110]. As an immediate application, By applying it to the observation of magnetospheric potential structures, present simulations enable us to address the origin of somewhat infrequent tripolar electric structures besides a frequent bipolar variation already interpreted as SEH in the magnetospheric wideband data (WBD) of the four spacecraft Cluster quartet [18, 19].

The chapter is organized in as follows, in Sec. 4.2, the analytic SEH formulation relevant to the electron acoustic regime explored in the present work is discussed and the cases considered in the present study are described with corresponding parameters. In Sec. 4.3, the evolution of SEH is presented in the present Vlasov simulations beginning from the equilibrium analytic solutions of the Vlasov-Poisson set of equations in the phase-space. Characterization of the results and correspondence of their spatiotemporal form with the observations in magnetospheric plasmas is also discussed. Summary and conclusions are presented in Sec. 4.6.

4.2 Analytic structure of electron acoustic SEH

In Chapter 3 the simulated structures were recovered to confirm with the solutions of the electron hole formulation prescribed by H. Schamel [36]. The analysis therefore indicated that in system free from any free-energy source (e.g, electron drift/current) the analytic electron hole solutions should be stable and can be used as an ideal initial condition to avoid an initial transient. This *a-priori* assumption is tested in this chapter and initial condition of the studied structures are chosen

to be SEH solutions [1] obtained in the desired electron-acoustic regime. For a formal introduction to our initial condition and its origin, below, we present the necessary analytic prescription for SEH solutions in the electron acoustic regime following Schamel [1].

The analytic SEH solutions of the Vlasov Plasma system essentially involve ion mobility in the low frequency regime where the ions can additionally be trapped in the potential nonuniformity besides electrons. Coherent SEH solutions in the electron acoustic velocity regime lying between the electron plasma wave and ion acoustic wave phase velocities, $v_{thi} < v_p < v_{the}$, are obtainable in slow ion response limit for simplification. Although these solutions are used in the present simulations as initial conditions, the evolution of interacting structures is done in presence of fully mobile ions in the numerical scheme in order to study the stability of SEH structures with respect to the ion response. Among the cases examined here are: (I) two identical electron holes, counter-propagating in the reference frame of the uniform plasma, colliding, (II) two non-identical counter-propagating solitons having unequal phase velocities, colliding, (III) two non-identical solitons co-propagating with a finite relative velocity where the faster soliton overtakes the slower one and (IV) two non-identical solitons co-propagating with a finite relative velocity, such that $\Delta v_0^2 < \psi$, where ψ is the potential amplitude of the structures. In all the first three cases (Case I- III) the relative velocity, Δv_0^2 is greater than ψ, $(\Delta v_0^2 > \psi)$.

4.2.1 Electron distribution for stable electron acoustic SEH

The initial analytic solutions adopted for all the cases presented in this chapter belong to solitary solutions in electron acoustic regime are consistent with unperturbed ions and a solitary electron hole phase-space distribution, as already discussed in Chapter 3 [33],

$$f_{\text{EH}}(x,v) = \frac{1 + k_0^2 \psi / 2}{\sqrt{2\pi}} \left[\theta(\epsilon) \exp \left\{ -\frac{1}{2} (\sigma \sqrt{2\epsilon} - v_{\text{eff}})^2 \right\} \right.$$
$$\left. + \theta(-\epsilon) \exp \left(-\frac{v_{\text{eff}}^2}{2} \right) \exp \left(-\beta \epsilon \right) \right], \qquad (4.1)$$

where, as originally introduced in Sec. 3.2, the lengths and velocities are normalized to $\lambda_{\mathrm{D}} = \sqrt{T_e/4\pi n e^2}$ and $v_{\mathrm{the}} = \sqrt{T_e/m_e}$, respectively, $\theta(\epsilon)$ represents the Heaviside step function, $\sigma = sg(v)$ is the sign of velocity, $v_{\mathrm{eff}} = v_e - v_0$, where the quantities v_e and v_0 are the velocities of the Maxwellian (with respect to the plasma) and the velocity of the electron acoustic solitary hole (with respect to the plasma), respectively. Note that in absence of drift, $v_e = 0$ and the first term in (4.1) is a Maxwellian shifted by the hole velocity where the positive and negative values of v_0 correspond to forward and backward propagating holes seen by the Maxwellian, respectively. The choice of parameter k_0 allows using (4.1) to obtain various categories of potential solutions having special values of potential gradients at the points where ϕ approaches its unperturbed value, conventionally chosen as $\phi = 0$. For example, the variations with $k_0^2 > 0$ and $k_0^2 = 0$ correspond to an oscillatory solution and a SEH solution, respectively. The variable $\epsilon = \frac{v^2}{2} - \phi(x)$ is constant of motion for collisionless electrons, such that f_{EH} satisfies the Vlasov equation obeyed by electrons and ions,

$$\frac{\partial f_{e,i}}{\partial t} + v\frac{\partial f_{e,i}}{\partial x} \pm \frac{\mathrm{d}\phi}{\mathrm{d}x}\frac{\partial f_{e,i}}{\partial v} = 0. \tag{4.2}$$

Accordingly, the initial electron distribution for present cases is set as $f_i \equiv f_{\mathrm{EH}}$, while the initial ion distribution is set to be Maxwellian $f_i \equiv f_{\mathrm{M}}$ given by (3.2), and although the analytic electron acoustic SEH formulation summarized below assumes negligible ion participation in the electron acoustic regime, the evolution of ion distribution in the numerical simulation is fully enabled.

4.2.2   Solitary solutions and Nonlinear Dispersion Relation

In order to obtain a Nonlinear Dispersion Relation for electron acoustic SEH the Poisson equation is to be solved using a non-perturbative approach requiring densities of electron and ions from the above distributions. A Taylor expansion of Eq. (4.1) followed by a velocity integration produces, in the limit $\phi \ll 1$, the total electron density density (omitting the subscript e),

$$n(\phi) \approx \left[1 + \frac{k_0^2\psi}{2} - \frac{1}{2}Z'_r(v_0/\sqrt{2})\phi - \frac{4}{3}b(\beta, v_0)\phi^{3/2}\right] \tag{4.3}$$

Table 4.1: Parameters ψ, v_0 and β in various cases.

Cases	(ψ_1, ψ_2)	(v_{01}, v_{02})	(β_1, β_2)	Δv_0^2
I	(0.04, 0.04)	(0.4, -0.4)	(-6.7947, -6.7947)	0.64
II	(0.02, 0.04)	(0.4, -0.4)	(-9.9571, -6.7947)	0.64
III	(0.04, 0.02)	(0.6, 0.3)	(-6.1263, -10.3071)	0.09
IV	(0.04, 0.02)	(0.4, 0.3)	(-6.7947, -10.3071)	0.01

which excludes the square nonlinearity term and has the nonlinearity $O(\phi^{3/2})$ produced exclusively by the trapped particles. Here $Z_r(x) = -2e^{-x^2}\int_0^x dt \exp(t^2)$ is the real part of the plasma dispersion function and $b(\beta, v_0) = \frac{1}{\sqrt{\pi}}(1 - \beta - v_0^2)e^{-v_0^2/2}$. The potential $\phi(x)$ is also required to satisfy the Poisson equation,

$$\frac{\partial^2 \phi}{\partial x^2} = \int [f_{\text{EH}}(x, v) - f_i(x, v)]dv, \tag{4.4}$$

with $f_i(x, v)$ uniform. The parameter k_0 relates to rest of the parameters in Eq. (4.1) via a Nonlinear Dispersion Relation (NDR) [4]. However, for the pure soliton solutions $k_0^2 = 0$, such that the other variables relate to each other via the NDR independent of k_0 and the NDR takes the form,

$$-\frac{1}{2}Z_r'(v_0/\sqrt{2}) \approx \frac{16}{15}b(\beta, v_0)\sqrt{\psi}, \tag{4.5}$$

prescribing the analytic solitary form of the $\phi_a(x)$ as,

$$\phi_a(x) = \psi \, \text{sech}^4\left[\sqrt{\left(\frac{b(\beta, v_0)}{15}\sqrt{\psi}\right)}x\right]. \tag{4.6}$$

While $v_e = 0$ for stationary distribution for all the above cases examined, the values of ψ, β and v_0 for the soliton pairs in them are provided in Table 4.1.

4.2.3 The pseudo-potential for electron acoustic SEH solutions

The Sagdeev pseudo potential $\mathcal{V}(\Phi)$ associated with the Poisson equation (4.4) in the electron acoustic regime can additionally be defined describing the soliton spatial potential structures as the motion along the separatrix of the pseudo-potential
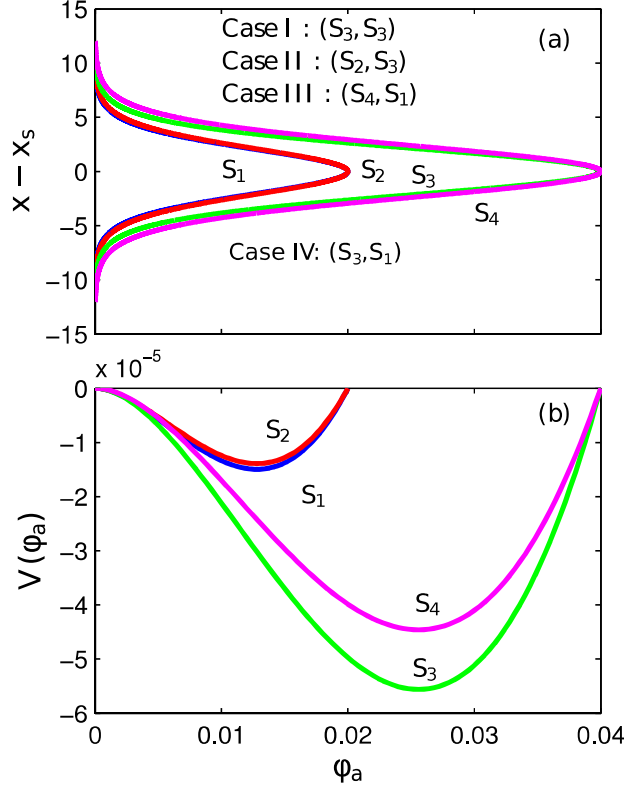
Figure 4.1: (a) Analytic solitary potential solutions $\phi_a(x)$ located at $x = x_s$ and (b) associated Sagdeev potential $\mathcal{V}(\Phi)$ corresponding to the initial phase-space structures implemented in the cases I, II, III and IV of the present simulations. Evolution of a pair of two solitons, selected from the initial profiles S_1, S_2, S_3 and S_4 plotted in (a), is simulated in each of the four cases. The pair of soliton profiles chosen in each case is listed in (a).

$\mathcal{V}(\Phi)$ in the regime of electron acoustic perturbations (treating ions to be infinitely massive)

$$ -\mathcal{V}(\Phi_a) = \frac{8}{15} b(\beta, v_0) \Phi_a^2 (\sqrt{\psi} - \sqrt{\Phi_a}). \tag{4.7} $$

The potential $\mathcal{V}(\Phi_a)$ and the associated spatial profile of the soliton electrostatic potential $\phi_a(x)$, located at $x = x_s$, are plotted in Figs. 4.1(b) and (a), respectively. The four profiles marked as S_1, S_2, S_3 and S_4 for the SEH solutions are used as initial conditions in the present simulations corresponding to the parameters provided in Table 4.1.

4.3 Vlasov simulations of interacting SEH structures

In the regime applicable to Eqs. (4.1)-(4.6) the time evolution of initial EH distribution (4.1) is investigated by solution of Eqs. (4.2) and (4.4) on a 1536×512 dual x-v mesh for case (I-III) and 2048×1024 dual x-v mesh for case (IV), using the generalized flux balance method, discussed in Chapter 2, for both electron and ion phase space [8, 27] of a hydrogen plasma ($m_i/m_e = 1836$) with $T_e/T_i = 20$. In Figs. 4.2(a), (c), (e) and (g), the profiles of analytic distribution $f_{\mathrm{EH}}(x,v)$ used as initial condition, are plotted for the cases I-IV, respectively. These profiles are featuring two initial solitons at $x = 8$ and 40 in cases I and II, $x = 10$ and 40 in case III and $x = 16$ and $x = 48$ in case IV (in order to prevent the wider first soliton in case III and case IV from interfering with the boundary).

4.3.1 Recovery of stably propagating SEH structures

As the very first and important observation, the analytic form of electron distribution (4.1) chosen as initial conditions for the simulations shows a propagation without much distortion or radiation unless perturbed by other structures, validating the *a-priori* adoption of them as most suitable initial conditions. Although the evolved stable SEH in the simulations have additional attributes when compared to rather approximate analytic solutions given by (4.6), they show only reasonable deviations from the analytic structure (largely related to numerical aspects), not detrimental to their analytically predicted stability under the adopted SEH formulation [1]. The physics of this *a-posteriori* validated stability is discussed in more detail in Chapter 6 where the aspects related to EH stability are addressed by means of simulations.

4.3.2 Electron distribution during SEH interaction

The time evolved versions of the electron distribution function at instantaneous hole locations are also presented in Fig. 4.2 where a distribution profile, nearly unperturbed by the introduced hole, as extracted from location $x = 0$ is plotted for the reference (dashed line) in the periodic simulation zones with $0 < x < L = 48$ for cases I-III and with $0 < x < L = 64$ for case-IV. While the ion velocity

distribution f_i is largely unaffected, the time evolved f_e for the cases I, II, and III are plotted at the time and location t_c and x_c, of passage through each other of these propagating holes, in Figs. 4.2(b), (d) and (f), respectively. In Fig. 4.2(h) the time evolved f_e in case-IV is plotted at time $t = t_c^{(3)}$, i.e., during the time when two holes pass through each other for the 3$^{\text{rd}}$ time. After which these two holes merge into one (where the superscripts of t_c and x_c, wherever displayed, correspond to index of consecutive crossings of the holes through each other in the periodic setup). Note that while cases I and II have counter-propagating holes, both the holes propagate in same direction in the cases III and IV. Initial relative velocity, Δv_0, between two holes is 0.8 in cases I and II, 0.3 in case-III and 0.1 in case-IV. The initially trailing faster soliton in case III and IV therefore takes a longer time, $t_c \sim 15.28\omega_{pe}^{-1}$ and $\sim 47.5\omega_{pe}^{-1}$ respectively, to approach the leading slower soliton and overtake it, showing lower collision frequency between structures than that in I and II.

As observed from Figs. 4.2(e) and (f), although the holes in case-III have a noticeable overlap in the intervals of velocity space they initially occupy, they shift suitably away from each other, avoiding this usual overlap, temporarily during their passage through each other. But in case IV, where the velocity difference between two propagating holes is smaller than $\sqrt{2\psi}$, the stronger hole causes the weaker hole to partially decay each times they pass through each other. Finally, after about their third interaction, or at $t = t_c^{(3)}$, the smaller one almost merges with the larger one to form a single solitary structure, as observed in Figs. 4.2(g) and (h).

4.3.3   Multiple interactions of propagating SEH

The density profiles for $t > 0$ are also plotted in Figs. 4.3(a), (c), (e) and (g) showing propagation of these solitons and their first collision or overtake for all the four cases (seen in fifth profile from the bottom in cases I, II and IV, and seventh profile from the bottom in case III). In Fig. 4.3(g) the tenth profile ($t = 105.99$) is showing the smaller soliton loosing its strength after first collision as compare to the first profile at ($t = 0$). A long time evolution of density profile is shown using color scale in Figs. 4.3(b), (d), (f) and (h) for case I-IV showing multiple passage of the original solitons through each other. The time between interaction of holes for smaller relative velocity is much longer which is evident from the observation,
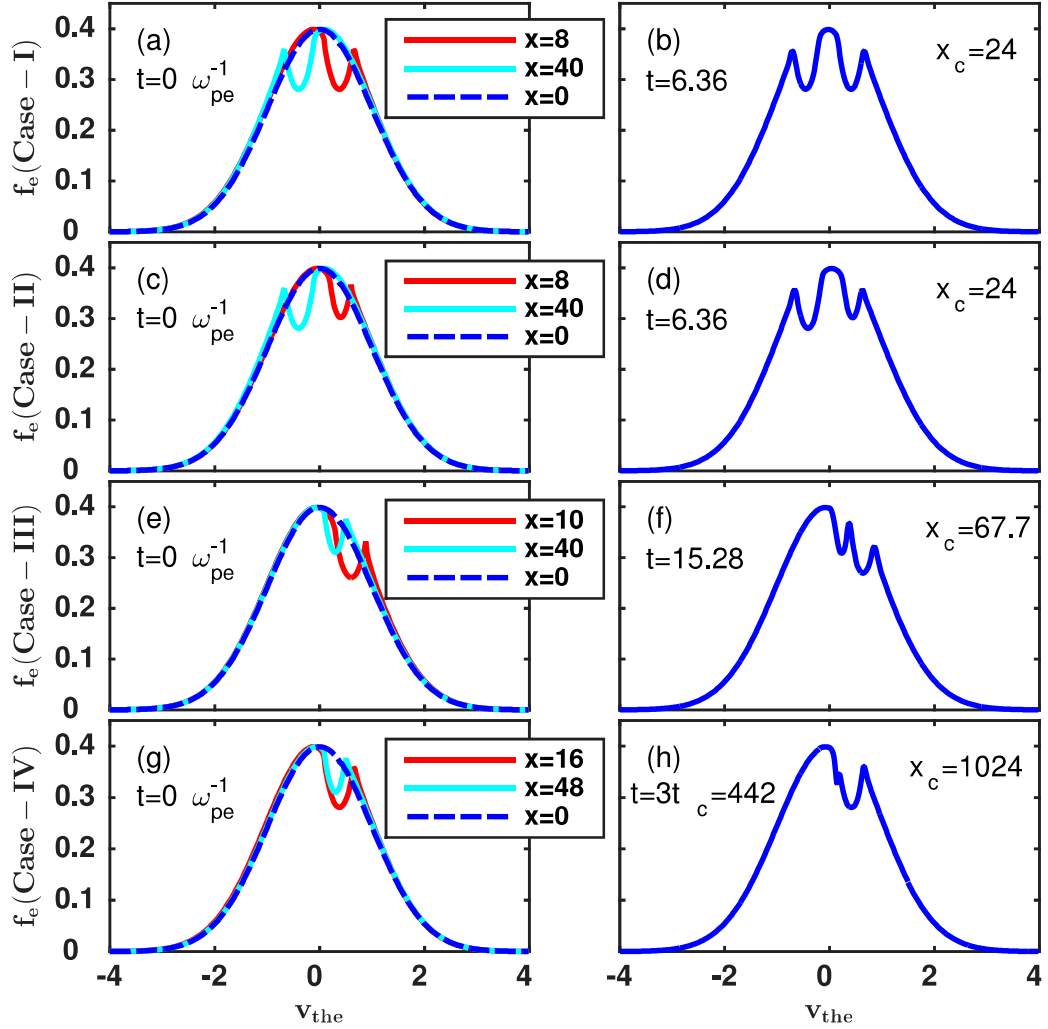
Figure 4.2: Profiles of initial electron distribution $f_{\mathrm{EH}}(x, v)$ plotted at the locations of the first and second holes (solid lines with separate shades), and at an unperturbed location $x = 0$ (dashed line), for the cases (a) I, (c) II, (e) III and (g) IV. Profiles of f_e at t_c and x_c, time and location of passage through each other of two holes, for the cases (b) I, (d) II and (f) III. In (h) f_e for case IV is plotted at the time when the two propagating holes pass through each other 3rd times.

for example, in case III and IV where the faster soliton, chasing the smaller one, passes more than once through its initial location ($x = 10$ in case III and $x = 16$ in case IV) before crossing the slower one. This coherent propagation of the initial structures in the system is visible in Figs. 4.3(b), (d), (f) and (h) where a much longer time sequence of the spatial density distribution is plotted using color scale
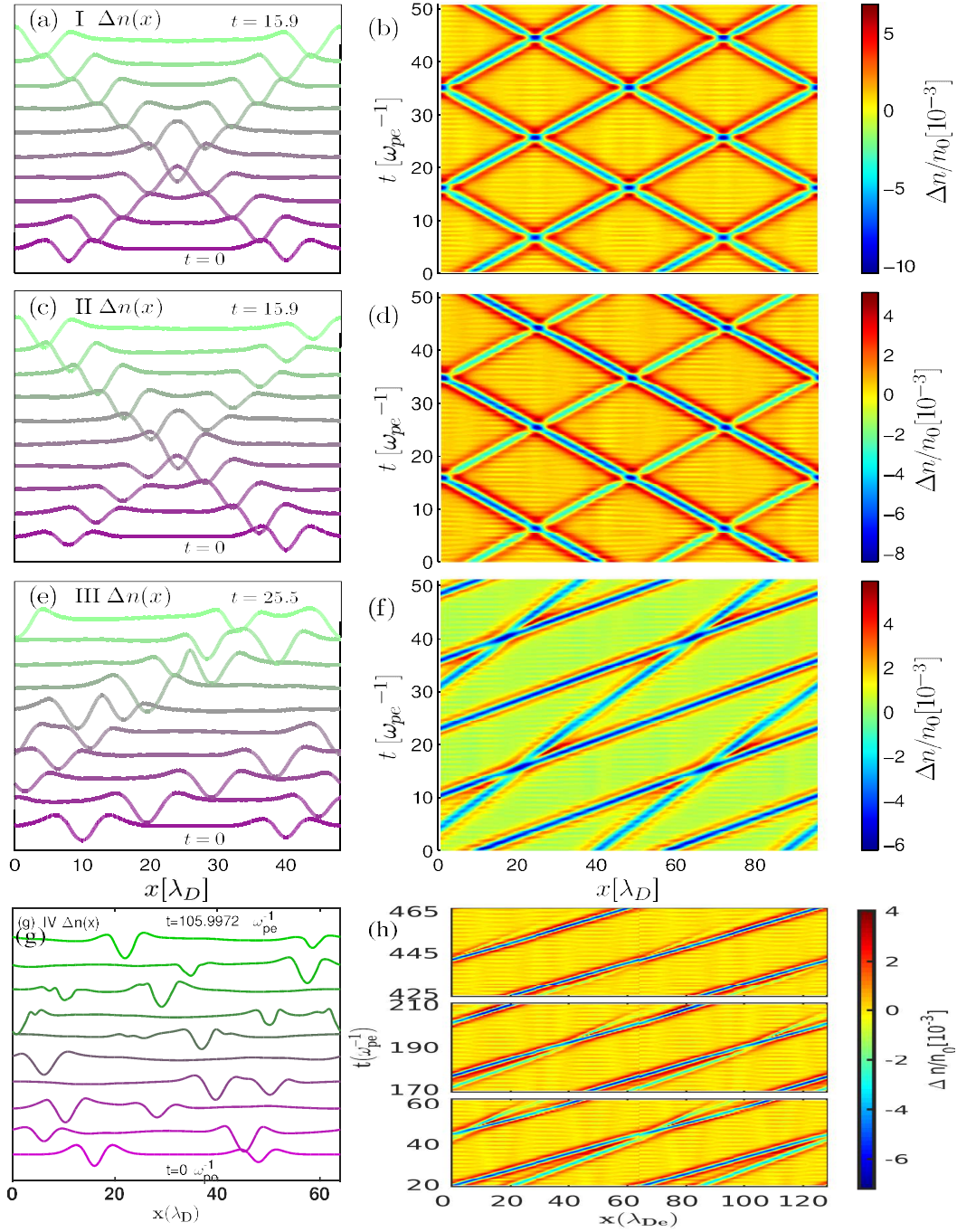
Figure 4.3: Time evolution of the density difference profiles in cases I-IV at (left) short and (right) long times (values on color scale). Subplots in (h) present time evolution of density in case-IV during the 1st ($t_{c1} = 47$), 2nd ($t_{c2} = 194$) and 3rd ($t_{c3} = 442$) times of passage of two holes through each other.

for the density in cases I-IV, respectively. Since the collisions in cases I-IV take place at the boundary, the original data is repeated in these figures in the region $48 < x < 96$ in cases I-III and $68 < x < 136$ in case IV, for clarity. In Fig. 4.3(h) there are three subplots showing the time evolution during their first ($t = 20$ to 60), second ($t = 170$ to 210) and third ($t = 426$ to 465) overtake. In each event of overtaking, the slower soliton partially decays and loses a part of its total strength. The deformation starts from its separatrix region of the structure. Finally after third collision ($t_c^{(3)} = 442$) it merges almost completely with the stronger/faster one. While in cases I-III the two solitary electron holes survive their multiple collisions.

4.3.4 Phase shift introduction during SEH interaction

Effects of nonlinearity and amplitude mismatch are visible in case II (III and IV) where the smaller soliton accelerates (slows down) by an amount more than the taller does during the interaction. For the interactions in cases III and IV where the time of interaction are longer, the smaller soliton is seen to re-emerge from the interaction region in a time slightly longer than what is estimated using its velocity of propagation during the non-interacting phase. Such a time delay is observable, for example, from the space-time trajectory of the smaller soliton in Figs. 4.3 (f) and (h) that shows a slight bend while entering and leaving the interaction process during each of the interactions. This time delay corresponds to a phase-shift incurred by the solitons during their interaction. This delay is also noted to be smaller for the larger soliton during an interaction between two unequal solitons. This dependence shows the asymmetry of the process with respect to strength of the interacting solitons and also indicates that an equal phase-shift will be produced in the case of two identical solitons interacting, as observed in case I. This can however be noted that given a larger relative velocity between solitons in cases I and II, the time of interaction remains considerably smaller in cases I and II, resulting in a relatively smaller phase-shift for them in comparison to cases III and IV.

4.3.5 Phase-space evolution of interacting SEH and entropy production

The time evolution of the electron velocity distribution in the phase-space for cases I-IV is presented in Fig. 4.4 covering the time and the region of phase-space around the nonlinearly interacting electron holes. In the cases I-IV the profiles in the third column from left correspond to time t_c of the solitons passage through each other. While in the cases I and II the phase space holes appear largely disjoint, the adiabatic mechanism [111, 112], preserving their identity becomes clear from case III where $\psi \sim \Delta v_0^2$ and their trapped particle distributions overlap on the velocity axis. Moreover, the trapped populations in case III are collectively pushed away from each other on the velocity scale during the interaction process. In a qualitative sequence, the particles trapped in the slower moving soliton, when approached from behind by a larger net potential dip, lose their kinetic energy, while those trapped in faster moving solitons see a net potential dip ahead and get accelerated, only to return to their original velocities following the interaction. Mutually opposite shifts along the velocity axis is thus noted in the interacting co-moving solitons in each case at t_c. This elegant symmetry of the process is seen preserved irrespective of the amplitude and speed of the interacting solitons as the comoving solitons additionally satisfy $\psi \sim \Delta v_0^2$ for an overlap in trapping region on the v axis.

A very distinct phase-space evolution, as compared to cases-I to III, is however observed in the case-IV. In case-IV where $\Delta v_0^2 < \psi$, the adiabaticity of their interaction mechanism does not remain intact and an irreversible deformation of the structure starts from the separatrix region with each event of interaction. The separatrix region of the smaller soliton shows strong distortion and a partial merger with the separatrix of bigger one during the period of interaction. Many particles originally trapped in smaller soliton are seen to irreversibly join the trapped population of the stronger soliton. As a result, the smaller soliton periodically undergoes a larger readjustment in its parameter, including the propagation velocity and amplitude. It therefore gradually losses its strength and finally merges completely with the bigger one. A net modification in the stronger soliton is also observed. Initially, they both move with different velocities given by the NDR 4.5, this initial relative velocity Δv_0, however, decreases during each interaction. Note
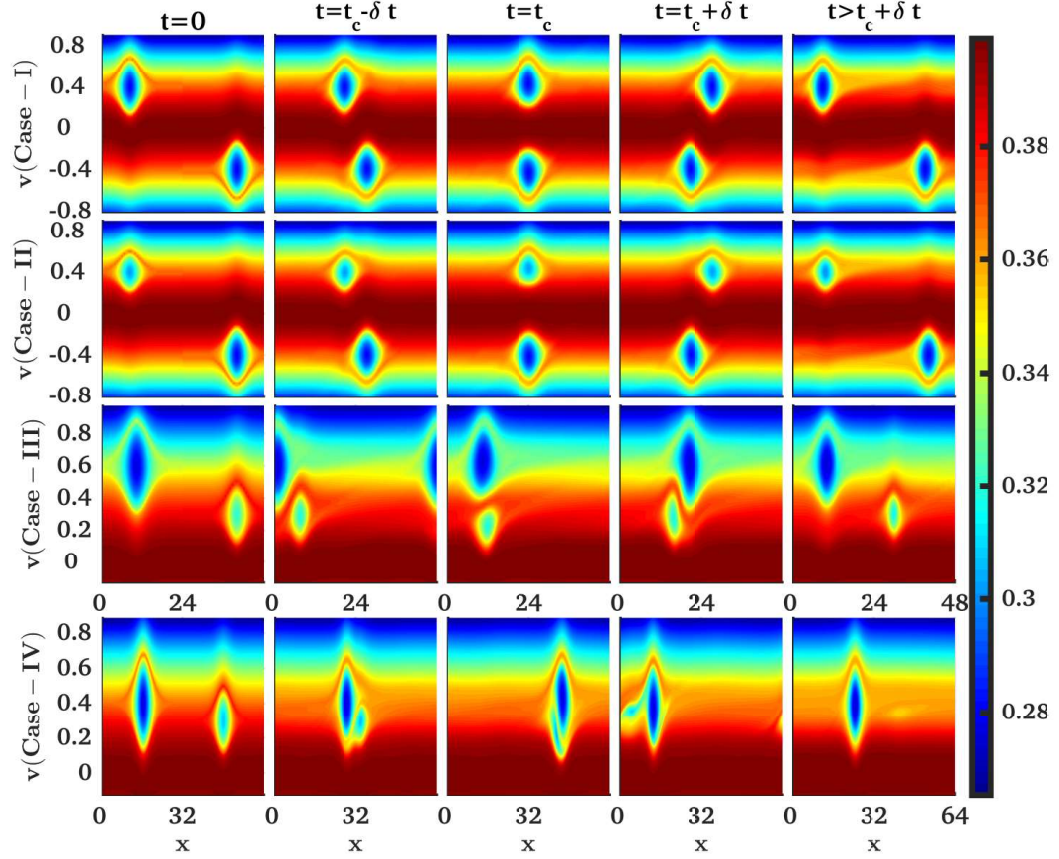
Figure 4.4: Time evolution of the electron holes in the electron phase-space for all the four cases, including $t = 0$, $t = t_c - \delta t$, $t = t_c$, $t = t_c + \delta t$ and $t > t_c + \delta t$, where δt is the small intervals about $t = t_c$. In case-IV the last subplot at $t > t_c + \delta t$ is plotted after crossing the holes through each other three times.

that because of this change in relative velocity, the time difference between two successive collision increases from $(t_c^{(2)} - t_c^{(1)} = 147)$ to $(t_c^{(3)} - t_c^{(2)} = 248)$, which is clearly noticeable in Fig. 4.3(h) also.

The above phase-space evolution Fig. 4.4 illustrates that the formation of fine structures in the phase-space during the interaction is responsible to production of entropy in numerical evolution and its analogous in associated experimental conditions. The present simulations show that the structures well separated by a relative velocity along the velocity dimension (e.g., cases-I-III $\Delta v_0^2 > \psi$) have only an adiabatic modification in the trapped particle distribution, not resulting in fine structures in the phase space. The cases of structures separated by smaller

relative velocity (e.g., case-IV $\Delta v_0^2 < \psi$), on the other hand, show generation of substructures (unresolved by coarser resolutions) in the trapped particle populations because of longer time of the interaction. Sharper phase-space gradients existing over longer duration results in larger diffusion in the phase-space, indicating a larger rate of entropy production.

4.4   Characterization of trapped particle nonlinearity

The simulated solitons in their initial arrangement are in well separated and noninteracting state. A near recurrence of this initial soliton arrangement can be noted in each case due to the periodicity used at the system boundaries. This recurrence allows one to readily determine the preservation of the soliton attributes by comparing the time evolved soliton structures at the time of recurrence, t_r, with their initial forms at $t = 0$. Such a comparison is done and displayed in Fig 4.5. The comparison between potential profiles where the high frequency EPW oscillations are exclusively seen, additionally allows us to carry out a Fourier decomposition based analysis to identify and characterize the kinetic nonlinearity underlying these small amplitude solitary structures and isolating them from a coexisting set of high frequency, nearly decoupled, linear modes that follow superposition principle.

4.4.1   Coexisting linear and kinetically-coupled nonlinear modes

The spatial profiles of the density, obtained from the initial distribution $f_{\mathrm{EH}}(x, v)$ integrated with respect to the velocity, correspond to the profiles marked with $t = 0$ plotted in Figs.4.5(a), (c) and (e), featuring two holes at $x = 8$ and 40 in the cases I, II and $x = 10$ and 40 in the case III. The density profiles evolved past the time of their interaction and at the time t_r where they nearly exhibit a recurrence of their initial arrangement are also shown for all these cases. While these time evolved forms of the electron density profiles are readily comparable with their initial forms, a similar comparison of the evolved states of the analytic initial solitary electrostatic potential is complicated due to an additional potential variation present as a result of the approximations entering in the analytic

density and potential expression used for generating the initial conditions for the simulations.
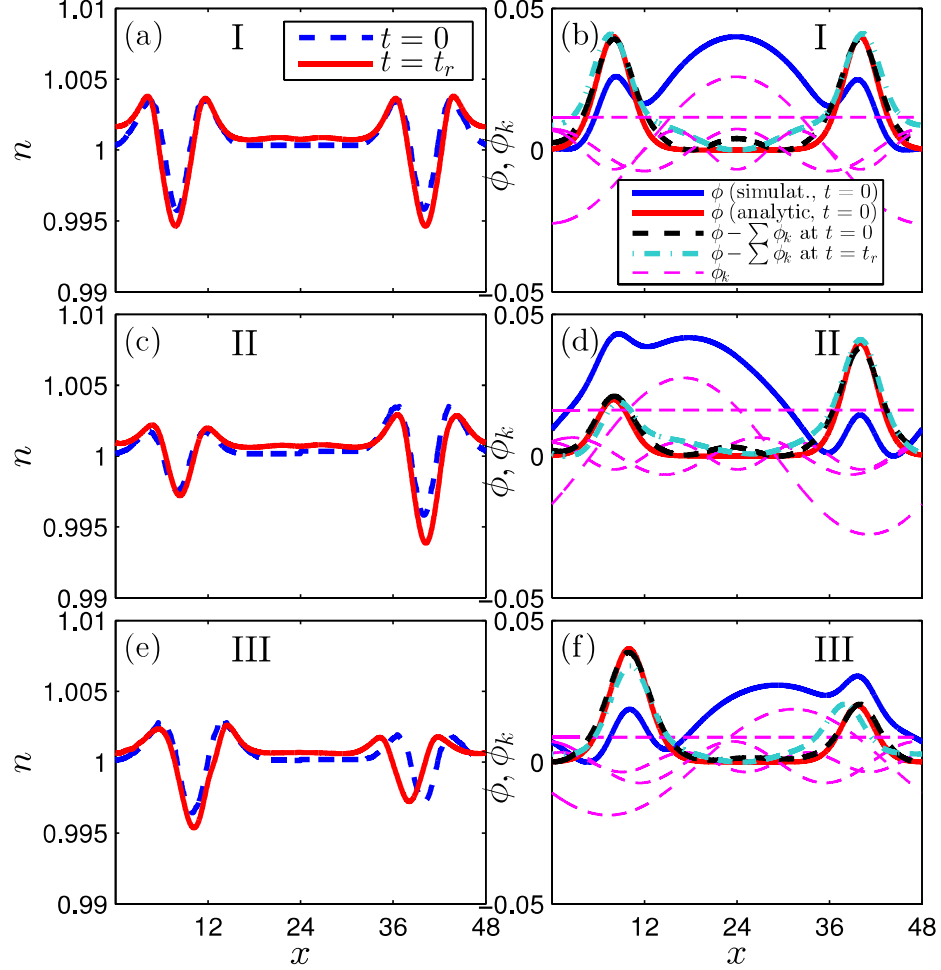
Figure 4.5: Profiles of the computed plasma density at $t = 0$ (solid red line) and at $t = t_r$ (dashed line) plotted in frames (a), (c) and (e), for the cases I, II and III, respectively. Profiles of the computed potential ϕ at $t = 0$ (thick solid blue line) in frames (b), (d) and (f) for the cases I, II and III, respectively. The Fourier modes of the plasma oscillations (thin dotted lines), the evolved potential profiles after eliminating the oscillating Fourier modes at $t = 0$ (thick dotted black line) and $t = t_r$ (thick dot-dashed green line) are also shown in (b), (d) and (f) for the cases I, II and III, respectively.

The profiles of electrostatic potential computed at initial time $t = 0$ and at the time of recurrence $t = t_r$ are plotted for cases I, II and III in Figs. 4.5(b),

(d) and (f), respectively. Use of exact velocity integration of f_{EH} to obtain initial potential in the simulations, in combination with approximate forms of certain analytic expressions from (4.3)-(4.6), seeds additional fast electron plasma oscillations in the set up at $t = 0$. While these oscillations have a passive presence and only cause appearance of a finer texture with frequency $\sim \omega_{pe}$ in the density evolution presented in Figs. 4.3(b), (d) and (f), their visibility is rather pronounced in the potential profiles. As visible from Figs. 4.5(b), (d) and (f), the potential ϕ computed at $t = 0$ in the simulations (plotted using thick solid blue line) by using the Poisson equation has an additional potential modulations superimposed on the analytic potential ϕ_a given by the expression (4.6) (plotted using thick solid red line). The simultaneous evolution of this additional potential modulation in time makes it difficult to easily follow the evolution of the solitary structures and requires additional efforts for separating the two from this modulation described as follows.

4.4.2 Separation and spectral reconstruction of linear mode evolution

When decomposed in its Fourier modes, ϕ_k, the additional potential modulation superimposed on soliton potential structure in the computed potential shows a simpler composition that includes a dominant $m = kL/2\pi = 1$ mode and a series of small amplitude higher m modes,

$$\phi - \phi_a = \sum_m \phi_m = \sum_m a_m \varphi_m \tag{4.8}$$

where φ_m are the elements of the orthogonal Fourier basis and a_m are the corresponding Fourier coefficients. The first four of these linear Fourier modes, $m = 0, 1, 2$ and 3, at $t = 0$ are plotted (using dotted lines) in Figs. 4.5(b), (d) and (f) for cases I, II and III, respectively. As can be noted from the three cases, the initial arrangement of these plasma modes at $t = 0$ is mainly determined by the locations of larger amplitude solitons, since the strongest $m = 1$ mode always has its minimum around the location of the larger soliton showing maximum correlation with it. For example, in case I, where there are two identical large solitons, the minimum of $m = 1$ is generated equally close to the two solitons, whereas, in the rest two cases where the other soliton is smaller in amplitude the minimum
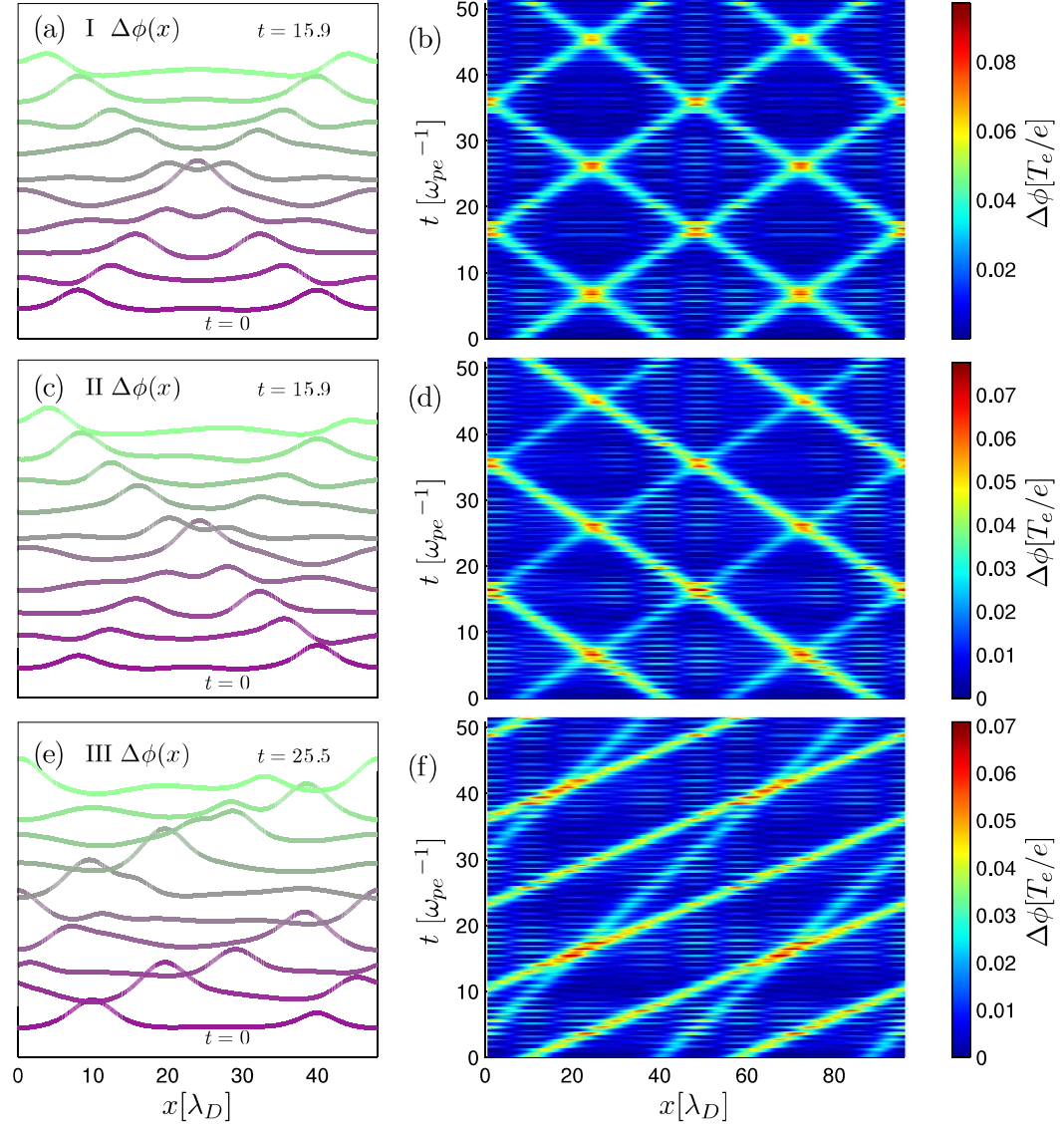
Figure 4.6: Time evolution of the potential profiles in cases I-III at (left) short and (right) long times (values on color scale).

of $m = 1$ mode is nearly at the location of the larger soliton, indicating that the soliton having smaller amplitude has relatively smaller contribution to this additional mode structure by being in better agreement with the analytic expression for potential.

Considering the smallness of the amplitudes of these additional Fourier modes of the potential (either comparable or below the already small amplitudes of soli-

tons), evolution of these modes can be treated as multiple linear plasma oscillations at frequency ω_p. Assuming that at this small amplitude they do not nonlinearly couple, either with each other or with small amplitude solitons, allows their oscillatory time evolution to be analytically eliminated from the entire time evolution of the potential profile to obtain a clearer soliton evolution. Accordingly, the compensated potential $\phi - \sum_m \phi_m$, featuring only solitons, can be obtained at all times from Eq. (4.8) by subtraction of the summation in the right hand side from the computed potential ϕ which includes this additional contribution from the oscillation. Result of this elimination at $t = 0$ and $t = t_r$ is presented in the Figs. 4.5(b), (d) and (f) using dashed line and dotted-dashed line which correspond to the potential profile with such compensation at $t = 0$ and $t = t_r$, respectively. These compensated profiles showing presence of only two propagating soliton structures indicate that the superposed fast modulations are indeed well modeled by the systematic mutually noninteracting linear plasma oscillations which also do not interact strongly enough with the solitons of nearly same amplitude. Since the equally small amplitude solitons propagate coherently without oscillations at velocity much smaller than the phase velocity of the electron plasma wave, their constituent modes are clearly coupled via the alternate means provided by the strong trapping of a large density of resonant particles within these localized structures.

The detailed time evolution of the compensated electrostatic potential, $\phi(x,t) - \sum_m \phi_m(x,t)$, plotted in Fig. 4.6 features, in addition to featuring the soliton solutions (4.6), the standing electron plasma modes with $k \sim m2\pi/L$ (e.g., profile marked with $t = 0$ in Fig. 4.6(a)). In the short range evolution presented in Figs. 4.6(a), (c) and (e), the solitons show a robust presence despite their interaction with this wave activity and frequent passage through the other soliton. The contribution from small amplitude large m modes also shows weak signs of temporal dependence of frequency and wavelength on the slowly time varying soliton separation Δx. The possible origin of this dependence is in the relatively large amplitudes of the solitons as compared to waves. The barrier produced by solitons generates reflected and transmitted parts of the faster Fourier modes (usually neglected in the linear regime). The temporal variation in the wave parameters results from the changing separation between solitons and leaves the residual noise in the Fourier reconstructed form of the solitons at larger times. Also presented

in Figs. 4.6(b), (d) and (f), is the long time potential evolution showing multiple crossings of the solitons, using the compensated potential profiles obtained by eliminating the small m oscillations from the simulated potential ϕ, for cases I-III, respectively.

4.5 Comparison to interacting SEH in laboratory and space plasmas

We finally discuss and present some of very long standing and rather recent experimental observations directly relevant to the simulation results presented in this chapter. While the observations of two holes attracting each other like particles of negative mass are long identified as mutually merging phase-space structures in laboratory plasmas, a strong evidence of two holes interacting via an identity preserving interaction in space (or magnetospheric) plasma might have been only very recent. The profiles from our simulations highlight the characteristics of such identity preserving interaction in magnetospheric data which has been largely understood since their recent observations, in the form of a tripolar pulse of electric field, measured by a cluster of spacecrafts. We have summarized these two categories of experiment and their relevance to our data in the following subsections.

4.5.1 Interacting SEH in Q-machines and magnetic mirrors

A number of observation exist where the interaction of holes and their subsequent merger is observed and interpreted in term of a negative-mass like instability of the attracting phase-space holes. In the single ended Q machine experiments by Saeki et $al.$ [13] two holes close to each other and having almost equal velocity were excited from an electric pulse. These holes merge or coalesce in a collision process described by Saeki et $al.$ as inelastic. Among similar observations, Berk et $al.$ [39, 81] in a mirror experiment performed in DCX-1 reported development of stable proton clusters as a result of the negative mass instability. The time of coalescence of the electrostatic signals from DCX-1 was found to be explainable by phase-space evolution of two coalescing electrons holes under a simplistic $water$ bag $model$ indicating that the electrostatic signals do correspond to coalescing trapped-

electron structures.

4.5.2   Interacting SEH in magnetospheric plasmas

Recently the electric field data from the Wideband Plasma Wave Receiver located on each of four Cluster spacecraft, as reported by Pickett *et al.* [18, 19], showed existence and interaction-like activity of the SEH in the magnetospheric plasma including certain poorly understood features routinely observed in our data [9]. We present the potential and electric field profiles in Fig. 4.7 from various cases at selected stages of evolution showing that while the non-interacting solitons correspond to a bipolar electric field variation as seen in Figs 4.7(a) and (b) for case III, the pairs of dissimilar solitary electron holes in cases II and III produce, during the initial phase of their passage through each other, a tripolar (two smaller positive pulses separated by a large negative pulse) electric field pulse, as seen in Figs. 4.7(c)-(d) from case-II and (e)-(f) from case-III, respectively. Additionally, an inverted tripolar electric field pulse (i.e., two small negative pulse separated by a larger positive pulse) reported in many observations by Pickett *et al.* [18, 19] is recovered in the events when the solitary phase space holes separate after completing their nonlinear interaction, as plotted in Figs. 4.7(g)-(h) for case-III. Within the
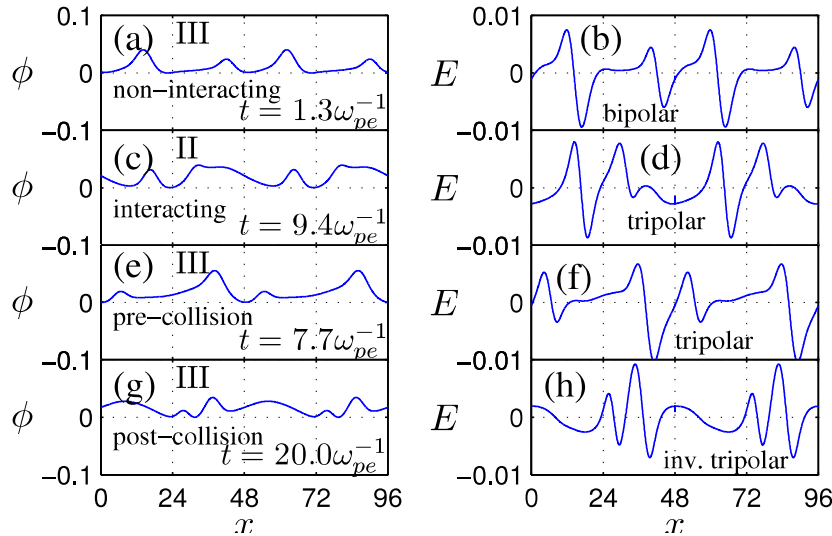
Figure 4.7: (left) Potential and (right) electric field, $E = -\partial\phi/\partial x$, profiles for indicated, cases, times and phases of SEH interaction.

band resolved by the spacecraft data the reported ratio of bipolar to tripolar pulse length (760 μs to 2 ms, [20]) is in reasonable agreement with the spatial tripolar pulse width $\sim$ 2-3 times the bipolar pulse width in the present simulations. The ratio of frequency of detection of these two events of about an order, e.g., 2199:248 from 17:00-17:40 hrs on February 10, 2002 or 872:80 from 08:31-08:57 hrs on May 26, 2002 [20], indicates the expected skewed probability of detecting them in random sampling of a large collection of interacting solitary structures studied as above. For a localized or inhomogeneous source, say at upstream locations in the magnetosphere, the majority of interactions sampled would be of case-III type where the frequency of the observed tripolar pulses is expected to be even lower.

4.6   Summary and conclusions

The phase-space vortex structures, or SEH, seen in chapter 3 to be generated from unstable plasma modes that grow in amplitude, trap particles, and subsequently enter a trapped particle governed nonlinear limit, motivated studies in this chapter. The stable propagating analytic solutions of a long existing formulation of such structures are used in this chapter as a means of studying the interaction between the SEH structure in a distinct regime of relatively faster, electron acoustic modes, where the ion participation in SEH dynamics remains negligible. The theoretical results, neglecting ion mobility, are treated as initial conditions for the simulations that fully account for evolution of both electron and ion kinetic distributions. It is understood that in the absence of external driving, the structures tend to develop isolated, near equilibrium, trapped particle distributions and therefore are well described by the SEH formulations based on this approach. The present simulations suggest that such model for the trapped particle distributions remains largely valid for the laboratory and natural plasmas, including those in magnetospheric plasmas that could be well described by the present simulations.

The motivation that the stable analytic SEH solutions must propagate as natural nonlinear excitations of the collisionless plasma is validated based on the understanding that the numerical simulation indeed evolve a near thermodynamically equilibrated population of the particles trapped in the coherent structures. This population produces a strong trapped particle nonlinearity arising from its sensitivity to wave/structure amplitude, bringing, in turn, an amplitude depen-

dence in its dispersion, characteristic of nonlinear waves and coherent structures. The main conclusions in this relation from the present chapter are as following.

The analytic form of electron distribution implemented as initial conditions for the SEH simulations shows propagation without much distortion or radiation unless perturbed by other structures, validating the *a-priori* adoption of them as most suitable initial conditions. Although the evolved stable SEH in the simulations have additional attributes when compared to rather approximate analytic solutions given by (4.6), they show only reasonable deviations from the analytic structure (largely related to numerical aspects), not detrimental to their stability predicted under the adopted analytic SEH formulation [36].

The formation of fine structures in the phase-space during the interaction is responsible to production of entropy in numerical as well as is associated experimental condition. The present simulations show that the structures well separated by a relative velocity along the velocity dimension ($\Delta v_0^2 > \psi$) have only an adiabatic modification in the trapped particle distribution, not resulting in fine structures in the phase space. The cases of structures separated by smaller relative velocity ($\Delta v_0^2 < \psi$), on the other hand, show generation of substructures in the trapped particle populations because of longer time of the interaction. Sharper phase-space gradients existing over longer duration results in larger diffusion in the phase-space, indicating a larger rate of entropy production.

A comparison between the initial and time evolved states of SEH is possible because of a near recurrence of the former in our periodic system. This comparison between potential profiles showing high frequency EPW oscillations additionally allows us to carry out a Fourier decomposition based analysis to identify and characterize the kinetic nonlinearity underlying the small amplitude solitary structures and isolating them from a coexisting set of high frequency, nearly decoupled, linear modes that follow superposition principle. A successful elimination, using the Fourier reconstruction, of the high frequency linear modes from the solitary wave data, indicates that the superposed fast modulations are indeed well modeled by the systematic mutually noninteracting linear plasma oscillations which also do not interact strongly enough with the solitons of nearly same amplitude. Since the equally small amplitude solitons propagate coherently without oscillations at velocity much smaller than the phase velocity of the electron plasma wave, their constituent modes are clearly coupled via the alternate means provided by

the strong trapping of a large density of resonant particles within these localized structures.

The reasonable agreement of electron hole observations in nature and laboratory experiments with both kinds of interactions, where the structures interaction produces minimum modification to individual solitons and where the solitons are fast modified and merge, is noted in respective regimes. These comparisons must allow quantitative determination of thermodynamic regimes of the finite amplitude plasma structures, or the plasma turbulence at large, in specific cases of interest in advanced studies of plasma waves, instabilities and turbulence. In two sets of the relevant comparisons we have shown in the first set: that in the cases of the first kind of interaction (identity preserving), the electric field profiles from selected stages of evolution show the non-interacting solitons correspond to a bipolar electric field, while the pairs of dissimilar solitary electron holes produce, during the initial phase of their passage through each other, a tripolar (two smaller positive pulses separated by a large negative pulse) electric field pulse. In the second set of comparison with various existing observations in laboratory plasmas it is highlighted that, as seen in second kind of interaction (non-identity preserving) at small relative velocity between two coherent structures two holes attract each other like particles of negative mass and coalesce, for example, in Q machine experiment by Saeki *et al.* [13]. In another example, the stable proton cluster developed from the negative mass instability, experimentally observed in Oak Ridge DCX-1 mirror machine, were compared to two-stream instability simulated by Berk *et al.* [39, 81] showing the similar merger using a simplistic *water bag model*.

5

Evolving trapped particle structures with implications on plasma stability

5.1 Introduction

The investigations in this chapter are motivated by the strong presence of undamped coherent structures in finite amplitude collective activity in plasmas, routinely detected such as in space, laboratory and fusion plasmas where coherence is identified by its robustness and stationarity. In this study such coherence arising from underlying kinetic characteristics of warm plasmas, witnessed in preceding chapters, leads us to further exploration of possible alternate regimes of instability of an ideal, nondissipative plasma. The concept of essentially linear nature of evolution at small amplitude governs the approach to plasma stability, thereby only linear modes that follow the superposition principle, are recovered and understood to grow by sources of free energy. The linear thresholds are therefore tied to the conventional discrete plasma modes, and, in turn, do not cover the stability of small amplitude nonlinear modes that might follow more general or independent growth mechanism in such, otherwise, subcritical or linearly stable regimes. The presence of equally small amplitude nonlinear structures, validated by both the kinetic simulations and analytics, therefore highlights an alternate mechanism for the turbulence to operate in the collsionless plasmas. It is thus essential to explore the evolution of such small amplitude nonlinear structures in the linearly subcrit-

ical regime and investigate their characteristics with respect to the well explored linear eigenmodes of the collisionless plasma.

In order to achieve the above objective, we consider a current-driven, 1D, collisionless plasma as a paradigm of driven intermittent plasma turbulence and anomalous transport with the focus on *undamped coherent* electrostatic structures. The study explores the concept of plasma instability in terms of more general fundamentally nonlinear structures, outside the conventional linear regime which is limited to covering largely the collisional plasma eigenmodes, additionally subjected, by use of Vlasov equation, to interaction with resonant particles. Simulations are once again employed to explore evolution of more relevant forms of perturbations in the species phase-space producing undamped collective structures. In the analysis of simulation output, however, a wave description is employed which in its fundamental form is maintained through all stages of sophistication, allowing also a direct comparison with the already vast literature on the underlying trapped particle modes.

Although a wealth of literature is available dealing with the topic of current-driven plasma and the ion-acoustic instability, only a few examples are mentioned here and attempt is made to cite and discuss many of them later, during the analysis. The growth of these nonlinear equilibria, possible in a subcritical plasma, was addressed analytically in the past by Dupree [5] who concluded that amplitude of these structures must grow due to scattering of particles for propagation velocities in the range where ion and electron distribution function have opposite signs of velocity derivatives. Simulations by Berk *et al.* [21] recovered spontaneous hole - clump pair creation close to the linear threshold for instability. Lesur *et al.* [22, 23] in their numerical simulations of these structures also recovered growth in subcritical regime resulting from exchange of momentum with other species or with the wave pseudo-momentum. Similarly, the growth of ion phase-space structures were recovered, by Petkaki et al. [87] in a Vlasov simulation, generating anomalous resistivity that exceeds the quasilinear estimates driving the reconnection. Another mechanism of subcritical hole excitation was recently proposed by Lesur *et al.* [88], augmenting the Berk-Breizman model [89], namely, by wave coupling with a linearly unstable (supercritical) mode.

The high resolution computer simulation results presented in this chapter illustrate an evolution of realizable, but rather noise-like, phase-space perturbations

which excite undamped coherent structures traveling at phase velocities far from their linear prescription, and simultaneously excite the familiar undamped linear plasma modes located at a variety of time and spatial scales. Keeping the regime of our multispecies, exact-mass-ratio, and fully kinetic computer simulations in view, we hence treat a current-driven, two-component plasma, which in the unperturbed background state is characterized by a drift between electrons and ions (v_D), a temperature ratio ($\theta = T_e/T_i$) and a mass ratio ($\delta = m_e/m_i$). Throughout this chapter v_D is chosen *below* the linear critical drift velocity v_D^* such that a linear instability [2] is excluded from the outset.

We begin this chapter by presenting the results of our computer simulations, recovering the evolution of a non-topological initial perturbation that evolves into a variety of normal modes as well as coherent phase-space structures, forming the basis of our subsequent general analytic formulation. In the first part of analytic description of our simulation, we mainly show that how Landau's formulation deviates from van-Kampen's one. This discussion brings nonlinear trapping in attention and shows the close correlation between *coherency* and *trapping*, which defy both these linear approaches. We identify, within the linear Vlasov approach, the parameter λ which is responsible for the appearance of the well known van-Kampen continuum and, on the other hand, the rise of discreteness of the plasma normal mode spectrum. In the second part of analytic description of results, we further replace λ by an appropriate nonlinear trapping parameter B (see Sec. IV). The separatrix $B = 0$ represents then, in this extended description, the familiar undamped dispersion relation (dispersion branch), which must however to be understood as a nonlinear trapped particle mode, while $B \neq 0$, i.e. the region surrounding the separatrix, is populated by a continuum of nonlinear structures (non-dispersion branches). Showing existence of a pseudo-potential $\mathcal{V}(\Phi)$, that allows charge separation to be representable by its derivative $\partial \mathcal{V}(\Phi)/\partial \Phi$, the coherence of nonlinear structures with a single phase velocity, unlike and independent of linear fluid-modes resonating with particles at their individual phase velocities, is highlighted. This illustrates a mechanism provided by trapping that synchronizes the phases at small amplitudes and therefore allows growth of resulting coherent structures by unusual mechanism, independent of the linear Vlasov stability theory, and in terms of the parameters other than the sole linear parameter, namely, the wave amplitude. As a main outcome, we reconcile our observations, of structures

having such unusual propagation velocity, with the collective structures located on a common, general Nonlinear Dispersion Relation (NDR) [36] featuring regions of separate fast and slow branches. This essentially indicates the presence of kinetic nonlinearity driven collective structures, perhaps ready to grow and drive most of the hot plasma turbulence (see Chapter 6), besides the linear set of eigenmodes of an essentially collisional (Maxwellian) plasma.

We concentrate on weak excitations and assume that without loss of generality the electrostatic potential ϕ satisfies $0 \leq \phi \leq \psi \ll 1$, where ψ is the amplitude of the perturbation and serves as a smallness parameter. An ideal beginning is the inspection of the plasma response in terms of a valid evolution of the Vlasov-Poisson system to a non-topological, eddy-like, initial perturbation (a locally scarce electron population about *any* velocity, preferably on the rising side of a drifting $f_e(v)$), as presented in Sec. 5.2. The simulated response is employed to draw the general picture in Sec. 5.3 and 5.4 in the following order: In Sec. 5.3 we consider the linear Vlasov theory of Landau and van Kampen. The latter two, however, cannot provide an adequate description due to their limitations, namely, (i) a subtle non-resolution of a velocity interval resonant with a coherent unstable structure (indeed present at the arbitrarily chosen velocity) and (ii) the neglect of nonlinearity introduced by the amplitude dependent final strength of the stable trapped particle population remaining therein. The interpretation of the overall picture that emerged from our simulation results is finally completed in Sec. 5.4 where we systematically include this nonlinearity and develop a general Nonlinear Dispersion Relation (NDR), capable of displaying all the observed familiar and unfamiliar responses in their corresponding limits.

5.2 Development of undamped collective structures in a subcritical plasma

Having examined the destabilization of solitary holes by a large electron drift in Chapter 3, and evolution of stably propagating and mutually interacting solitary structures in a plasma free from any source of free energy (drift) in Chapter 4, we now examine the evolution of perturbations in a subcritical plasma, or in the conditions where the drift is below the minimum strength prescribed by the linear stability theory of the collisionless plasmas [28]. This is the limit where the initial

small amplitude perturbations must stay at their noise level without developing larger amplitudes to enter into their nonlinear stage. We however seed a rather unconventional phase-space-eddy-like small amplitude perturbations in these conditions.

5.2.1 Plasma distributions for simulations in subcritical regime

In order to represent a current carrying plasma in the 1D electrostatic simulation set up of present study, an initially stationary Maxwellian velocity distribution is used for the ions, while the drifting electrons are represented by a shifted Maxwellian velocity distribution. The amount of current present in the system is
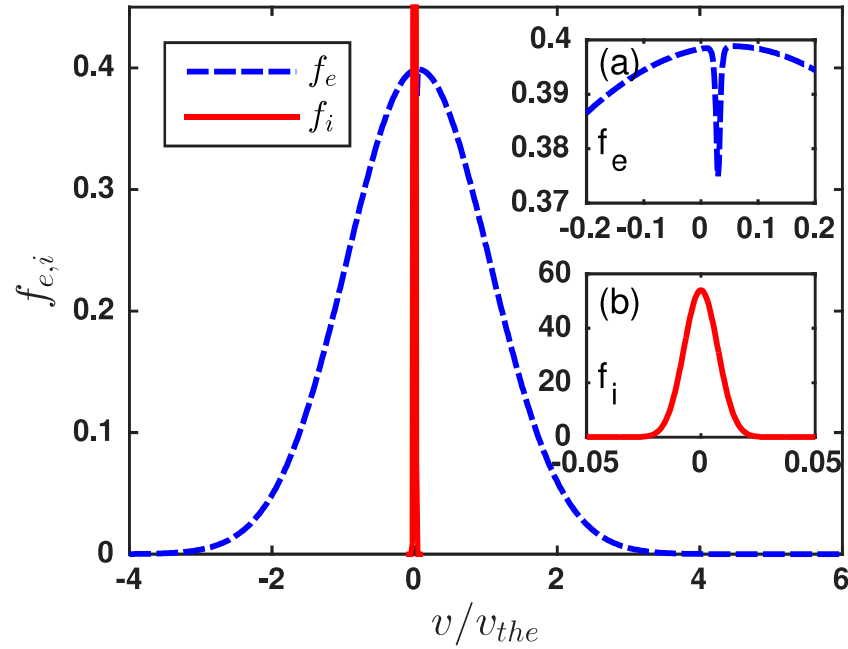
Figure 5.1: Plot of electron (dashed line) and ion (solid line) distribution function at $t = 0$. Subplot (a) presents f_e at $x = 15\lambda_{De}$. Subplot (b) presents ion distribution function f_i.

then determined from the drift velocity of the electrons. In terms of normalized variables introduced in Sec. 3.2, the initial electron and ion distribution functions
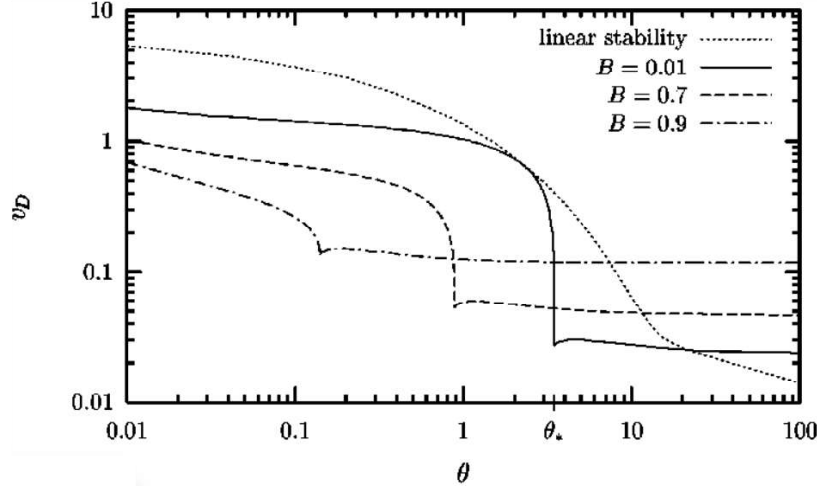
Figure 5.2: The threshold drift value for linear stability (dotted line) as a function of temperature ratio $\theta \equiv \Theta$ as originally obtained by Fried and Gould [2]. The addition curves represent nonlinear stability threshold for solitary electron holes obtained by Griessmeier *et al.* [113] for the indicated values of parameter B.

in this setup are thus represented by,

$$f_e(x, v, t = 0) \;\; = \;\; \frac{1}{\sqrt{2\pi}} (1 + f_1(x, v)) \exp\left[-\frac{(v - v_D)^2}{2} \right], \qquad (5.1)$$

$$\text{and} \quad f_i(x, u, t = 0) \;\; = \;\; \frac{1}{\sqrt{2\pi}} \exp\left[-\frac{u^2}{2} \right], \qquad\qquad (5.2)$$

respectively. In this study we evolve distributions, by implementing flux balance, of both electrons and the hydrogen ions with their exact mass ratio $m_i/m_e = 1836$ and have again used a periodic boundary condition at the ends of the simulation zone of length L.

At $t = 0$ the following eddy-like seed perturbation is given to the electron distribution function,

$$f_1(x, v) = -\epsilon_1 \, \text{sech} \left[\frac{v - v_1}{L_1} \right] \text{sech}^4(kx), \qquad (5.3)$$

where L_1 and v_1 determine the width and position, respectively, of the perturbation along the velocity dimension. The quantity k determines the width of the perturbation in the x direction. In order to avoid the (questionable) presence of

104

an instability given in the linear sense by linear Landau theory [2, 28], for our parameters ($T_e = 10T_i$), $v_1 = 0.03$, $L_1 = 0.003$, $k = 2\pi/0.3$ and the length of the simulation box 30, the drift velocity of electrons is chosen below the linear threshold $v_D^* =$ 0.056 given by $v_D = 0.05 < v_D^*$ with a perturbation strength $\epsilon_1 = 0.06$. As reproduced from Griessmeier *et al.* [113], Fig. 5.2 presents the curve representing threshold drift value v_D for linear stability (dotted line) as a function of temperature ratio $\theta \equiv \Theta$, originally obtained by Fried and Gould [2]. The addition curves corresponding to the alternate, nonlinear stability threshold, for solitary electron holes as obtained by Griessmeier *et al.* for the values of parameter $B = 0.01$, 0.7 and 0.9, respectively. In our present 1D simulation 16384×32768 dual $x - v$ mesh grid is used for solving Vlasov equation numerically for both electrons and ions. The phase space resolution is selected such that structures with sharpest gradient are well resolved. It has been ensured that increasing the resolution further does not allow appearance of newer and sharper structures. Required number of grid points have been calculated by implementing $\delta v \ll f/\nabla_v f$ and $\delta x \ll f/\nabla_x f$, where δv and δx are the grid sizes along v and x dimensions respectively. While the time step for the evolution during $t > 0$ in the simulation is $\Delta t = 0.02$, Fig. 5.1 presents the initial electron and ion distribution functions at $t = 0$. Subplot (a) presents the electron distribution function at the middle of the simulation box x=15 and at the velocity location of the velocity perturbation $v_1 = 0.03$.

5.2.2   Time evolution of initial phase-space perturbations

The time evolution of the electron distribution function and the densities of both electrons and ions is presented in Fig. 5.3. The perturbation f_1 applied at $t = 0$ to the equilibrium distribution f_0 is visible at the velocity location 0.03 and has an associated electron density dip at x=15. Since no structuring occurs in ion phase space due to the relatively fast electronic perturbation, an ion density plot suffices to exhibit the macroscopic ionic response. The corresponding initial electric field localized at this position produces an electron plasma oscillation and a localized ion density modulation consisting of a dip surrounded by two smaller humps. While the dip propagates with ion acoustic phase-velocity, the trailing hump breaks into two structures which also propagate with the ion acoustic velocity in backward and forward directions, respectively, without any visible growth in their initial
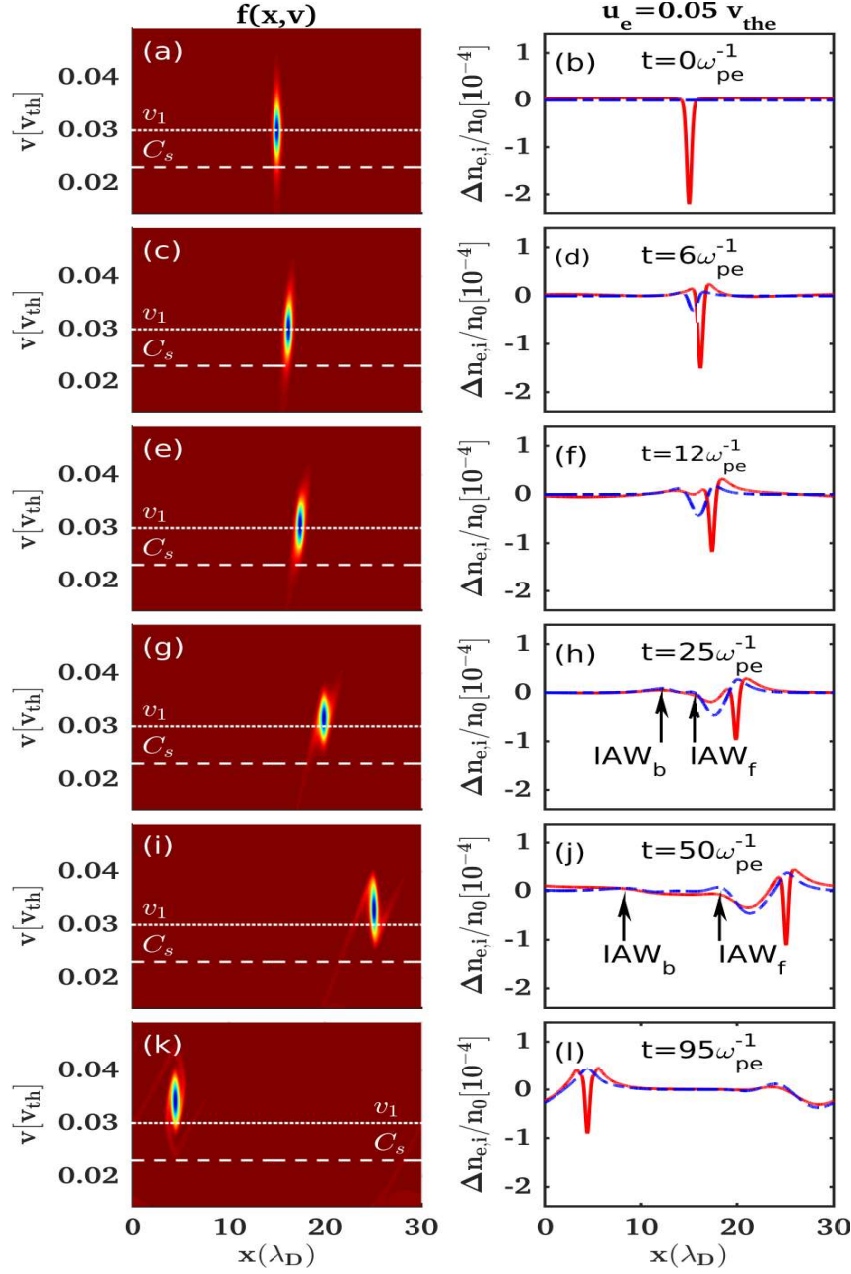
Figure 5.3: Time evolution of electron phase-space (in a, c, e, g, i and k) where frames correspond to indicated times and dotted and dashed horizontal lines mark the seed velocity and ion acoustic velocity, respectively. Corresponding electron density (solid line) and ion density (dashed line) (in b, d, f, h, j and l) at indicated times. The forward and backward propagating IAW structures visible in frames (h) and (j) are indicated as IAW_f and IAW_b, respectively.

amplitude. However, the leading ion hump forms an attractor for the surviving fraction of the initial electron density dip as they are seen to accelerate together to the same phase velocity (about 50 % larger than the ion acoustic velocity) with a visible growth in their amplitudes over a significant duration, before attaining a near saturation at this higher phase velocity. This phase of evolution corresponds to frames (g)-(l) of the Fig. 5.3. The electrons that are trapped in this growing coherent structure, visibly create a stable undamped electron phase-space hole structure. The final propagation velocity of this coherent wave/structure is 0.033 which is greater than the velocity $v_1 = 0.03$ chosen for seeding initial scarcity of the electrons (upper, dotted line in left frames of Fig. 5.3). While the fast electron response and slow ion responses are readily identifiable as the conventional electron plasma wave (EPW) and Solitary Ion Acoustic Waves (IAW), respectively, to accuracy of finite thermal corrections in its characteristic dispersion parameters, the saturation velocity 0.033 of the undamped fast coherent structure far exceeds the ion acoustic velocity ($c_s \sim 0.023$, lower, dashed line in left frames of Fig. 5.3). Thus, the coherent structure with propagation velocity 0.033 can not be suitably located on the conventional discrete spectrum of the linear plasma modes. Moreover, its phase-velocity value depends on the strength of the initial perturbation, exhibiting a fundamental departure from the linear character of any underlying instability. The similar undamped coherent structures with almost no ion participation can be excited as well [9], although by growing/propagating at somewhat higher velocity, essentially in presence of even higher drift velocities, they may not be ideal examples of a growth below the linear threshold value of the drift velocity.

The time evolution of the simulated potential and electric field is presented in Fig. 5.4. The potential structure corresponding to the nonlinear structure is visible more clearly when the counter-propagating components of the standing EPW are in the opposite phase and correspond to a flat EPW potential profile, e.g., at the time $t = 95$ as shown in Fig. 5.4(k). The corresponding electric field shows a bipolar profile at structure location as visible in Fig. 5.4(k). The initial perturbation has thus produced, asymptotically, a combination largely of two undamped structures, namely, a conventional high frequency electron plasma oscillation (EPW) and a slow coherent structure with trapped electrons whose dispersion characteristics are yet to be ascertained in the conventional framework of
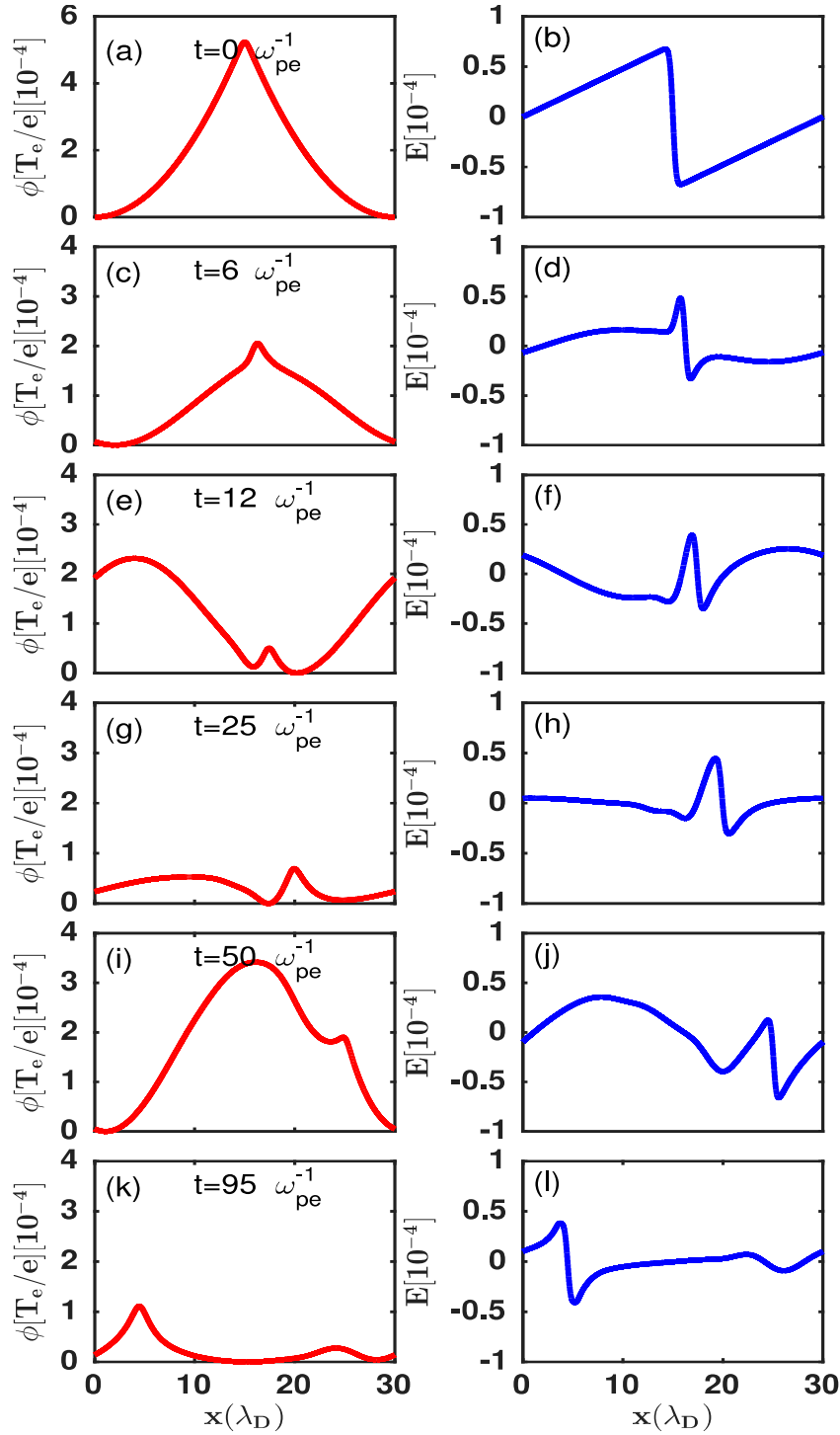
Figure 5.4: Time evolution of potential (in a, c, e, g, i and k) and electric field (in b, d, f, h, j and l) at indicated times.

the plasma instability allowing no growth below the linear threshold of the electron drift. This identification procedure is undertaken in a comprehensive three-level development of a generalized dispersion framework of plasma instability made in the following sections. Before discussing this generalized dispersion framework, we present the evolution of the same initial perturbation using a linear Vlasov simulation code, yielding a very dissimilar evolution.

5.2.3   Evolution using linearized Vlasov simulation procedure

In order to investigate the evolution that the linear Vlasov theory [28] would produce, we simulate the phase-space evolution of the perturbation (5.3) using a linearized simulation procedure that implements the flux balance only for the perturbed part of the distribution

$$f_1(x, v, t) = f(x, v, t) - f_0(v). \tag{5.4}$$

Therefore simulating, effectively, the evolution of f_1 according to the linearized Vlasov equation,

$$\partial_t f_1 + v \partial_x f_1 - E_1 \partial_v f_0 = 0, \tag{5.5}$$

where the information of initial unperturbed distribution function f_0 is preserved by this procedure and is used at all future times in the form of $\partial_v f_0$ appearing in the Eq. (5.5). Note that the total distribution function $f(x, v, t)$ in (5.4) at all $t > 0$ in this procedure is essentially dissimilar to that in the full nonlinear Vlasov procedure described in Chapter 2 where instead of $\partial_v f_0$, the full $\partial_v f$ determines the evolution of f, conserving, in turn, each of the norms listed in Chapter 2.

The corresponding evolution obtained by a linear Vlasov code implementing the above procedure under identical initial conditions is seen in Fig. 5.5. It essentially exhibits the undamped electron plasma oscillations (EPO) associated by a ballistic electron motion but no electron hole generation. The initial seed density dip is simply transformed into the two oppositely propagating Langmuir waves. In the nonlinear run, Fig. 5.3, instead the initial seed is deformed by the nonlinear trapping effect and settles within a few plasma periods into a nonlinear hole like
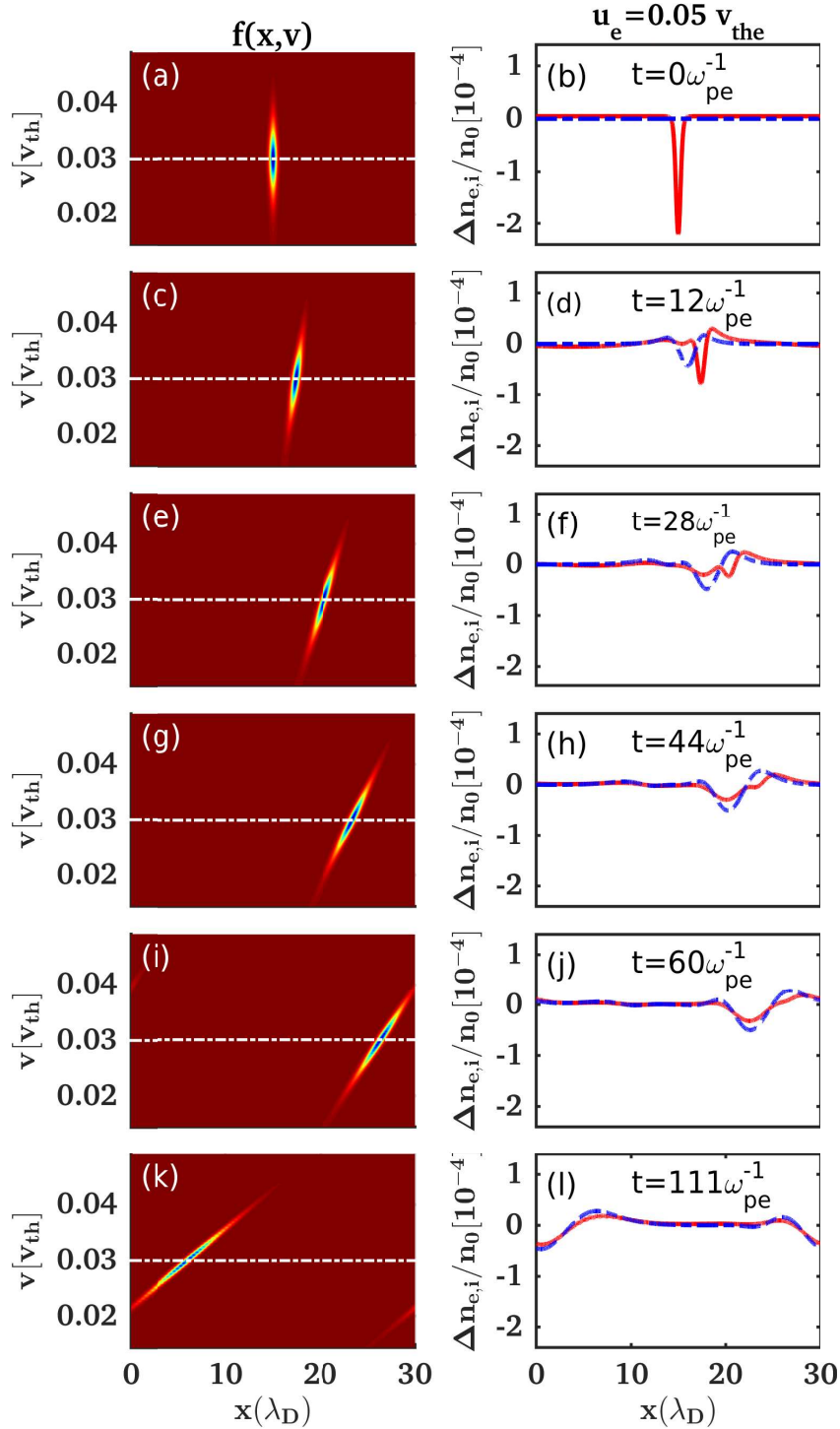
Figure 5.5: Time evolution of electron phase-space and corresponding electron density (solid line) and ion density (dashed line) at indicated times obtained by a linear Vlasov code.

structure, self-consistently. There is no trace of Landau damping/growth or phase mixing of this structure unlike 5.5. Note that the slight increase of its phase velocity by a slight increase of its amplitude is in close agreement with theory (see Fig. 3 of [114], where v_0 has to be replaced by $\tilde{v}_D$, being quantities to be defined later) provided that the fast trapping process is more or less terminated and hence β nearly constant.

5.2.4   Requirement of a general description of nonlinear equilibria

Since nonlinear collective structures of much smaller amplitudes are shown to exist at the noise level that follow independent growth mechanism of more general kind, the linear growth mechanism remains a rather non-unique mechanisms for the collisionless plasma turbulence to operate. The focus in rest of the analysis therefore is on the nonlinear structures recovered above and their interpreting their dispersive properties as well as their stability which is discussed in more detail in Chapter 6.

An identification procedure for the nonlinear structures recovered above is undertaken in following analysis in a comprehensive three-level development of a generalized dispersion framework of plasma instability. The structures are finally located on a nonlinear dispersion relation which has the well-known discrete structure of undamped linear plasma modes seamlessly embedded in its nonlinear continuum. In order to achieve this it is desired to introduce the conventional linear approaches within this generalized description, beginning from more familiar linear formulations, namely, Landau and van-Kampen. Having covered in Chapter 1 the most primitive first level description where electrons and ions are described by fluid equations, we now describe the kinetic Vlasov formulations in their linear and nonlinear regimes.

5.3   Linear Vlasov descriptions for structures and stability

Let us begin with the linear descriptions which would recover the more familiar linear structures, e.g., the electron plasma oscillations/waves or EPW generated in

the above simulations [10]. In this next step of sophistication we describe the electrons as an incompressible, 2D phase space fluid, the density (distribution function) of which being governed by the normalized Vlasov equation (2.3) with $\eta = \eta_e = 1$. In this mean field approach, where discreteness effects are suppressed, the mean electric field E is represented by: $E(x,t) = -\partial_x \phi(x,t)$, which is again assumed to be small and self-consistently coupled with the immobile ions through Poisson's equation (2.5). If $f_0(v)$ represents the homogeneous background distribution we can split f into $f(x,v,t) = f_0(v) + f_1(x,v,t)$ and linearize (2.3) with respect to f_1 to get the linearized form of the Vlasov equation (5.5). Mathematically speaking, (5.5) is an inhomogeneous, linear partial differential equation of first order, the characteristics of which being straight lines. The unperturbed distribution $f_0(v)$ is generally assumed arbitrary, sufficiently smooth and normalizable. The additional constraint, that its slope vanishes at phase velocity, i.e., $f_0'(v_0) = 0$, as imposed in Landau's approach (see later), is, however, not considered generic by us. An unperturbed distribution can logically not anticipate the action of a perturbation i.e. one should not confuse cause with effect.

In our present current-carrying case $f_0(v)$ is given by the shifted Maxwellian

$$f_0(v) = \frac{1 + k^2 \psi/2}{\sqrt{2\pi}} e^{-\frac{1}{2}(v - v_D)^2}, \tag{5.6}$$

where we have already anticipated the presence of a periodic structure analogous to (A.4). The validity of the linearized Vlasov approach demands the smallness of the velocity gradient of f_1:

$$|\partial_v f_1| \ll |\partial_v f_0|, \tag{5.7}$$

which has to be satisfied in the entire phase space and during the whole time span of evolution, which includes the initial condition $f_1(x, v, 0)$.

5.3.1 van-Kampen's linear dispersion relation

It is worth mentioning and almost trivial that (5.7) can be violated despite the smallness of the initial perturbation, $|f_1| << |f_0|$. A stationary solution of (5.5), traveling with v_0, can easily be found by the Ansatz $f_1(x - v_0 t, v), \phi(x - v_0 t)$. Its insertion into (5.5) immediately gives: $(v - v_0)\partial_x f_1 + \phi' \partial_v f_0 = 0$, which is generally

solved by

$$f_1(x - v_0 t, v) = - \left[P \frac{f_0'(v)}{v - v_0} + \lambda \delta(v - v_0) \right] \phi(x - v_0 t). \qquad (5.8)$$

In the last step we used the two well known expressions: $xP\frac{1}{x} = 1$ and $x\delta(x) = 0$, where P is Cauchy's principle value and $\delta(x)$ the delta function distribution. To establish self-consistency we solve (2.5) by inserting $f = f_0 + f_1$ in $n = \int dv(f_0 + f_1)$ and get with (5.8),

$$\phi'' = n - 1 = \frac{k^2 \psi}{2} - \left[P \int dv \frac{f_0'(v)}{v - v_0} + \lambda \right] \phi =: -\mathcal{V}'(\phi), \qquad (5.9)$$

where the term $k^2 \psi/2$ of f_0 in (5.6) is negligible here being of higher order. The pseudo-potential then becomes: $-\mathcal{V}(\phi) = \frac{k^2 \psi}{2} \phi - \left[P \int dv \frac{f_0'(v)}{v - v_0} + \lambda \right] \phi^2/2$, from which we get by the obvious demand. $\mathcal{V}(\psi) = 0$, the linear dispersion relation (LDR):

$$k^2 - P \int dv \frac{f_0'(v)}{v - v_0} \equiv k^2 - \frac{1}{2} Z_r'(\frac{v_0 - v_D}{\sqrt{2}}) = \lambda, \qquad (5.10)$$

where $Z_r(x)$ is the real part of the complex plasma dispersion function [115] for real arguments. This is the van-Kampen relation [12], which can be considered as a linear dispersion relation (LDR) since it determines the phase velocity $v_0 = \omega_r/k$ in terms of k, λ and v_D. The general equilibrium solution within the linearized Vlasov description is hence given by the LDR (5.10) and the pseudo-potential $\mathcal{V}(\phi)$, given by (A.10). The LDR could be analyzed in more detail already here but we postpone it to the next section where a similar, however better founded dispersion relation arises.

5.3.2 Landau's linear dispersion relation

The reason why we have to discard the linear solutions, given by van-Kampen description, everywhere respected solution (5.8) is its invalidity. The underlying prerequisite, namely (5.7), is massively violated in the resonant region due to the two singularities of f_1 in (5.8), the giant principal value singularity (see in case of doubt Fig. 2 of [1]) and the delta-function singularity. Moreover, even within the linear Vlasov approach there are contradicting aftermath, as there is a discrepancy

between the van-Kampen approach, presented here, and the Landau approach [11]. Whereas van-Kampen's approach holds for any $f_0(v)$, Landau needs for his analysis an additional zero slope at the phase velocity. He solves the initial value problem by the Fourier-Laplace technique and justifies the use of the Landau contour in his analysis to obtain time-asymptotically the LDR

$$k^2 - \frac{1}{2} Z' \left(\frac{\omega - k v_D}{\sqrt{2} k} \right) = 0. \tag{5.11}$$

In doing so he uses continuity of the solution when the pole in the complex v-plane, $v = ip/k$, where p is the Laplace variable $p = -i\omega$, transits from $p > 0$ to $p < 0$ corresponding to $\gamma > 0$ to $\gamma < 0$, respectively, where $\gamma = Im\omega$. It should, however, be mentioned that the involved perturbed distribution f_1 is by no means better suited than the van-Kampen one, as it shows through the use of the Landau contour, and of the Sokhotskyi-Plemelj formula, the same type of non-acceptable singularities (for more details see e.g. [28]).

5.3.3   Coincidence between van-Kampen and Landau LDR: recovery of fluid limit

Through his procedure Landau achieves a unique expression for γ, namely $\gamma \sim f_0'(\omega_r/k)$, valid for $|\gamma| \ll \omega_r$ and for both signs, $\gamma > 0$ (growth) and $\gamma < 0$ (damping). From this, one immediately recognizes that there is a coincidence between van-Kampen and Landau only when $\lambda = 0$ in (5.10) and $f_0'(v_0) = 0$ are satisfied simultaneously, otherwise they disagree. This is mainly the reason why in van-Kampen's theory the continuous spectrum, being associated with $\lambda \neq 0$ and giving rise to a continuum of modes with arbitrary $v_0 = \omega_r/k$, is sometimes called "off-dispersion spectrum" since it is not included in (5.11). In other words, Landau misses by his procedure the van-Kampen continuum and needs a zero slope of $f_0(v_0)$ to describe his stationary solution, and with it his threshold for instability. The general resolution of this discrepancy is of course that none of them are valid unless $\lambda = 0$ and $v_0 \gg 1$, such that $f_0'(v_0) \to 0$. In this limit, however, we are set back to our previous fluid solution of no resonant particles at all. Indeed, using

$$-\frac{1}{2} Z_r'(x) = -\frac{1}{2x^2} \left(1 + \frac{3}{2x^2} + ... \right), \tag{5.12}$$

valid for $|x| \gg 1$, one can easily see that (5.10) with $\lambda = 0$ and (A.8) are identical, still leaving the phase velocity $v_0 \sim 0.033 \ll 1$ of the structure recovered in simulation unexplained.

Finally, we emphasize that van-Kampen's and Landau's undamped solutions cannot be distinguished microscopically, i.e. by the use of $\phi(x)$ and of the LDR alone. One has to go into the microscopic phase space to see the difference between both. As we shall show in the next section, this property will be strengthened since there is in fact an infinity of infinitesimal, but nonlinear wave solutions (like the one recovered by us in the simulation at $v_0 \sim 0.033 \ll 1$), all being governed by the same macroscopic dispersion relation. We also note that although it is so simple to recognize the inconsistency of the van-Kampen and Landau solutions in case of resonant particles, it will be rather difficult to assess its repercussion on plasma stability.

5.4 Nonlinear Vlasov description for coherence at small amplitude

The fully nonlinear pseudo-potential method introduced in Chapter 4, acknowledging the finite trapped particle population is shown here to lead also to a general nonlinear dispersion relation (NDR) that accommodate, among its various limiting cases, both the linear dispersive and the nonlinear trapped-particle structures recovered in the simulations. Besides these recoveries, it allows the understanding of linear Vlasov description and its relation to particle trapping regime in a common framework. Here, following Schamel's [1] pseudo-potential based nonlinear method introduced in Chapter 4 we treat in the following the two cases with immobile and mobile ions, respectively.

5.4.1 Immobile ion regime: NDR for electron response and trapping

Considering first the fast propagating coherent structures ($v_0 \gg c_s$) we then treat ions as immobile and use, for the electron distribution, the formal solution of their time-independent Vlasov equation written in the structure's frame given by (4.1) with $v_{\text{eff}} = v_D - v_0$ and k replaced by a more specific symbol k_0. We note that

$f(x,v)$ is a function of two constants of motion, ϵ and σ, which is a necessary requisite for the propagation of a wave, when $v_{\text{eff}} > 0$.

The first part in (4.1) represents the free, the second part the trapped electrons. Although their distribution can in principle be chosen arbitrarily, see [45], we prefer here a distribution, which is continuous at the separatrix $\epsilon = 0$ and has regularly trapped electrons. The trapping parameter β turns out to be decisive for getting physically meaningful equilibria and should not be replaced simply by zero (corresponding to a plateau-like trapped particle distribution). The reason, why we have replaced k by k_0 in the normalization of $f(x,v)$, is that in case of more complex periodic solutions, deviating from a single harmonic wave and being cnoidal in character (see later), k_0 is no longer the correct wave number k (but is of course related to it). For more details we refer to Sec. VII.C. of [36]. To get a better intuitive feel for the Ansatz (4.1) please note that in the limit of a vanishing perturbation, $\psi \to 0$, it holds $\sigma\sqrt{2\epsilon} \to v$ such that $f(x,v)$ becomes a shifted Maxwellian, as it should.

The density (4.3) obtained by a velocity integration of (4.1) under the approximation of the small amplitude produces, on its insertion in into Poisson's equation (4.4) (considering $n_i = 1$), a nonlinear dispersion relation,

$$k_0^2 - \frac{1}{2}Z_r'\left(\frac{v_{\text{eff}}}{\sqrt{2}}\right) = B \tag{5.13}$$

and a general version of the pseudo-potential (4.7) as below for a nonharmonic potential that we represent by Φ rather than ϕ used for harmonic (dispersive) cases following superposition (for which no single $\mathcal{V}(\Phi)$ can be constructed associated with an aggregate structure obtained by their instantaneous superposition, i.e., the curvature/charge-separation $\phi''(x)$ is no longer representable by a $\mathcal{V}'(\phi)$, or the coherent character of ϕ is lost),

$$-\mathcal{V}(\Phi) = \frac{k_0^2}{2}\Phi(\psi - \Phi) + \frac{B}{2}\Phi^2\left(1 - \sqrt{\frac{\Phi}{\psi}}\right), \tag{5.14}$$

where

$$B = \frac{16}{15}b(\beta, v_{\text{eff}})\sqrt{\psi} \tag{5.15}$$

116

and

$$b(\beta, v_{\text{eff}}) = \frac{1}{\sqrt{\pi}}(1 - \beta - v_{\text{eff}}^2)\exp(-v_{\text{eff}}^2/2). \qquad (5.16)$$

There are two noteworthy improvements with respect to van-Kampen's treatment and van-Kampen LDR (5.10): firstly, the parameter λ is replaced by B, which results from trapping, and secondly, an additional, solitary-like term appears in the modified pseudo potential $\mathcal{V}(\Phi)$ (5.14), which reflects the trapping nonlinearity (TN) and introduces non-harmonic contributions to Φ. As shown more explicitly in [1], the potential $\Phi(x)$ itself becomes cnoidal in character, i.e., it is generally described by Jacobian elliptic functions [116].

5.4.2 Locating simulated structures on the NDR

To be a valid solution, B has to satisfy $-2k_0^2 \leq B$, coming from (-$\mathcal{V}'(0) \geq 0$,- $\mathcal{V}'(\psi) \leq 0$), which affects, for a given k_0, the trapping parameter β. The nonlinear
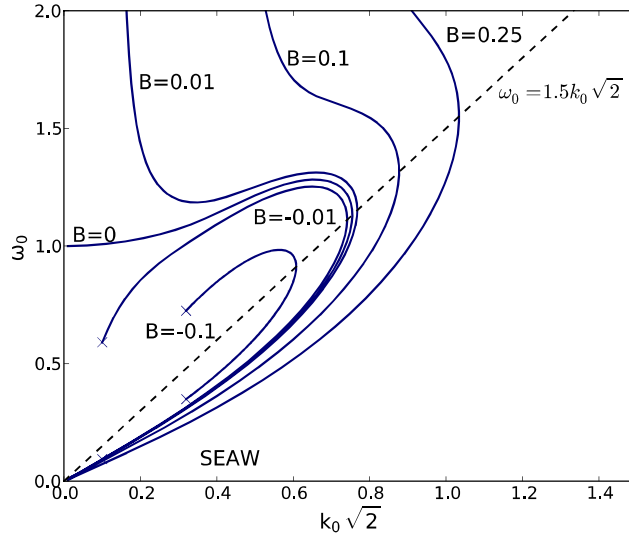
Figure 5.6: The nonlinear dispersion relation (NDR) Equation (5.13) for constant B with $\omega_0 := k_0 v_0$ and $v_D = 0$.

dispersion relation (NDR) (5.13) looks similar to van-Kampen's LDR but is now well founded. Its exploration - see Fig. 5.6, which is identical with Fig. 5 of [1] and is presented for $v_D = 0; v_0 = \omega_0/k_0$ - exhibits (i) a one-parametric continuum of fast and a slow wave branches, the slow ones being associated with the slow

electron acoustic waves (SEAWs) and the fast ones with high frequency (hf) waves among which is the Langmuir wave with $B = 0$, $k_0 \ll 1$, (ii) a line $\omega_0 \simeq 1.5\sqrt{2}k_0$ where both sets of branches meet and (iii) a lower cut-off in k_0 for the hf branches : $\sqrt{B} < k_0$ in case of $B > 0$). As a consequence there is a continuum of phase velocities v_0 (analogous to the van-Kampen continuum) a stationary structure can attain, and not only the "dispersion branch" $B = 0$ with its thumb-like shape.

5.4.3 Relationship between linear and nonlinear Vlasov equilibria

We are now in the position to clarify the relationship between linear and nonlinear Vlasov equilibria. We do this by asking the question as to whether there is, for a given $k_0^2 > 0$, a harmonic wave limit $B \to 0$ in (5.13)-(5.14) which can be interpreted in the linear sense as $\psi \to 0^+$, namely that at least one of the linear solutions are accessed. A positive answer could then be interpreted as a justification of the standard wave description which forms basis for linear threshold based operating mechanism of plasma instability.

Assuming for the sake of simplicity, which does however not affect the outcome, a non-drifting electron species, $v_D = 0$, we can write

$$B = \frac{16}{15\sqrt{\pi}}(1 - \beta - v_0^2)\exp(-v_0^2/2)\sqrt{\psi} \tag{5.17}$$

and see that there are three factors which can account for a zero B.

1. One solution for $\psi = \epsilon > 0$ is $v_0 \gg 1$, which is however nothing else but our previous fluid-like Langmuir wave solution where resonant particle effects are negligible. This yields no new information.

2. A second zero is provided for $\psi = \epsilon > 0$ by the first bracket, and becomes $-\beta = v_0^2 - 1$. This is clearly a trapped particle equilibrium with a tiny width of the trapping region, $2\sqrt{2\phi}$, in which the trapped electron distribution $f_t(x, v)$ is depressed (concave) since $v_0^2 > (1.307)^2 \simeq 1.71$ and consequently β negative.

3. The only possibility left over of getting a linear limit is by letting $\psi = \epsilon \to 0^+$, in which case the third, the square root of the amplitude ψ would become

responsible for the harmonic wave limit. In this case, however, we are still confronted with trapped particle equilibria since the trapping width, $2\sqrt{2\phi}$ is still non zero as long as $\epsilon \neq 0$. But then we have an infinity of nonlinear solutions since β can attain any value. All of them belong to the same NDR (5.13) which is formally equivalent with (5.10) in the limit $v_D = 0, \lambda = 0$ or with (A.8) in the limit $\omega = \omega_0, k = k_0$.

In other words, the dispersion relation is shared by an infinity of extremely small amplitude wave solutions which are well-behaved as long as trapping is an admitted physical process. Hence, up to infinitesimal amplitudes nonlinear trapping remains a vivid process regularizing singularities in the phase space. A plasma has an infinity of nonlinear choices of circumventing singular solutions and it would be rather unnatural to ignore them.

5.4.3.1   Solitary nonlinear equilibria without linear analogue

We can deepen and support this conclusion by considering, in addition, the localized perturbations. Indeed, assuming $0 < B \leq 1$ but $k_0^2 = 0$, we find solitary electron holes of the form $\Phi(x) = \psi \ \text{sech}^4 \left(\frac{\sqrt{B}x}{4} \right)$, the phase velocity of which being given by the solution of (5.13) (with $v_D = 0$ for simplicity) lying in the range $0 \leq v_0 < 1.307$. For small B satisfying $0 \leq B \ll 1$ the latter becomes $v_0 = 1.307(1 - B)$. A non-zero value of B in the infinitesimal amplitude limit $\psi \to 0^+$ is easily compensated and achieved by $-\beta \propto B/\sqrt{\psi}$ representing a tiny density dip in phase space at resonant velocity [33].

5.4.3.2   Independence of fluid and kinetic wave equilibria

The analysis based on above model suggests that *coherent wave equilibria are either fluid-like (such as Langmuir waves) or kinetic hole equilibria with a non-ignorable trapped particle component* [1, 36, 45, 54]. Moreover, since Landau's solution coupling them fails, in turn, for $\gamma = 0$ we have to accept by employing continuity that the whole Landau scenario of growth or damping near threshold becomes questionable as well, at least, as long as tiny seed fluctuations are present to trigger the hole evolution, rather the characteristics of noise in most plasmas generated via nonequilibrium processes. This can happen well below linear threshold, and happen in terms of parameters other than amplitude (which is sole growth pa-

rameter in linear approximation), as discussed further based on additional cases in Chapter 6.

5.4.4   Mobile ion regimes: NDR accommodating ion trapping

In our simulations we witness a finite ion mobilization, especially for the perturbations at slow velocities from noise, equally probable in an ideal noise, such that the ion response is essentially present. In order to accommodate our present simulations that addressed such seed-like perturbation of low velocity with drift, we may give up the fixed ion approximation and replace it in Eq. (4.4) by the ion density, which is related to the ion Vlasov equation. (Note that fixed ions are reproduced in the following equations by the limit $\Theta \to 0$ or $T_i \to \infty$). We shorten, however, the incorporation of ions by referring to Sec. IV of [36], which itself rests on [4], and also in favor of the simulations in this regime discussed in the next Chapter. When ion trapping is acknowledged, the two important relations, the NDR and $\mathcal{V}(\Phi)$, respectively become,

$$k_0^2 - \frac{1}{2}Z_r'(\frac{\tilde{v}_D}{\sqrt{2}}) - \frac{\Theta}{2}Z_r'(\frac{u_0}{\sqrt{2}}) = B_e + B_i \tag{5.18}$$

$$-\mathcal{V}(\Phi) = \frac{k_0^2}{2}\Phi(\psi - \Phi) + \frac{B_e}{2}\Phi^2(1 - \sqrt{\frac{\Phi}{\psi}}) +$$

$$\frac{B_i}{2}\left(\Phi(3\Phi - 5\psi) + 2\psi^2[1 - (1 - \frac{\Phi}{\psi})^{5/2}]\right). \tag{5.19}$$

In these expressions the following abbreviations have been used: $u_0 = (\Theta/\delta)^{1/2}v_0$, B_e is identical with B, defined above, and B_i is given by,

$$B_i = \frac{8}{5}b(\alpha, u_0)\Theta^{3/2}\sqrt{\psi}, \tag{5.20}$$

α being the ion trapping parameter corresponding to the electronic one β. We mention here that due to ion mobility a second discrete mode, the ion acoustic mode, enters in the picture which however may operate in absence of ion trapping. Such structures, recovered by the additional cases simulated, are presented in the next chapter along with the associated effects and aspects related to stability of nonlinear structures.

120

5.5   Summary and conclusions

In this chapter, a current driven, 1D, collisionless plasma is considered as a paradigm of driven intermittent plasma turbulence and anomalous transport with the focus on additionally excited *undamped coherent* electrostatic structures excited alongside the familiar undamped linear plasma modes. The simulation presented have thus explored the concept of plasma instability in terms of more general fundamentally nonlinear structures, outside the conventional linear regime which is limited to covering largely the undamped collisional plasma eigenmodes, that are additionally subjected, by means of Vlasov equation, to interaction with resonant particles. Simulations explore evolution of more relevant forms of perturbations in the species phase-space and display activity of undamped structures that are small amplitude trapped particle equilibria existing alongside the conventional collective linear wave equilibria of the thermalized plasmas recovered in collisional fluid-like limit. In the analysis of simulation output, a wave description is employed which, in its fundamental form, accommodates the nonlinear aspects arising from the kinetic effects like particle trapping and recovers the linear Vlasov descriptions as one of its limiting cases.

The simulations, beginning from small amplitude phase-space eddy like initial perturbations realizable in a nonthermal noise, evolve the distributions to show undamped coherent structures, apart from the well known linearly undamped modes of the thermal plasmas, namely the electron plasma and ion acoustic waves. Numerically, a rapid relaxation within about 100 plasma periods is seen, released by an eddy-like initial fluctuation, in which both types of structures emerge time asymptotically. The additional undamped structures traveling at an unusual phase velocity (about twice c_s) disagree with linear description and are absent from the simulations performed using a linear Vlasov simulation procedure.

In our analytic description based on three different levels, we have constructed stationary electrostatic structures, which constitute a continuous spectrum, determined by electron trapping. Members of this mode continuum are the well known discrete modes (Langmuir, ion acoustic), which arise in the limit of vanishing trapping at high phase velocities (with respect to electron thermal and ion thermal velocity, respectively), and the cnoidal electron and ion holes, which are entirely due to trapping and belong to the non-dispersion branches of the non-

linear dispersion relation. There is no general way to establish a link between the linear discrete mode spectrum, being masked by singularities in the associated distributions, and the class of well-behaved nonlinear trapped particle structures even in the infinitesimal amplitude limit. This has the consequence that in case of coherency the onset of instability as described by Landau is generally absent when seen realistically from the standpoint of the complete Vlasov-Poisson system. It is replaced instead by a more complex, highly unknown destabilization process in phase space, in which this manifold of trapped particle equilibria with its attracting negative energy property together with the explicit initial perturbation will play an important role. This renders plasma destabilization multifaceted and as a rule - no longer one-dimensional in parameter-space, i.e., involving growth not only in the amplitude that remains sole parameter in all linear theories.

Based on the above simulating results and multilevel analysis this can be concluded that the perturbative linear and nonlinear treatments of plasma instability can be generalized to include the contribution of nonlinear small amplitude coherent structures. A limited number of existing studies, e.g., Dupree [5] and Tetreault [117] proposed the coherent modes as possible candidates as growing structural elements, in addition to linear eigenmodes. In our study, the coherent structures are characterized in the stationary regime by the existence of a pseudo-potential $\mathcal{V}(\Phi)$. This means that $\partial_{xx}\Phi(x) = -\partial_\phi \mathcal{V}(\Phi)$ holds, or the curvature of Φ (or charge separation) can be expressed by Φ again through the pseudo-potential $\mathcal{V}(\Phi)$. For a composite superposition of linear eigenmodes (e.g., Landau or van-Kampen), on the other hand, $\partial_{xx}\phi(x)$ is no longer representable by a $\partial_\phi \mathcal{V}(\phi)$, i.e., the coherent character of ϕ is lost. An additional singular limit encountered under the linear theory in the limit of zero damping rate is further discussed in detail in final conclusions of the thesis presented in Chapter 7 with reference to relevant work in this subject by Mouhot and Villani [118, 119], Wesson [120] and Belmont *et al.* [121]. The non-uniqueness of the linear asymptotic solutions was indicated by Belmont *et al.* [121] however by ignoring nonlinear trapped particle effects. This effect is captured more strongly by general $B \neq 0$ solutions of the presented analytic approach [1]. The relevance of the linear Landau approach thus emerges to be limited to special parameter and temporal regimes where deviations from the prerequisites of nonlinear theory can reestablish the standard linear wave concept as discussed in broader detail in Chapter 7.

122

We conclude this chapter by providing examples of observations of subcritical plasma instabilities associated with structure formation in, simulations of driven plasmas [22, 54, 85, 122–124], in space or laboratory observations, such as [15, 125] and also in particle accelerators where its signatures are noted in the form of coasting and bunched beams in synchrotrons and storage rings, well represented by Vlasov-Poisson systems. In the Fermi Main Ring, for example, operating near stability limit [52], sharp gaps or notches have been witnessed in the response function [62], which correspond to depletion zones in the momentum distribution function. This is seen at the lowest measurable signal level and sheds light on the spectrum of small amplitude perturbations, proving the incompleteness of linear and associated nonlinear wave theories in the kinetic regime [54, 113, 126–128]. A similar phenomenon, namely stable, coherent, longitudinal structures superimposed on bunched beams [63], has been observed during "rf activity" in stochastic cooling studies [64, 65]. A well documented excitation of holes below linear threshold could be seen also in numerical simulations of pair plasmas in [85] as well as in the laboratory experiments of Moody and Driscoll [61]. And finally, it would be an intriguing task for future investigations to link the present nonlinear destabilization mechanism with the observed reorganization into coherent structures of driven collisionless magnetospheric plasmas at increasing turbulence levels [129].

6

Electron hole instability of subcritical plasma phase-space perturbations

6.1   Introduction

The stability of plasma state is determined by the capacity of a free energy source to grow small amplitude perturbation into larger amplitude collective structures that are usually recovered as undamped eigenmodes of linearized plasma equations. These small amplitude solutions follow the principle of superposition, eliminating the amplitude as an active parameter of the dynamics such that the instability thresholds are recoverable purely in terms of the driver strengths. Results in Chapter 5 importantly concluded that the amplitude itself is a threshold parameter since the *modes* might couple at a threshold amplitude to produce an alternate set of undamped solutions of the exact equations having an independent destabilization mechanism, capable of replacing the mathematical eigenmodes of the linearized approximate equations that are ideal and hence must follow the superposition principle when used for analytic convenience. The destabilization mechanism of the plasmas can therefore fundamentally differ from what prescribed by the linear stability, with profound implication for the plasma turbulence theory and its underlying, presently linear, operating mechanism.

A threshold in terms of amplitude is shown in the preceding analysis, strongly aided by computer simulations, to depends on more complex factors, like rate of en-

tropy increase, however, for the perfectly collisionless Vlasov plasmas this threshold must approach the zero amplitude, hence ruling out any equivalent linear regime. Moreover, even for the cases with finite rate of entropy production, the threshold are no longer tied to discrete eigenmodes of the linearized Vlasov equations and rather to a continuum of trapped particle equilibria that are exact coherent undamped eigenmodes of collisionless plasmas. The latter, fundamentally nonlinear modes, are however destabilized by radically nonconventional means, e.g., by defying the (de)stabilizing strength of velocity derivative $\partial_v f(v_0)$ (i.e., drifts) in favor of alternate factors like coupling with other unstable modes/nonuniformities of the plasma, and, more remarkably, displaying destabilization in terms of the parameter (like phase velocity) other than the structure amplitude, that remained sole parameter representing destabilization in linear cases.

The results of next set of high phase-space resolution simulations [8–10] elucidate these growth mechanisms where the infinitesimal amplitude trapped-particle equilibria, or phase-space holes, subcritically grow in amplitude, and mode convert. Quite analogous to the linearly undamped eigenmodes $\phi(x)$ contained in an initial perturbation that get destabilized by phase-mixing-away the unsupported transient in the linear Vlasov evolution (shown in Fig. 5.5), the destabilization here is shown to take place of the undamped mode-coupled nonlinear structures $\Phi(x)$ contained in an initial small amplitude phase-space eddy-like perturbation. When the latter are evolved in a linearly subcritical plasma, we see additionally undamped structures that obey the existing analytic description of such mode-coupled structures prescribed to replace discrete eigenmodes of the linearized approximate Vlasov equation in a nonperturbative exact plasma stability analysis. The coherent $\Phi(x)$ generated at a slower phase velocity is further seen to be destabilized by defying the sign of $\partial_v f(v_0)$ and grow, rather in their phase-velocity dimension than amplitude, to effectively mode convert into a more stable, ion acoustic electron hole. The linearly undamped modes, namely, the EPW and IAW modes excited by the initial perturbation are duly recovered stable because of the evolution done in a subcritical drift regime, unlike the strong drift cases where ion acoustic mode displayed stronger growth while no phase-space eddy perturbation were seeded preventing independent electron hole structures to grow.

Among most successful analytic models of small amplitude trapped particle undamped equilibria are Schamel structures [1, 36] which are solitary in nature

because they incorporate and combine the essential dispersive and nonlinear attributes. Although purely ideal in their treatment (obeying zero amplitude threshold) of the phase-space separatrix, they are employed here as basis for generating and interpreting the simulation results, allowing to explain the tolerable deviation of simulations from the ideal electron-hole model they represent, to the order of the complex (irreversible) physics which the latter excludes at the separatrix.

In the present chapter, we present in Sec. 6.2, the analytic expressions for non-conventional phase-space perturbations for exciting a combination of linear plasma modes and the mode-coupled undamped structures at two distinct spatial scales. The evolution of both kinds of undamped structures as simulated by these initial perturbations are presented in Sec. 6.3. Two distinct regimes of instability of small amplitude undamped nonlinear plasma equilibria are identified qualitatively in Sec. 6.4, while their operating mechanism is discussed more quantitatively in Sec. 6.5 based on flux and electrostatic energy conservation in the simulations. The analytic basis of the observed growth mechanism is described by employing the general nonlinear dispersion relation involving both electrons and ion response which is discussed in Sec. 6.5.2 and summary and main conclusions from the chapter are presented in Sec. 6.6.

6.2 Perturbations for mode-coupled undamped structures

The study in this chapter is based on results of two cases of high-resolution Vlasov simulations with two small phase-space perturbations, developing into stable and unstable hole structures depending on the initial set of parameters. The instability recovered in the latter case is combination of (i) an intrinsic hole instability arising from the initially developed hole being a less negative energy structure and (ii) a parametric instability arising from coupling of the electron hole to a plasma nonuniformity created by the initial perturbation. The evolution shows that the electron holes can be destabilized by coupling to conventional collective modes of collisionless plasmas.

For the present simulations we have once again used a well localized initial phase-space perturbation in the electron distribution function of the following an-

alytic form,

$$f_1(x, v) = -\epsilon_1 \operatorname{sech}\left[\frac{v - v_1}{L_1}\right] \operatorname{sech}^4[k(x - x_1)] \tag{6.1}$$

where ϵ_1 is the amplitude of the perturbation, L_1 is the width of the perturbation in the velocity dimension and k^{-1} is its spatial width. The background equilibrium velocity distribution of the electrons and ions are thermalized Maxwellian with finite temperatures T_e and T_i, respectively,

$$f_{0j}(x, v) = F_{0j} \exp\left[-\frac{m_j(v - u_j)^2}{2T_j}\right] \tag{6.2}$$

where subscripts $j = e, i$ correspond to electron and ion species, respectively, and appropriate F_{0j} ensures net charge neutrality in the simulation box.

In this study we include evolution of total electron distribution $f_e = f_{0e} + f_1$ in two cases with different values of the parameter set (v_e, v_1) given below. It is expected in each case that out of the continuum of solutions, the initial perturbations must excite the closest undamped trapped electron equilibrium. We use the Debye length λ_D, electron plasma frequency ω_{pe} and electron thermal velocity v_{the} as normalizations for length, time and velocities, respectively. In a plasma with $T_i/T_e = 10$ and $m_i/m_e = 1836$, considering the linear instability threshold drift velocity, $v_e^* = 0.053$, we have selected two subcritical combinations of electron drift and perturbation velocity, $(v_e, v_1) = (0.052, 0.05)v_{the}$ and $(0.01, 0.01)v_{the}$. In both these cases the perturbation is chosen to be located at the center, $x = 15\lambda_D$, of the simulation box having dimension $L = 30\lambda_D$. The phase-space widths of the perturbation is chosen as $L_1 = 0.01v_{the}$ along the velocity dimension and $k^{-1} = 10\lambda_D$ along the spatial dimension x in the expression (6.1).

6.3   Evolution of undamped potential structures

The corresponding outputs of above two cases in terms of time evolution of f_e in the phase-space and associated density profiles are presented in Fig.6.1 and Fig.6.2, respectively. Unlike their evolution in the linearized Vlasov regime where the electron holes get treated as transient and immediately buried, the two identical initial perturbations, differing merely in the initial velocity of their launch, show

a remarkably distinct evolution in which the latter case undergoes a set of strong nonlinear hole instabilities.

6.3.1 Stable evolution of faster perturbation

For the first perturbation case at $v_1 = 0.05v_{the}$, the time evolution of the contours of electron distribution function $f_e(x, v)$ in phase-space is presented in left column of Fig. 6.1, showing that the core of the initial phase-space cavity like perturbation is largely intact and after a marginal readjustment of its phase-space widths continues its propagation with nearly the original velocity, $0.05v_{the}$ of the perturbation. For the second slower perturbation case at $v_1 = 0.01v_{the}$, however, the phase-space structure presented in left column of Fig. 6.2 is seen accelerating to a higher velocity after a noticeable change in its topology in the phase-space. While we expect the initial positive potential structure setup by the electron deficient perturbation to decay gradually by expelling ions over ion response time $\sim \omega_{pi}^{-1} = \sqrt{m_i/m_e}\omega_{pe}^{-1}$ we see a distinct response of plasma in each of these two cases. In a simpler looking first case, we witness a much faster saturation of this ion expulsion (potential decay) and an immediate set up of a coherent propagation of the structure via the following mechanism.

The local scarcity of electrons from the phase-space ($f_1 < f_0$) in a small velocity interval translates in an electron density dip (potential hump) at x_1, instantly introducing a phase-space separatrix about (x_1, v_1). A slowly varying separatrix corresponds to an adiabatic invariant, with a response time (time for the separatrix to modify) longer than that of untrapped ions ($\tau_{\text{adiabatic}} \gg \omega_{ip}^{-1}$). In order to restore the quasineutrality on a faster time scale, therefore, the initial non-equilibrium perturbation structure begins to expel ions. An inward flux of ions is expected, on the other hand, driven by deficiency in thermal (streaming/untrapped) electron population at the hole location that causes lower streaming electron pressure $[(n_sT_s)_{\text{in}} < (n_sT_s)_{\text{out}}]$ and motivates the surrounding ions to bunch at the hole location [130]. Clearly, in a stably propagating solitary electron-hole structure, these two fluxes must balance and a comoving ion density hump must exist, as seen in Fig. 6.1(j). More noticeably, supplementing the response of ions that bunch creating a central positive charge, the cold trapped electron population dispels itself away from the center, strengthening this net central charge density, as again seen in Fig. 6.1(j). This imparts the structure an electron acoustic element. Moreover,
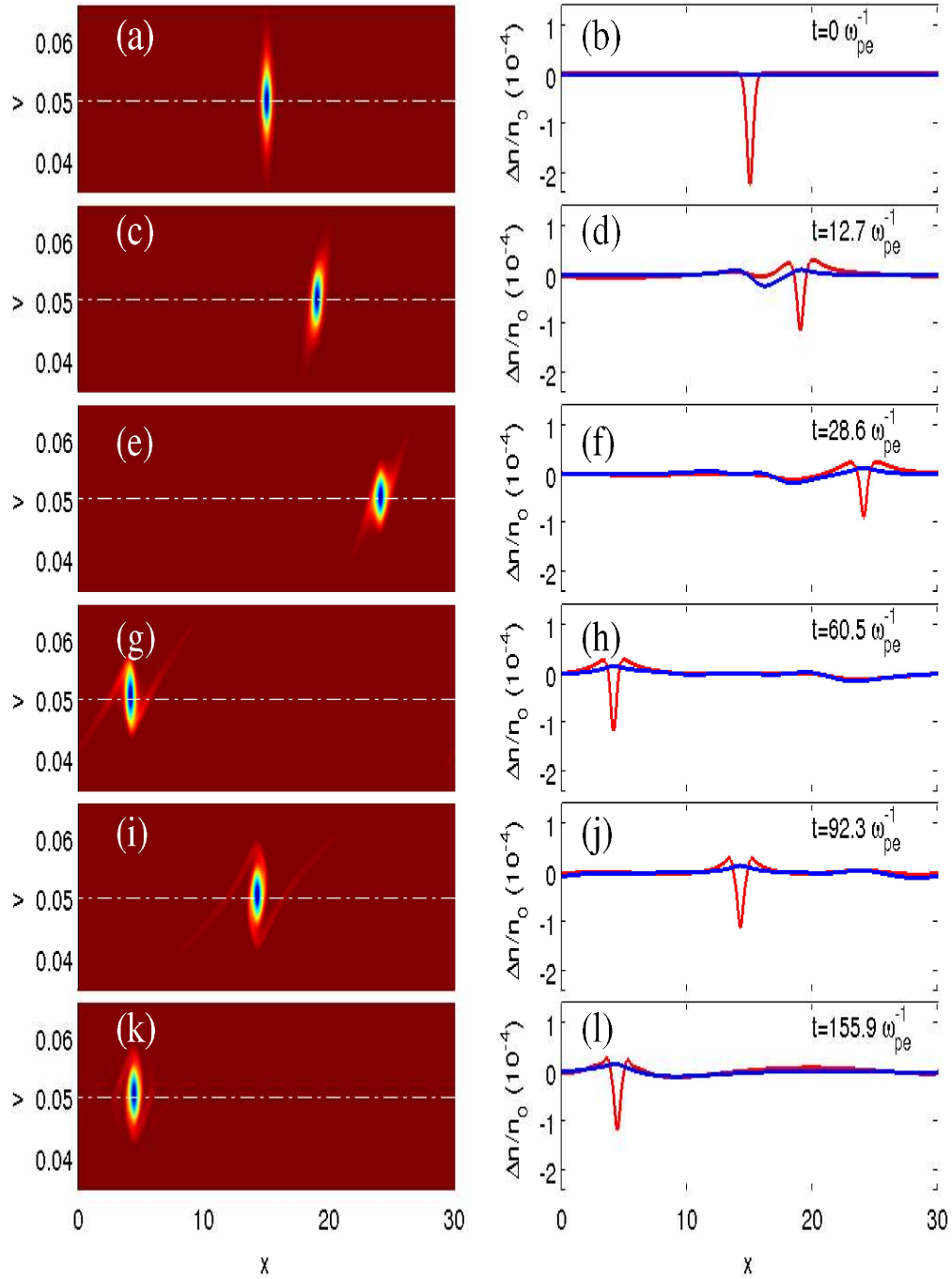
Figure 6.1: Evolution of the phase-space perturbation initially introduced at $(x_1, v_1) = (15, 0.05)$.
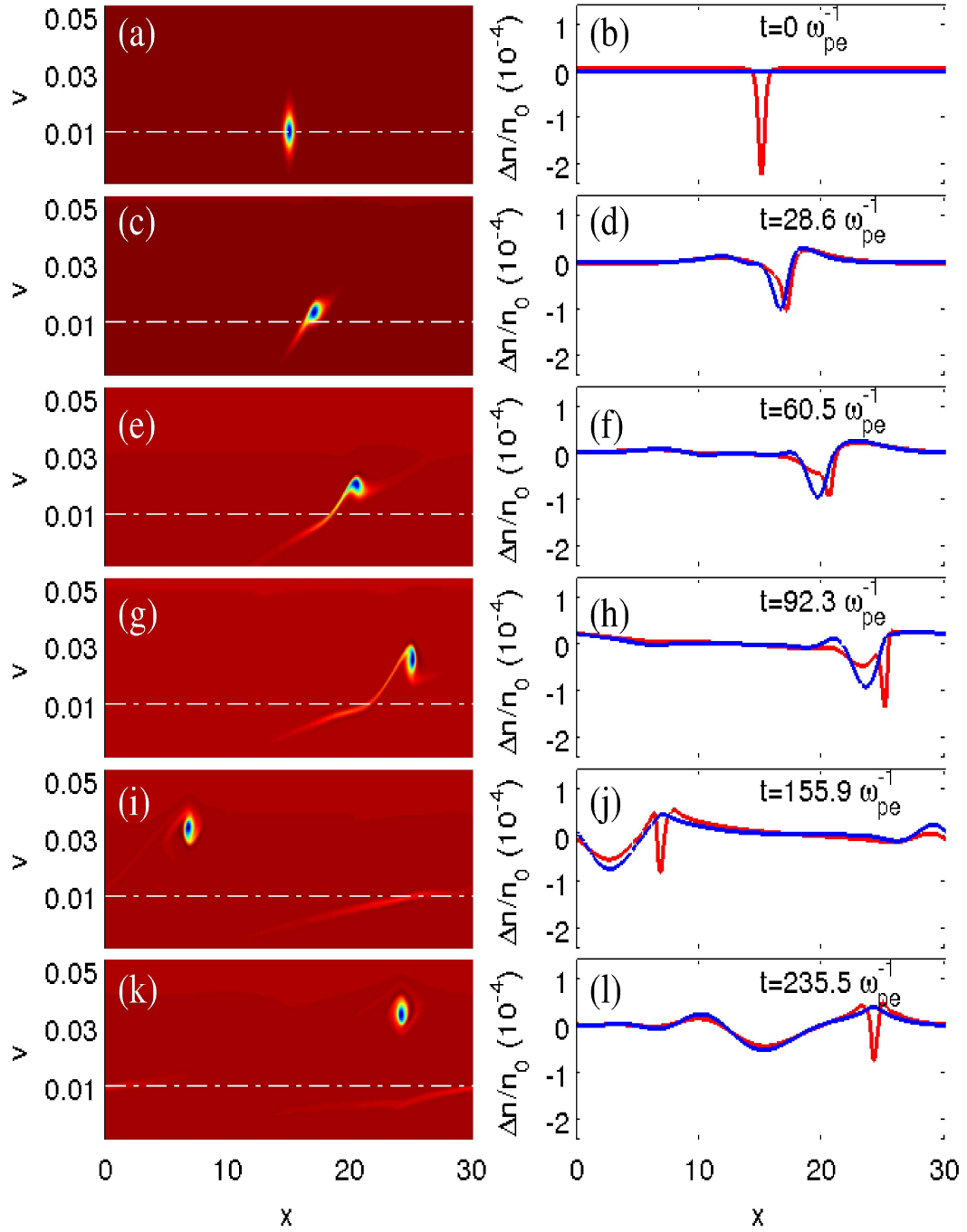
Figure 6.2: Evolution of the phase-space perturbation initially introduced at $(x_1, v_1) = (15, 0.01)$.

the faster structures are increasingly electron acoustic in nature as ions get smaller time to bunch strongly enough.

6.3.2 Unstable evolution of slow perturbation

The evolution of initially slower perturbation of the second case with $(v_e, v_1) = (0.01, 0.01)v_{the}$, presented in Fig. 6.2, clearly shows a rather distinct two-phase evolution. The initial perturbation in this case remains unshielded for a considerably longer time and thus manages to expel a large ion density out of the slowly moving perturbation cavity before forming a slow electron hole structure. The passage of this saturated slow electron hole through the initially created ion nonuniformity further generates a strong acceleration of this and slowly converting it into an supersonic ion acoustic electron hole where ions can effectively participate in its dynamic shielding process.

6.4 The electron hole instabilities

The above two evolutions allow us to identify, qualitatively, two unstable SEH growth regimes where a perfect shielding of propagating electron hole structures can not be achieved and the structures contained in the initial perturbation must make an approach to their corresponding stable states, including an electron hole and the conventional linear plasma modes. In the secondary stage of evolution the structures interact with each other and further destabilize each other, parametrically. These two unstable phases are described as two distinct instabilities of the electron hole contained in the perturbation, as below.

6.4.1 Electron hole instability: hole formation

The initial phase where the perturbation develops into an undamped stable hole by the action of both streaming and trapped electrons. sees ions to be expelled from the initial electron cavity while the streaming electrons to bunch at the cavity location. The process leads to creation of the electron hole and achieves its shielded form without significant modification of the separatrix. This phase is therefore identified as an electron hole instability, because, although it uses the initial field energy contained in the perturbation to create an electron hole, the

final state is a lower free energy state resulting into a stably propagating electron hole equilibrium structure, besides, of course, the conventional ion acoustic and electron plasma wave equilibria. We note that this unstable phase for the first case of faster initial perturbation lasts for shorter period. However, in the second case of slower perturbation it lasts for a considerably long duration, involving greater ion expulsion.

6.4.2 Parametric electron hole instability: hole mode conversion

This phase corresponds to the second phase of electron hole evolution after its formation by electron hole instability. For the present slow perturbation case, this phase sees an increase in the strength of electron acoustic characteristics of the developed electron hole while decrease in the strength of its ion acoustic character. In this unstable phase, the electron hole is destabilized, parametrically, by interaction with the plasma uniformity present, e.g., in the form of the ion acoustic wave such that the electron hole accelerates and gains higher phase velocity, characteristics of the electron acoustic hole regime examined in Chapter 3, rather than the slow ion acoustic regime examined in Chapter 2. This parametric instability phase can be seen in second case to last over a considerably longer period as compared to the first, electron hole instability phase.

6.5 The instability mechanism

Both these unstable phases of evolution are absent from the first case (Fig. 6.1), but visible in the second case presented in Fig. 6.2, where a slow perturbation, unshieldable for a longer period (see below) is able to create a wider plasma nonuniformity before a charge flux balance is achieved, forming an initially weak SEH (phase-1: Figs. 6.2(a) to (d)) via a hole instability. The SEH then traverses the originally created plasma nonuniformity to grow in its strength, and thereby in velocity (phase-2: Figs. 6.2(e) to (j)), via the parametric version of the hole instability.

6.5.1   Flux and energy balance in simulation data

The growth in the net electrostatic energy in non-oscillatory modes for two cases can be identified from that plotted in two cases in Figs. 6.3(b) and (d). A clear partition of initial total energy of the perturbation between that of the coherent modes (bottom level) and the oscillatory modes (high frequency oscillating top) is identifiable by the plots of the total electrostatic energy in both figures. While in case-I (Fig. 6.3(b)) the energy in coherent (non-oscillatory) mode is nearly constant, in case-II (Fig. 6.3(d)) the initially weak coherent mode formed in phase-1 ($t < 8\omega_{pe}^{-1}$) gains the energy, parametrically, by an unstable evolution triggered by a pressure imbalance of streaming electrons ($50 < t < 120\omega_{pe}^{-1}$). To substantiate presence of this mechanism we have presented, in Figs 6.3(a) and (c), the profiles of net electron density (dashed gray line) and streaming electron density (blue line). While the net density shows a dip, the streaming density is recovered to still have a peak in accordance with conventional variation, $n_e = \exp(\phi)$, (dashed dotted red line) for an acoustic mode [28]. This means that the streaming electron pressure in the unstable phase of SEH is highly imbalanced across the SEH (Fig 6.3(c)) leading to a net growth in the hole amplitude until this imbalance is removed and the growth saturates. During the saturated stable phase, however, the electron pressure profile shows a state of equilibrium (Fig 6.3(a)) and hence a stably propagating SEH.

We now show that via (i) the non availability of SEH solutions at smaller velocities and (ii) a SEH amplitude-velocity relationship, both well accommodated in Schamel's nonperturbative SEH approach [1], the unstable phase-1 and phase-2 of case-II, are categorically explained. They, respectively, correspond to the (i) initial failure of plasma in shielding the slow SEH-like perturbation and (ii) a subsequent growth and acceleration of the small amplitude SEH structure with changing ambient density.

6.5.2   Unstable regions of EH parameter space

The growth of the electron hole structures can be predicted by a nonlinear analytic model based on formal solutions of Vlasov equation, given by H. Schamel [1]. The
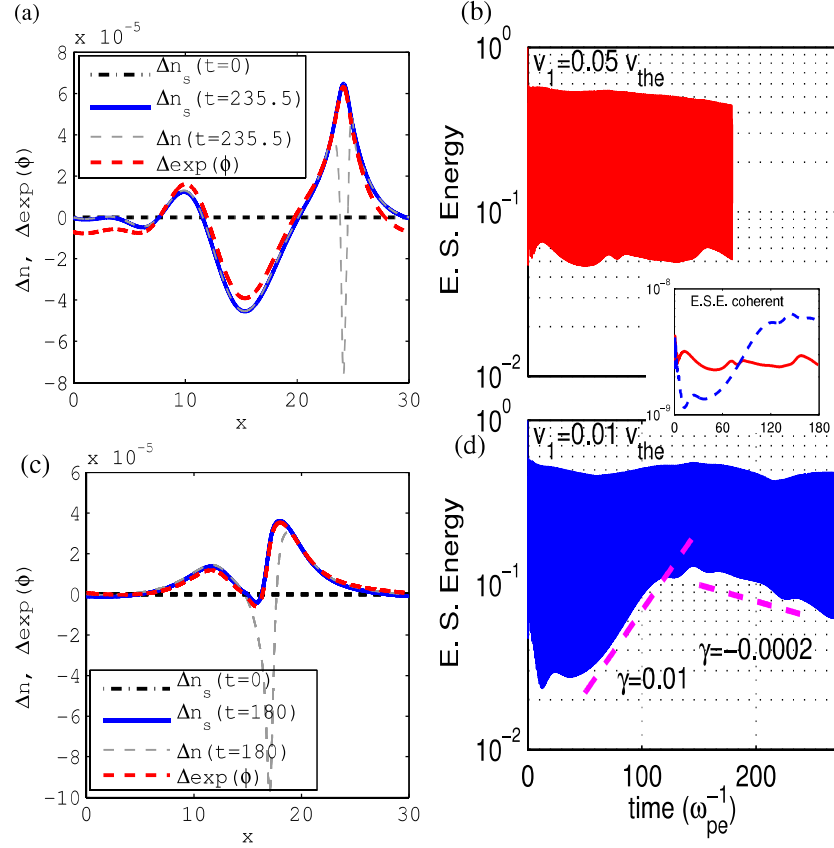
Figure 6.3: (a) Streaming and net electron density perturbations and that obtained from the inertia free electron momentum balance for a stable hole and (c) for a unstable growing hole. (b) Total electrostatic energy of the system for the case $v_1 = 0.05v_{\text{the}}$ and (d) for $v_1 = 0.01v_{\text{the}}$.

expression for distribution functions for electrons and ions are [1]:

$$f_e(x,v) = \frac{1+K}{\sqrt{2\pi}} \begin{cases} \exp\left[-\frac{1}{2}\left(\sigma_e\sqrt{2\epsilon_e} - v_{\text{eff}}\right)^2\right], & \epsilon_e > 0 \\ \exp\left(-v_{\text{eff}}^2/2\right)\exp\left(-\beta\epsilon_e\right), & \epsilon_e \leq 0; \end{cases}$$

(6.3)

$$f_i(x,u) = \frac{1+A_e}{\sqrt{2\pi}} \begin{cases} \exp\left[-\frac{1}{2}\left(\sigma_i\sqrt{2\epsilon_i} + u_0\right)^2\right], & \epsilon_i > 0 \\ \exp\left(-u_0^2/2\right)\exp\left(-\alpha\epsilon_i\right), & \epsilon_i < 0; \end{cases}$$

(6.4)

In these equations K and A_e are the normalized constant for electron and ion distribution function respectively. $\sigma_e = sg(v)$ is the sign of electron velocity, $\sigma_i = sg(u)$ is the sign of ion velocity, $\epsilon_e := \frac{v^2}{2} - \phi(x)$ is the single particle energy for electron, $\epsilon_i := \frac{u^2}{2} + \Theta(\phi(x) - \psi)$ is the single particle energy for ion and $v_{\text{eff}} = v_D - v_0$, where v_D describes a given constant drift between electron and ion existing already in unperturbed state. The unperturbed distributions, (6.3)-(6.4), are assumed to be shifted Maxwellian formulated in a frame moving with v_0 in the electron phase space and with u_0 in the ion phase space. $u_0 = \mu v_0$, where $\mu := (m_i T_e / m_e T_i)^{1/2} \equiv (\Theta/\delta)^{1/2}$, T_e and T_i are the electron and ion temperatures, respectively, Θ and δ are the temperature and mass ratios, respectively. Using these two distribution functions in the Poisson equation one can derive the nonlinear dispersion relation (NDR) [1],

$$
\begin{aligned}
k_0^2 \quad &- \quad \frac{1}{2} Z_r' \left(v_{\text{eff}}/\sqrt{2} \right) - \frac{\Theta}{2} Z_r' \left(u_0/\sqrt{2} \right) \\
&= \quad \frac{16}{15} \left[\frac{3}{2} b(\alpha, u_0) \Theta^{3/2} + b(\beta, v_{\text{eff}}) \right] \psi^{1/2} = B,
\end{aligned}
\tag{6.5}
$$

where, $Z_r(x)$ is the real part of the plasma dispersion function. The quantities $b(\alpha, u_0)$ and $b(\beta, v_{\text{eff}})$ are given by,

$$
b(\alpha, u_0) = \frac{1}{\sqrt{\pi}} \left(1 - \alpha - u_0^2 \right) \exp(-u_0^2/2)
$$

$$
b(\beta, v_{\text{eff}}) = \frac{1}{\sqrt{\pi}} \left(1 - \beta - u_0^2 \right) \exp(-v_{\text{eff}}^2/2)
$$

where β and α are the trapping parameters for electrons and ions, respectively, $\alpha = 1$, corresponding to no trapping of ions. The NDR (6.5) determines the phase velocity of structures (v_0 and u_0) in terms of v_D, k_0^2, Θ, ψ, α and β. Depending upon the values of k_0^2 and B, four type of solutions are possible: solitary electron hole (SEH) ($k_0^2 = 0$), harmonic wave ($B = 0$, $k_0^2 > 0$), solitary potential dip (SPD) ($B < 0$ and $k_0^2 > 0$) and cnoidal electron holes (CEH) ($B > 0$ and $k_0^2 > 0$). In present simulation $\alpha = 1$, since ions are not trapped in the coherent structures $\psi \sim 10^{-4}$, $v_D = 0.05$ and $\Theta = 10$. Using these values in NDR, v_0 can be obtained as a function of ψ for fixed values of k_0^2 and β. Solid lines in Fig. 6.4 present this relationship using $k_0^2 = 0$ (required for SEH solutions) and $\beta = -60, -80, -100, -120$ and -140, respectively.
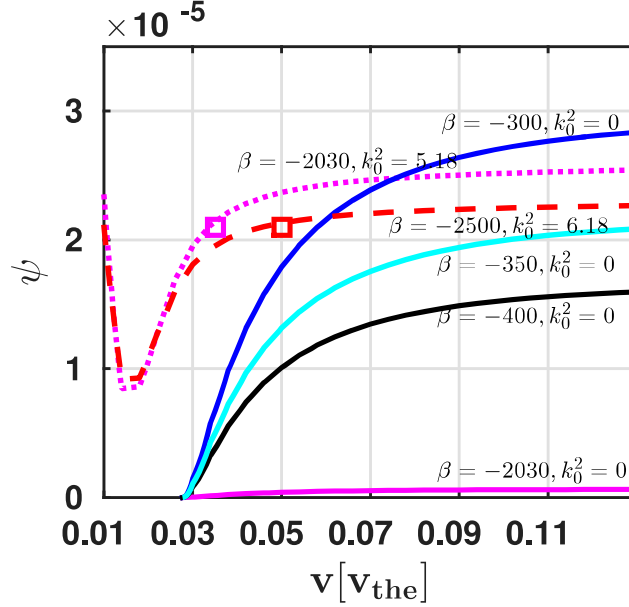
Figure 6.4: Plot of maximum potential ψ of electron hole vs. velocity v for $v_D = 0.05v_{the}$ and $\Theta = T_e/T_i = 10$. Contours of $k_0^2 = 0$ (SEH) are plotted for different value of β value.

Two additional curves in Fig. 6.4 present this relationship for CEH-like solutions with $k_0^2\lambda_D^2 = 6.18$ (dashed line) and $k_0^2\lambda_D^2 = 5.18$ (dotted line). Each curve corresponding to $k_0^2 = 0$ starts with a minimum velocity $0.03v_{the}$ showing that no SEH ($k_0^2 = 0$) solutions are possible bellow this velocity at this temperature. The region below the solid curves presents the solution for $k_0^2 > 0$ (providing harmonic waves and CEHs solutions) while the region above them is unstable with $k_0^2 < 0$, or imaginary values of k_0 (providing only monotonic or shock-like solutions) meaning unstable evolution of SEH-like initial conditions, as in phase-1 of case-II. Note that for each curve the velocity of the structure (with fixed β and k_0^2) increases with increasing ψ, also explaining the phase-2 of parametrically unstable evolution where a net pressure imbalance results in higher ψ, thereby accelerating the structures to higher velocities.

We note that the coherent structures in our simulation have $\beta=$ -2030 and -2500 for $v_1 = 0.01v_{the}$ and $0.05v_{the}$, respectively, but they correspond to $k_0^2\lambda_D^2 = 5.18$ and 6.18, respectively, rather than $k_0^2 = 0$ expected of ideal SEH solutions. The two simulated cases are marked by square boxes at their respective velocities and amplitudes. Considering that the parameters from the center of the simulated
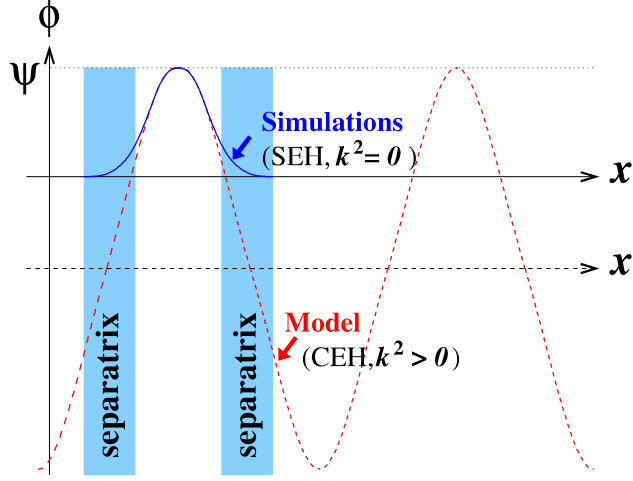
Figure 6.5: Schematic of structure in simulation and model

structure are substituted, this discrepancy can be traced in the ideal nature of the separatrix in the used SEH model. We find that despite the visible solitary nature of the simulated structures, they are associated with finite k_0^2 class of ideal solutions. Due to presence of a nonideal separatrix, these ideal high $|\beta|$, finite k_0^2 solutions misread the background plasma potential as rather deeper than ψ in simulation. In simulations, ψ is smaller when measured with respect to the value $\phi = 0$ of the plasma background. An ideal background plasma, as perceived by the model for the ideal finite k_0^2 solutions is shown schematically by dotted line in Fig. 6.5. The ideal SEH model nevertheless analytically describes the unstable evolution of the SEH in the simulations, and perhaps in nature, with sufficient clarity, identifying their growth as driving turbulence in the collisionless plasmas.

6.6   Summary and conclusion

The results and analysis in this chapter numerically verified key predictions of Chapter 5 based, themselves, on results of Chapter 3 and 4 where the trapped particle equilibria in ion acoustic and electron acoustic regimes were examined, respectively. The simulations using two cases of initial conditions are used to verify the conclusions from Chapter 5, that the plasma stability is rather defined by nonlinear structures that might destabilize by non-conventional means. The growth could appear, for example, in terms of parameters other than amplitude of

the eigenmodes of linearized Vlasov equation or by an effective mode conversion from ion dynamics dominated regime to electron dynamics dominated regime.

Analogous to the linearly undamped eigenmodes $\phi(x)$ contained in an initial perturbation that get destabilized by phase-mixing-away the unsupported transient in the linear Vlasov evolution, the destabilization here is shown to take place of the undamped mode-coupled nonlinear structures $\Phi(x)$ contained in an initial small amplitude phase-space eddy-like perturbation. When the latter is evolved in a linearly subcritical plasma, we see additionally undamped structures that obey the existing analytic description of such mode-coupled structures prescribed to replace discrete eigenmodes of the linearized approximate Vlasov equation in a nonperturbative exact plasma stability analysis. The coherent $\Phi(x)$ generated at a slower phase velocity is further seen to be destabilized by defying the sign of $\partial_v f(v_0)$ and grow, rather in their phase-velocity dimension than in their amplitude, to effectively mode convert into a more stable, ion acoustic electron hole. The linearly undamped modes, namely, the EPW and IAW modes excited by the initial perturbation are duly recovered to be stable because of the evolution done in a subcritical drift regime, unlike the strong drift cases where ion acoustic mode displayed stronger growth while no phase-space eddy perturbation were seeded preventing independent electron hole structures to grow.

Unlike their evolution in the linearized Vlasov regime where the electron holes get treated as transient and immediately buried (or damped), the two identical initial perturbations, differing merely in the initial velocity of their launch, show a remarkably distinct evolution in which both the cases evolve not only to show electron holes as undamped structures alongside the undamped linear eigenmodes, the latter, slow initial perturbation cases undergoes a set of strong nonlinear hole instabilities as well.

Among two kinds of unstable evolution identified in the simulation at a faster and slower rate, respectively, in the first unstable phase the perturbation makes and approach to a set of undamped modes including an electron hole and the conventional linear plasma modes, namely the EPW and IAW. In the secondary stage of evolution these undamped structures interact with each other and further destabilize each other, parametrically. These two unstable phases of nonlinear structure growth/mode-conversion are described as two distinct instabilities, namely, the electron hole instability and a parametric instability arising from mutual coupling

between the undamped linear and nonlinear structures.

In analytic description of the observed growth of undamped structure is provided where the basis of the mechanism is analyzed by employing the general nonlinear dispersion relation involving both electrons and ion response. It is quantitatively displayed that in a graphical characterization of the NDR, each curve corresponding to $k_0^2 = 0$ starts with a minimum velocity $0.03v_{the}$ showing that no SEH ($k_0^2 = 0$) solutions are possible bellow this velocity at corresponding temperature. The region below the curves representing solitary solutions of the formulations presents the solution for $k_0^2 > 0$ (providing harmonic waves and CEHs solutions) while the region above them is unstable with $k_0^2 < 0$, or imaginary values of k_0 (providing only monotonic or shock-like solutions) meaning unstable evolution of SEH-like undamped structures, as recovered in the later phase of slowly propagating initial perturbations.

The discrepancy of evolution in simulation visible with respect to the analytic characterization is traced in the ideal nature of the separatrix in the used SEH model. We find that despite the visible solitary nature of the simulated structures, they are associated with finite k_0^2 class of ideal general solutions. Due to presence of a nonideal separatrix, these ideal high $|\beta|$, finite k_0^2 solutions misread the background plasma potential as rather deeper than ψ in simulation. In simulations, ψ is smaller when measured with respect to the value $\phi = 0$ of the plasma background. The ideal SEH model nevertheless analytically describes the unstable evolution of the SEH in the simulations, and perhaps in nature, with sufficient clarity, identifying their growth as driving major part of turbulence in the collisionless plasmas.

7

Conclusion and Future Scope

The collective excitations and structures are at the heart of the physics of the plasma state of matter. They fundamentally characterize any quasineutral collection of charge particles as plasma [28, 131–135]. The character of collective activity in plasmas as well as complexity and rigor of the formulations that describe these collective plasma excitations assume quite different dimensions depending upon the parameter regime of the plasma, especially the parameters that determine its collisionality. In collision-less regime the long range coulomb force is much more important than the interaction with near neighbours or collisions. This is mostly in terms that hot collisionless plasmas do not admit many routine assumptions that can generate extensive simplification to produce a certain standard order in the nature of collective structures in collisional plasmas where species distribution functions are highly thermalized and have a common equilibrium form [28].

The strong collisionality allows use of fluid theory and the features like nonlinearity appear only at large amplitudes that are sufficient to affect full thermalized distribution function, or entire population of species at any given spatial location of interest. As opposed to this, nonthermal distributions allow resonant effects where only a resonant part of population of species, within certain small velocity interval, can cause spatial nonuniformities that persist and evolve deterministically over longer times due to adiabaticity of the species distributions. While formulations based on thermalized or equilibrium distributions remain applicable to the majority of collision-dominated plasmas, more general notions and formulations based on kinetic or nonthermal distributions apply to physics of collective structures in hot collisionless plasmas, as addressed in the studies presented in this

thesis. Apart from dynamical properties of collective structures, these generalizations have implications for many conventional aspects of basic plasma theory of collective structures and plasma stability. Below we present a brief specific discussion on them, followed by more general conclusions from individual chapters.

The central conclusions from this work relate to the advanced structure of theory of plasma collective structures and stability. The simulation results and their analysis done here highlighted that although the linear kinetic approaches adopted by Landau [11] and van-Kampen [47] presented an apparent contrast in their conclusions, they addressed two fundamental aspects of equal importance. While the linear approach proposed by L. D. Landau usefully provided a prescription, and an essential set of elements, for development of a stability theory for the plasmas, the van-Kampen's conclusions hinted about the prescription for the generalization of the same plasma stability theory.

As it is clear from the aspects related to entropy in collisionless system briefly discussed in Sec. 1.4.1 and 1.4.5, the Landau theory admitted thermalization, via entropy maximization, of the entire *equilibrium distribution* f_0 by considering limited number of poles corresponding to the discrete normal modes of this thermalized distribution. The Landau theory approximated further evolution via an entropy conserving process, and by considering finite number of modes (poles) of a thermalized distribution at fixed phase velocities, limited the possibility of modification of the collective structures by kinetic nonlinear effects that would essentially modify the poles by modifying the phase velocities. The attempt, by H. Schamel, to develop a more advanced theory of plasma collective structures, and therefore of the plasma stability, extended the realistic idea of thermalized distributions, by entropy maximization, to the next higher level of the particles trapped in the collective structures. Admission, by Schamel, of an explicit and parametrized trapped particle distribution, achieved once again by entropy maximization at trapped particle level, effectively fixed the shortcomings of two most important alternate futuristic models of plasma collective structures, namely, the linear van-Kampen model and the fully nonlinear BGK model. The Schamel structures are rather closer to small amplitude constituents of the noise required by the turbulence to operate. It is hence expected that their destabilization mechanism must also be closer to fundamental operating mechanism of the turbulence and would generalize the linear Landau theory based threshold nature of the plasma stability paradigm.

142

These general destabilization mechanisms predicted by Schamel [25] however remain largely unfamiliar at the present stage of the plasma stability theory. In this respect, the simulations in the present thesis have attempted to illustrate their limited examples (e.g., in Chapter 6), once again by making only little excursion out of the boundaries of strongly thermal equilibria considered for both streaming and trapped particle distributions, and in a limited range of plasma parameters. Coincidentally, the same limitations apply to more generalized approaches, e.g., Schamel, which therefore find excellent agreement with both simulations and accessible classes of laboratory and natural plasmas.

In the following text we present a chapter wise description of conclusions from the individual chapters of the thesis.

The **Introduction** of the thesis, or the first chapter, reviewed important aspects of the plasma physics in the light of existing formulations of plasma collective structures and theories of plasma stability in collisionless plasmas. The content of Introduction mainly highlight the physics that, the fast electron response to electrostatic perturbations is inhibited, for example, by the kinetic effects where resonant electrons are either reflected or get trapped by even small potential nonuniformities. The oscillations of trapped particles add to the degrees of freedom [32] and result into phase-space vortices [24] that can modify the spatial nonuniformities associated with the vortex depending up on the trapped particle density as well as the amplitude of nonuniformity. The analytic structure of trapped particle equilibria is extensively analyzed in various limits, e.g., where trapped particles can be maintained in isolated non-thermal states and the exact nonlinear solutions are obtained as Bernstein-Greene-Kruskal (BGK) modes [3], and for the cases where the trapped particles are well approximated as having an equilibrium distribution with finite *temperature* [1, 25, 46]. In the later limit, considered analytically in great detail by H. Schamel, it was shown [1] that the nonlinearity introduced by the amplitude dependent density of trapped particles influencing the local potential, can substitute the more conventional sources of nonlinearities in plasmas to produce an alternate range of interesting nonlinear solutions. Their mathematical forms include a potential hump or solitary electron hole (SEH), a cnoidal electron hole wavelet (CEHWL), and a solitary potential dip (SPD) [1]. A large class of structures in laboratory and natural plasmas perhaps follow this description which admits a far restricted entropy production rate and hence displays a wider agree-

ment with a range of structures recovered both in experiments and in computer simulations.

The phase-fluid continuity of the collisionless Vlasov-Poisson system, forming the basis of the numerical model developed and implemented to carry out present studies, is described in Chapter 2. Standard electrostatic plasma modes and their dispersion properties are shown to be successfully recovered by performing test runs of the simulation with typical plasma parameters and system size. The adopted numerical procedures is additionally shown to have high potential for an efficient parallelization and the detailed scheme for the parallelization based on the MPI and Open-MP standards is described with the achieved effective speed up as a function of increasing number of computing nodes.

The numerical characterization and physical validation of the procedure using electrostatic plasma mode simulations are resulted in the following conclusions. For the cases where the electrostatic energy corresponding to the electron plasma waves damps with a faster Landau damping rate, the residual oscillations in the conserved quantities correspond to the periodic displacement of the distribution function in the phase-space, arising from the periodic interaction of counter-propagating collective ion acoustic wave structures. The displaced distribution function yield displacement dependent values of velocity integral performed with limited velocity space boundaries as opposed to those ideally located at infinity. For physically acceptable numerical solutions, the oscillations in the conserved quantities and norms are suitably ensured within a tolerable limit by choice of the velocity space boundaries for the individual species.

The agreement of simulation results with standard analytic physical results is successfully recovered for typical plasmas for which standard sinusoidal perturbation was used to excite 1D electrostatic modes in a finite electron and ion temperature Maxwellian distribution of both the species. Apart from recovering the real frequencies of the electrostatic electron plasma and ion acoustic modes to a sufficient accuracy, the implemented simulation procedure also recovered the fundamental kinetic characteristics like collisionless Landau damping of these electrostatic modes. In the low k regime of weak Landau damping, the examination of regions of ions and electron phase-space close to the phase velocity of the respective modes reveals the existence of highly stable trapped particle equilibrium structures arising from trapping of charged species resonant with the phase veloc-

ities of the recovered electrostatic modes. These trapped particle equilibria and the nonlinearity associated with them are further analyzed in sufficient detail by means of the developed simulation procedure in rest of this thesis.

The adiabatic electron response and process of solitary wave generation by trapped particle nonlinearity are presented in Chapter 3. The coherent structures provide very effective first signatures of the nonlinearity in collective modes as discussed in Chapter 1. Among the electrostatic plasma modes the ion acoustic response shows most visible signature of nonlinearity by readily producing ion acoustic solitons and solitary waves for finite amplitudes. The ion acoustic structures therefore serve as an ideal paradigm for nonlinlinearity produced coherence in the plasma theory and their growing phase is investigated.

We have presented results of a two species Vlasov simulation featuring self-consistent generation of solitons produced from a stronger nonlinearity originating from the kinetic effects of trapped electron population in a finite amplitude ion acoustic acoustic wave driven unstable by a current driven microinstability. The numerical simulations presents a general time dependent evolution of the particle distribution functions that obey the collisionless Vlasov equation. The simulations are motivated by solitary structures predicted by nonlinear nonperturbative formulation based on the Vlasov-Poisson system that reduces into a m-KdV equation. In order to effectively compare the evolution usually recovered by conventional linear procedure using harmonic (cosine) density perturbations, the investigation is done by selecting this class of perturbations as initial conditions.

In the initial phase of evolution, a remarkable modification in the distribution function is visible at the ion acoustic velocity. Since generation of vortex like structures in electron phase space distribution results in the diminishing gradient of the electron distribution function $\partial f_e / \partial v_e$ at the resonant velocity which must be nonzero for the linear growth in the ion acoustic wave, the evolution the observed saturation in wave growth indicates a nonlinear saturation of the growth where the resonant particles act to flatten the zero order electron distribution, allowing $\partial f_e / \partial v_e \to 0$ at the phase velocity of the wave. We have noted that at an amplitude quite comparable to its initial sinusoidal stage at $t = 10\omega_{pe}^{-1}$, the strong nonlinear effects begin to appear in the IAW at $t = 31\omega_{pe}^{-1}$ and beyond. In the secondary phase the growing nonlinear wave, depending on the allowable k values in the simulation, either develops into a train of solitons of various heights and

speeds, or produces a single soliton structure. The amplitude evolution at longer times shows that the growth of this nonlinear wave or structures is arrested as the structures begin to trap the resonant electrons and, in turn, their amplitudes begin to approach corresponding saturation values. In this saturated phase a trapped particles (electrons) instability [37] is the mechanism responsible for the observable residual growth in the nearly saturated soliton amplitude that shows a modulation with the frequency equivalent to the electron bounce frequency ω_{be}.

The nonlinear coherent soliton structures have developed in the simulation are shown to follow the analytical solutions of mKdV equation that accounts for the stronger nonlinearity produced by the electron trapping in the structure. In the low k regime where the structures coexist and interact with the undamped high frequency electron plasma waves, the nonlinear soliton structures retain their modified nonlinear analytic structure as long as the trapped electron distribution is allowed to be in a thermodynamical equilibrium. For the structures where associated trapped electron equilibrium is perturbed by a time dependent variation of the trapping potential, it is difficult to characterize the trapped electron distribution using the equilibrium parameters. In the conditions where the developing ion acoustic structures are free from time dependent perturbations, the numerically simulated coherent structure could be characterized analytically, by finding from them the necessary parameter to construct the corresponding analytical solutions and carry out the comparison of the simulation results with the theoretical formulation that leads to a modified KdV equation with a stronger nonlinearity. The modified Sagdeev potential, $\mathcal{V}(\phi)$, corresponding to the numerically simulated solutions is also constructed and verified to confine the electrostatic potential $\phi(x)$ in the limits of the observed soliton structures.

Relatively small amplitude coherent structures coexisting with a periodic self-consistent potential perturbation are found to be most affected by the adiabatic response of the electrons. Presence of a self-consistent time dependent perturbing potential, present in the form of an EPW in the simulations, prevents the trapped electrons from reaching an equilibrium and forming stable BGK modes that are time independent stable solutions of the Vlasov equation. Although the coherent ion acoustic solitary structures with such a transient trapped particle population are observed and found to be reasonably stable. In the cases where EPW is undamped, it is well resolved in our simulations and visible as a well de-

146

veloped undamped BGK-like structure at the electron phase velocity v_{phase} in the electron distribution function. This indicates that for the cases where the electron bounce frequency exceeds the Landau damping rate of the EPW, $\omega_{be} > \gamma_{\text{L}}$, a stable BGK mode develops and arrests the linear Landau damping of the EPW, unlike the cases where $\omega_{be} < \gamma_{\text{L}}$ and a linear landau damping of EPW must result. We also compared the relative strengths of the kinetic nonlinearity generated by the trapped particles with the conventional fluid nonlinearity by means of the solutions of m-KdV equation 3.1 for the recovered solitary electron hole parameters. It is seen that with increase in the value of the coefficient $(1 - \beta)$ of the trapping nonlinerity, the solution modifies from soliton having only fluid nonlinearity to the soliton having only the trapped particle nonlinearity. In the present simulation of generation of IA-solitary waves in presence of current, we have recovered the solitary soluitons of sufficiently small amplitudes within the regime of trapped particle nonlinearity. Therefore, it can be suitably concluded that at small amplitude regime the trapped particle nonlinearity dominates over the fluid nonlinearity.

The physics of nonlinearly interacting trapped particle solitons in collisonless plasmas is presented in Chapter 4. The phase-space vortex structures, or SEH, seen in chapter 3 to be generated from unstable plasma modes that grow in amplitude, trap particles, and subsequently enter a trapped particle governed nonlinear limit, motivated studies in Chapter 4. The theoretical results of Schamel [1], neglecting ion mobility, are treated as initial conditions for the simulations that fully account for evolution of both electron and ion kinetic distributions. It is understood that in the absence of external driving, the structures tend to develop isolated, near equilibrium, trapped particle distributions and therefore are well described by the SEH formulations based on this approach. The present simulations suggest that such model for the trapped particle distributions remains largely valid for the laboratory and natural plasmas, including those in magnetospheric plasmas that could be well described by the present simulations.

The motivation that the stable analytic SEH solutions must propagate as natural nonlinear excitations of the collisionless plasma is validated based on the understanding that the numerical simulation indeed evolve a near thermodynamically equilibrated population of the particles trapped in the coherent structures. This population produces a strong trapped particle nonlinearity arising from its sensitivity to wave/structure amplitude, bringing, in turn, an amplitude dependence in

its dispersion, characteristic of nonlinear waves and coherent structures.

The analytic form of electron distribution implemented as initial conditions for the SEH simulations shows propagation without much distortion or radiation unless perturbed by other structures, validating the *a-priori* adoption of them as most suitable initial conditions. Although the evolved stable SEH in the simulations have additional attributes when compared to rather approximate analytic solutions given by (4.6), they show only reasonable deviations from the analytic structure (largely related to numerical aspects), not detrimental to their stability predicted under the adopted analytic SEH formulation [36].

The present simulations show that the structures well separated by a relative velocity along the velocity dimension ($\Delta v_0^2 > \psi$) have only an adiabatic modification in the trapped particle distribution, not resulting in fine structures in the phase space. The cases of structures separated by smaller relative velocity ($\Delta v_0^2 < \psi$), on the other hand, show generation of substructures in the trapped particle populations because of longer time of the interaction. Sharper phase-space gradients existing over longer duration results in larger diffusion in the phase-space, indicating a larger rate of entropy production.

A successful elimination, using the Fourier reconstruction, of the high frequency linear modes from the solitary wave data, indicates that the superposed fast modulations are indeed well modeled by the systematic mutually noninteracting linear plasma oscillations which also do not interact strongly enough with the solitons of nearly same amplitude. Since the equally small amplitude solitons propagate coherently without oscillations at velocity much smaller than the phase velocity of the electron plasma wave, their constituent modes are clearly coupled via the alternate means provided by the strong trapping of a large density of resonant particles within these localized structures.

The reasonable agreement of electron hole observations in nature and laboratory experiments with both kinds of interactions, where the structures interaction produces minimum modification to individual solitons and where the solitons are fast modified and merge, is noted in respective regimes. These comparisons must allow quantitative determination of thermodynamic regimes of the finite amplitude plasma structures, or the plasma turbulence at large, in specific cases of interest in advanced studies of plasma waves, instabilities and turbulence. In two sets of the relevant comparisons we have shown in the first set: that in the cases of the first

148

kind of interaction (identity preserving), the electric field profiles from selected stages of evolution show the non-interacting solitons correspond to a bipolar electric field, while the pairs of dissimilar solitary electron holes produce, during the initial phase of their passage through each other, a tripolar (two smaller positive pulses separated by a large negative pulse) electric field pulse. In the second set of comparison with various existing observations in laboratory plasmas it is highlighted that, as seen in second kind of interaction (non-identity preserving) at small relative velocity between two coherent structures two holes attract each other like particles of negative mass and coalesce, for example, in Q machine experiment by Saeki *et al.* [13]. In another example, the stable proton cluster developed from the negative mass instability, experimentally observed in Oak Ridge DCX-1 mirror machine, were compared to two-stream instability simulated by Berk *et al.* [39, 81] showing the similar merger using a simplistic *water bag model*.

The physics of evolving trapped particle structures and its implications on plasma stability are discussed in Chapter 5. In this chapter, a current-driven, 1D, collisionless plasma is considered as a paradigm of driven intermittent plasma turbulence and anomalous transport with the focus on additionally excited *undamped coherent* electrostatic structures excited alongside the familiar undamped linear plasma modes. The simulation presented have thus explored the concept of plasma instability in terms of more general fundamentally nonlinear structures, outside the conventional linear regime which is limited to covering largely the undamped collisional plasma eigenmodes, that are additionally subjected, by means of Vlasov equation, to interaction with resonant particles. Simulations explore evolution of more relevant forms of perturbations in the species phase-space and display activity of undamped structures that are small amplitude trapped particle equilibria existing alongside the conventional collective linear wave equilibria of the thermalized plasmas recovered in collisional fluid-like limit. In the analysis of simulation output, a wave description is employed which, in its fundamental form, accommodates the nonlinear aspects arising from the kinetic effects like particle trapping and recovers the linear Vlasov descriptions as one of its limiting cases.

The simulations, beginning from small amplitude phase-space eddy like initial perturbations realizable in a nonthermal noise, evolve the distributions to show undamped coherent structures, apart from the well known linearly undamped modes

of the thermal plasmas, namely the electron plasma and ion acoustic waves. Numerically, a rapid relaxation within about 100 plasma periods is seen, released by an eddy-like initial fluctuation, in which both types of structures emerge time asymptotically. The additional undamped structures traveling at an unusual phase velocity (about twice c_s) disagree with linear description and are absent from the simulations performed using a linear Vlasov simulation procedure.

In our analytic description based on three different levels, we have constructed stationary electrostatic structures, which constitute a continuous spectrum, determined by electron trapping. Members of this mode continuum are the well known discrete modes (Langmuir, ion acoustic), which arise in the limit of vanishing trapping at high phase velocities (with respect to electron thermal and ion thermal velocity, respectively), and the cnoidal electron and ion holes, which are entirely due to trapping and belong to the non-dispersion branches of the nonlinear dispersion relation. There is no general way to establish a link between the linear discrete mode spectrum, being masked by singularities in the associated distributions, and the class of well-behaved nonlinear trapped particle structures even in the infinitesimal amplitude limit. This has the consequence that in case of coherency the onset of instability as described by Landau is generally absent when seen realistically from the standpoint of the complete Vlasov-Poisson system. It is replaced instead by a more complex, highly unknown destabilization process in phase space, in which this manifold of trapped particle equilibria with its attracting negative energy property together with the explicit initial perturbation will play an important role. This renders plasma destabilization multifaceted and as a rule - no longer one-dimensional in parameter-space, i.e., involving growth not only in the amplitude that remains sole parameter in all linear theories.

Under these premises plasma stability theory is still in its infancy. Publications on this subject usually rest on perturbative nonlinear models in which linear wave theory provides the lowest order approximation (such as in [88, 89]). The impact of the trapping nonlinearity is typically not allowed for. An exception is the work of Dupree [5] in which, as described in the Introduction, the stability of a solitary ion hole in a current carrying plasma is investigated (see also [117]), however with a limited rigor. Especially his (and Tetreault's) very first questioning of the role of linear instability together with the discovery of a nonlinear threshold well below the linear one, must be considered are remarkable results. If approved by a

more straightforward stability strategy [136] they may pave the way for a better understanding of plasma stability. A new horizon for plasma stability may hence be seen, for example, by considering the whole family of cnoidal hole modes as potential candidates for growing structural elements. This would keep the demand that in the collisionless plasma limit the trapping nonlinearity has to be taken into account from the outset, or from their presence in initial nonthermal plasma noise.

In our study, the coherent structures are characterized in the stationary regime by the existence of a pseudo-potential $\mathcal{V}(\Phi)$. This implies that if the structure has a higher harmonic content $\Phi(x) = \sum C_k \exp[i(kx + \varphi)] + c.c.$, such as for a true cnoidal wave solution, the phase φ is common for all subharmonics and it holds for the whole wave packet $\partial_{xx}\Phi(x) = -\partial_\phi \mathcal{V}(\Phi)$, i.e. the curvature of Φ (or charge separation) can be expressed by Φ again through the pseudo-potential $\mathcal{V}(\Phi)$. This is different to the common linear superposition of harmonics in the linear framework, such as van-Kampen or Landau modes, $\phi(x) = \sum C_k \exp[i(kx + \varphi_k)] + c.c.$, in which each individual mode has its own phase φ_k, independent of each other. Although, through the linearity of the solution for which the superposition principle holds, the composite solution remains a solution, the curvature (charge separation) $\phi''(x)$ is no longer representable by a $\mathcal{V}'(\phi)$, i.e. the coherent character of ϕ is lost.

One underlying reason of incoherency is of course that within the linear approach a mechanism which can synchronize the phases is missing. For such a perturbation the only fate is damping due to phase mixing as proposed by Landau [11], as recently taken up again by Wesson [120]. For a perturbation with a spectrum of individual modes one can hence distinguish already on the macroscopic level the structureless perturbation $\phi(x)$, such as in a quasi-linear evolution, from the coherent structure $\Phi(x)$, see also [137–139]. In the latter, the kinetic trapping nonlinearity does the job of phase locking. Another verbal expression of the failure of linear wave theory in describing stationary coherent structures is simply its inability to describe with its straight line characteristics the curved orbits stemming from the wave-particle interaction process, a property being true up to infinitesimal amplitudes.

We mention that John Wesson [120] in his alternative treatment of the Landau approach, where he used real variables and straightforward algebra, nicely explains Landau damping by phase mixing of ballistic particles. The latter have

to be incorporated in order to get within the transition from damping to growth an identical expression for the growth- and the damping-rate, respectively, a constraint, which however lacks necessity and is simply imposed artificially. The well known expression, $\gamma \simeq f_0'(v_0)$, is then obtained by setting the out-of-phase part of the density perturbation equal to zero. It should be noted, however, that his analysis faces the same problem than Landau's one, namely that as $\gamma \to 0$ the distribution function becomes inevitably singular. In other words, the underlying linear Vlasov approach suffers a breakdown near $\gamma = 0$ in a manner such that the transition (in combination with coherency and resonant particles, the essential ingredients in case of zero damping or growth) is no longer feasible in the context of the full Vlasov equation.

On the other hand, this breakdown of the linear Vlasov approach is absent as long as one stays well in the damped region, as mathematically shown by Mouhot and Villani in their pioneering work [118, 119]. And indeed, in an another linear treatment, Belmont *et al.* [121] could find non-Landau solutions by essentially replacing van-Kampen modes through non-singular, decaying wave packets in their linear superposition procedure. As a result a weaker damping scenario could be achieved. Vanishing damping (or growth), however, was not contained and admitted in their wave spectrum. This is, however, not surprising because zero damping demands nonlinearity by which Landau's scenario of destabilization is generally abolished. Its correction by lifting the scenario on a higher, nonlinear level is, however, somewhat more intricate as plasma destabilization especially in the subcritical region will not only depend on the variety of hole modes (of negative energy modes preferably) but also on the initial perturbation. A threshold criterion depending on a single parameter, such as the drift velocity v_D, will as a consequence no longer exist or may exist only under very specific conditions, the latter being an open issue is investigated partially in Chapter 6

It is of interest to mention further that Belmont *et al.* [121] already found at the linear Vlasov level a sensitive dependence of the evolution on the initial conditions, implying a non-uniqueness of the linear, asymptotic solution, as we have discovered from the difference between a $\lambda = 0$ van Kampen and a $\gamma = 0$ Landau solution (ignoring their invalidity). Their prospect of "a change in our understanding of the role of the resonant particles" would have been complete, however, only if they had considered additionally nonlinear trapped particle effects. In case of

coherency the latter have a stronger, more profound influence than prognosticated by the authors. This is especially evident through our non-dispersive, $B \neq 0$ modes of the continuous spectrum.

Does this now mean that the concept of growth based on Landau's theory is completely out of the game? The short answer is no, only its validity is limited to special parameter and temporal regimes. In more detail, however: it does remain relevant as deviations from the mentioned prerequisites can reestablish the standard wave concept. If, for example, the plasma is sufficiently quiet and the initial fluctuation spectrum essentially broad band harmonic, uncorrelated and of topological type (i.e. (5.7) holds) then linear Vlasov description will be valid for some time and with it - the Landau's theory. In case of an *unstable* plasma, the growth (and damping) of modes will take place as in the linear sense up to the bounce time after which the saturation of the most growing mode by particle trapping will terminate the linear phase, initiating a delayed structure formation process. Time-asymptotically, an intermittent, steady state plasma turbulence will then arise being characterized by a collection of trapped particle and allied structures. An initial single harmonic and hence coherent perturbation, however, is already sufficient to invalidate the linear growth scenario, for trapping and the associated nonlinearity will dominate the evolution from the very beginning, as seen in the recent numerical simulations of Hou *et al.* [140, 141]. The adaptation of the system to a non self-consistent initial perturbation introduces particles that are in phase with the wave and undergo a resonant interaction and subsequent trapping process from the outset.

It is worth mentioning that subcritical plasma instabilities, being associated with structure formation and hence beyond any Landau scenario, are meanwhile omnipresently observed in plasma simulations of driven plasmas [22, 54, 85, 122–124], in space or laboratory observations, such as [15, 125] and last, but not least, in particle accelerators. This latter area of applications refers to coasting and bunched beams in synchrotrons and storage rings, represented by Vlasov-Poisson systems. In the Fermi Main Ring, for example, operating near stability limit [52], sharp gaps or notches have been witnessed in the response function [62], which correspond to depletion zones in the momentum distribution function. This is seen at the lowest measurable signal level and sheds light on the spectrum of small amplitude perturbations, proving the incompleteness of linear and associated nonlinear

wave theories in the kinetic regime [54, 113, 126–128]. A similar phenomenon, namely stable, coherent, longitudinal structures superimposed on bunched beams [63], has been observed during "rf activity" in stochastic cooling studies [64, 65]. A well documented excitation of holes below linear threshold could be seen also in numerical simulations of pair plasmas in [85] as well as in the laboratory experiments of Moody and Driscoll [61]. And finally, it would be an intriguing task for future investigations to link the present nonlinear destabilization mechanism with the observed reorganization into coherent structures of driven collisionless magnetospheric plasmas at increasing turbulence levels [129].

The electron hole instability of subcritical plasma phase-space perturbations, as recovered in the simulations, are elaborately presented Chapter 6. The results and analysis in Chapter 6 numerically verified key predictions of Chapter 5, based, themselves, on results of Chapter 3 and 4 where the trapped particle equilibria in ion acoustic and electron acoustic regimes were examined, respectively. The simulations using two cases of initial conditions are used to verify the conclusions from Chapter 5, that the plasma stability is rather defined by nonlinear structures that might destabilize by non-conventional means. The growth could appear, for example, in terms of parameters other than amplitude of the eigenmodes of linearized Vlasov equation or by an effective mode conversion from ion dynamics dominated regime to electron dynamics dominated regime.

Analogous to the linearly undamped eigenmodes [$\phi(x)$], contained in an initial perturbation that get destabilized by phase-mixing-away the unsupported transient in the linear Vlasov evolution, the destabilization here is shown to take place of the undamped mode-coupled nonlinear structures [$\Phi(x)$] contained in an initial small amplitude phase-space eddy-like perturbation. When the latter are evolved in a linearly subcritical plasma, we see additionally undamped structures that obey the existing analytic description of such mode-coupled structures prescribed to replace discrete eigenmodes of the linearized approximate Vlasov equation in a nonperturbative exact plasma stability analysis. The coherent $\Phi(x)$ generated at a slower phase velocity is further seen to be destabilized by defying the sign of $\partial_v f(v_0)$ and grow, rather in their phase-velocity dimension than in their amplitude, to effectively mode convert into a more stable, ion acoustic electron hole. The linearly undamped modes, namely, the EPW and IAW modes excited by the initial perturbation are duly recovered to be stable because of the evolution done in

a subcritical drift regime, unlike the strong drift cases of Chapter 3 where ion acoustic mode displayed stronger growth while no phase-space eddy perturbation were seeded preventing independent electron hole structures to grow.

Unlike their evolution in the linearized Vlasov regime where the electron holes get treated as transient and immediately buried (or damped) in Sec. 5.2.3, the two identical initial perturbations of Secs. 6.3.1 and 6.3.2, differing merely in the initial velocity of their launch, show a remarkably distinct nonlinear evolution in which both the cases evolve not only to show electron holes as undamped structures alongside the undamped linear eigenmodes, the latter, slow initial perturbation case, undergoes a set of strong nonlinear hole instabilities as well.

Among two kinds of unstable evolution identified in the simulation at a faster and slower rate, respectively, in the first unstable phase the perturbation makes and approach to a set of undamped modes including an electron hole and the conventional linear plasma modes, namely the EPW and IAW. In the secondary stage of evolution these undamped structures interact with each other and further destabilize each other, parametrically. These two unstable phases of nonlinear structure growth/mode-conversion are described as two distinct instabilities, namely, the electron hole instability and a parametric instability arising from mutual coupling between the undamped linear and nonlinear structures.

In analytic description of the observed growth of undamped structure is provided where the basis of the mechanism is analyzed by employing the general nonlinear dispersion relation involving both electrons and ion response. It is quantitatively displayed that in a graphical characterization of the NDR, each curve corresponding to $k_0^2 = 0$ starts with a minimum velocity $0.03v_{the}$ showing that no SEH ($k_0^2 = 0$) solutions are possible bellow this velocity at corresponding temperature. The region below the curves representing solitary solutions of the formulations presents the solution for $k_0^2 > 0$ (providing harmonic waves and CEHs solutions) while the region above them is unstable with $k_0^2 < 0$, or imaginary values of k_0 (providing only monotonic or shock-like solutions) meaning unstable evolution of SEH-like undamped structures, as recovered in the later phase of slowly propagating initial perturbations.

The discrepancy of evolution in simulation visible with respect to the analytic characterization is traced in the ideal nature of the separatrix in the used SEH model. We find that despite the visible solitary nature of the simulated structures,

they are associated with finite k_0^2 class of ideal general solutions. Due to presence of a nonideal separatrix, these ideal high $|\beta|$, finite k_0^2 solutions misread the background plasma potential as rather deeper than ψ in simulation. In simulations, ψ is smaller when measured with respect to the value $\phi = 0$ of the plasma background. The ideal SEH model nevertheless analytically describes the unstable evolution of the SEH in the simulations, and perhaps in nature, with sufficient clarity, identifying their growth as driving major part of turbulence in the collisionless plasmas.

7.1 Future work

As mentioned in the Introduction, despite the non-conventional evolution and analytic formulation of the present study, the examples presented here make only a moderate excursion from the highly thermalized free and trapped particle distributions. The present study therefore suggest a large scope for future studies. A few of these relevant future problems are listed as below.

7.1.1 Advanced analytical model for Vlasov equilibria

Most of the nonlinear analytical models of stable trapped particle structures, for example those given by H. Schamel, T. H. Dupree and Lynden Bell [5, 6, 25], invoke the entropy maximization at various stages. While the first two follow Maxwellian-Boltzmann distribution, the third proposes a distinct statistics for the trapped particle distribution. A common factor in them,is that all the microstates of trapped particles corresponding to a most probable equilibrium state are indistinguishable. Therefor, the reversibility from a final state to initial state is generally disallowed. The coherent structures, observed in laboratory plasmas and space plasmas where entropy increases due to the collisions, are coincidentally well modeled by these approaches. However, nearly ideal collisionless Vlasov systems (pure Hamiltonian system), e.g., very hot stellar plasmas, conserve entropy, and therefore must show reversibility between initial and final states. The pure Vlasov equilibria may evolve like FPU (Fermi-Pasta-Ulam) phenomena [48] where instead of equipartition of energy from a large amplitude initial perturbation to its fundamental modes, they exhibit a rather unexpected recurrence phenomena to the initial structure after a certain time, unless the pool of microstates with identi-

cal looking macrostates are really large. This feature must affect the evolution of the structures such that two similar structures might respond differently to a single perturbation. Therefore, the stability of the kinetic collective structure is an important open question and better analytic models are needed for quantitative studies for the systems in the class of hot plasma turbulence.

7.1.2 Entropy of a phase space hole: a statistical approach

The deterministically evolving trapped particle distribution functions in computer simulations present a paradigm for the systems that approach a thermodynamical equilibrium by alternate means. Their isolated state or a weakly open dynamics with slow rate of entropy generation determines whether their final unique equilibrium-like state in each case results from a thermodynamical process or a reversible deterministic evolution. This aspect in the simulations needs to be explored by an ensemble based statistical approach where an entire ensemble with distinct initial conditions is subjected to a unique dynamical evolution and development of their macroscopic features is to be studied. This constitutes a potential future study for evolving Vlasov Poisson systems and their possible analogues.

7.1.3 Extended study of collective structures in 2D and 3D geometries

All the results presented in this thesis are outcome of 1D electrostatic Vlasov simulations. An extended version of this procedure is to be applied to multi dimensional (2D and 3D) study of the issues that are addressed here. In this relation, formation and comparison of phase space eddies or electron hole in 1D, 2D and 3D simulation of two beam plasma were studied by R. L. Morse and C. W. Neilson [82]. They reported that phase space eddies are formed in 1D, but in 2D and 3D they begin to get destabilized and disappear. More detailed studies are required to explore the evolution and interaction of coherent structures and their impact on turbulence in 2D and 3D cases, allowing to study its implications on the stability paradigm.

Study of wave particle interaction in relativistic limit through Vlasov approach remains an interesting and widely open area that can be studied using rather extensive simulations. The present explorations that make only a little excursion out of the conventional equilibrium limits present a large scope of advanced studies,

A

Linear fluid description of the plasma modes

A mutually exclusive relationship between coherence and linearity can be illustrated by means of a 1D linearized fluid treatment of the collisional plasmas. In this most primitive description ions are treated infinitely massive and therefore fixed ($m_i \to \infty$ or $\delta = T_i/T_e = 0$), and the electrons are described by their fluid equations, namely, the continuity, momentum balance (with an adiabatic pressure law) and Poisson's equation, which are in normalized form given by

$$\partial_t n + \partial_x(nu) = 0 \tag{A.1}$$

$$\partial_t u + u\partial_x u = \partial_x \phi - 3\partial_x n \tag{A.2}$$

$$\phi'' = n - 1. \tag{A.3}$$

For the background, i.e. without any excitation (amplitude $\psi \equiv 0$), we assume,

$$n = 1; \quad u = v_D; \quad \phi = 0.$$

For the case with excitation ($\psi > 0$) we solve the linearized version of (A.1)-(A.3) by the following Ansatz:

$$n = 1 + k^2\psi/2 + N(x - v_0 t); \quad u = v_D + U(x - v_0 t);$$
$$\phi = \Phi(x - v_0 t) \tag{A.4}$$

where the $(k^2\psi/2)$-term in n stems from the normalization constant. It accounts for a positive curvature of $\Phi(x)$ at potential minimum $\Phi = 0$ (as seen later from (A.5)) and is tailored such that to establish contact with linear wave theory in the harmonic wave limit. A more general discussion of the normalization constants in connection with the choice of the extrema of $\Phi(x)$ can be found in [36].

We then get from the continuity and momentum equation, respectively, $U = (v_0 - v_D)N$ and $U = \frac{\Phi - 3N}{v_D - v_0}$, from which follows by equality of both expressions: $N = \frac{\Phi}{3 - (v_D - v_0)^2}$. The insertion of N into Poisson's equation then yields

$$\Phi''(x) = \frac{k^2\psi}{2} - \frac{\Phi}{(v_0 - v_D)^2 - 3} =: -\mathcal{V}'(\Phi), \tag{A.5}$$

where we have introduced in the last step the pseudo-potential $\mathcal{V}(\Phi)$, which has been introduced to plasma physics presumably at first by [142] (see also [4, 98]).

It allows one to integrate Poisson's equation directly resulting in the pseudo-energy

$$\Phi'(x)^2/2 + \mathcal{V}(\Phi) = 0 \tag{A.6}$$

which yields by a quadrature $\Phi(x)$ whence $\mathcal{V}(\Phi)$ is known. In the present case we have

$$-\mathcal{V}(\Phi) = \frac{k^2\psi\Phi}{2} - \frac{\Phi^2/2}{(v_0 - v_D)^2 - 3}, \tag{A.7}$$

where we have assumed without the loss of generality $\mathcal{V}(0) = 0$. The existence of a solution then demands $\mathcal{V}(\psi) = 0$, which gives

$$k^2 - \frac{1}{(v_0 - v_D)^2 - 3} = 0. \tag{A.8}$$

This is the linear dispersion relation (LDR) since it determines the phase velocity of the structure v_0 in terms of k (and of v_D). Setting $v_0 = \omega/k$ one has then two solutions

$$\omega_\pm = kv_D \pm \omega_L \tag{A.9}$$

where $\omega_L := \sqrt{1 + 3k^2} \equiv \omega_L(k)$ is the k-dependent Langmuir frequency.

With the help of LDR the pseudo-potential simplifies to

$$-\mathcal{V}(\Phi) = \frac{k^2}{2}\Phi(\psi - \Phi),$$

(A.10)

being the standard expression of a single harmonic wave of wave number k. The corresponding wave solutions are hence given by

$$\Phi_\pm(x,t) = \frac{\psi}{2}\bigg(cos[k(x - V_D t) \mp \omega_L t] + 1\bigg),$$

(A.11)

which represent two Langmuir waves propagating in opposite direction in the frame moving with v_D. Time dependent solutions can be obtained by a linear superposition of such modes with in general different k, ψ and phases. The particular solution of two equally intense Langmuir waves counterpropagating against each other in the frame moving with v_D yields the well-known plasma oscillation

$$\Phi_{osc}(x,t) := \frac{1}{2}[\Phi_+(x - v_{0+}t) + \Phi_-(x - v_{0-}t)] =$$
$$\frac{\psi}{2}\bigg(cos(\omega_L t)cos[k(x - v_D t)] + 1\bigg),$$

(A.12)

which is oscillating in time with Langmuir frequency and non-propagating in the v_D-shifted Galilean frame. The corresponding pseudo-potential of this composite single harmonic wave with time-oscillatory amplitude becomes

$$-\mathcal{V}(\Phi_{osc}) = \frac{k^2}{2}\Phi_{osc}(\psi - \Phi_{osc}) - \frac{1}{2}\left[\frac{k\psi}{2}sin(\omega_L t)\right]^2.$$

(A.13)

The coherent nature of this solution is again expressed by the standard harmonic expression for $\mathcal{V}$, whereas the time dependent amplitude results in a time dependent base of $\mathcal{V}$. The field energy in one wavelength $\lambda = 2\pi/k$ of this solution is then found to be,

$$w(t) := \int_0^\lambda \frac{1}{2}E_{osc}^2 dx = \frac{\pi k\psi^2}{8}cos^2(\omega_L t),$$

(A.14)

which is oscillating in time and has a first maximum at $\omega_L t = \pi$. As a supplement we mention that the superposition of two unequal counterpropagting waves of

different amplitudes $\psi_\pm = \psi \pm \Delta\psi$ yields

$$\phi(x,t) = \frac{1}{2}\left(\psi(\cos X \cos T + 1) + \Delta\psi \sin X \sin T\right), \qquad (A.15)$$

with $X := k(x - v_D t) + \varphi/2$ and $T := \omega_L t + \varphi/2$, where φ is the phase difference between both waves. The field energy for this wave is found to be

$$w(t) = \frac{\pi k}{8}[\psi^2 \cos^2 T + (\Delta\psi)^2 \sin^2 T], \qquad (A.16)$$

and shows non-zero minima of $w(t)$. However, such a composite perturbation with a small amplitude mismatch already shows features of incoherency as a corresponding $\mathcal{V}(\Phi)$ does not exist. This gives us the opportunity to postulate an intimate relationship between the physical phenomenon "coherency" and its mathematical analog on "$\mathcal{V}(\Phi)$".

In rest of this thesis we shall denote, by $\Phi(x)$, the solutions for which a consistent, i.e. valid $\mathcal{V}(\Phi)$ exists and call them "coherent" structures, whereas we term solutions for which such a property is missing "incoherent" and denote them by $\phi(x)$. Other, more intricate, time-dependent solutions could be investigated as well by superposition of undamped modes of different wavelengths, intensities and phases with the ultimate goal of studying phase mixing and/or recurrence phenomena in such highly incoherent wave packets, for example. We note also that it would not be very difficult to consider nonlinear effects with $\psi \geq O(1)$, too, but this is not pursued further here because we put a limit on weak perturbations. In a perturbative treatment, valid under $\psi < 1$, nonlinearity would appear in $O(\psi^2)$ and therefore the more negligible the smaller ψ.

We close this subsection by mentioning that wave-particle resonance effects were omitted which implies large phase velocities $v_0 = \omega_L/k >> 1$ or small $k << 1$. To incorporate shorter wavelengths we have hence to leave the macroscopic fluid description and enter into the kinetic Vlasov description.

Bibliography

[1] H. Schamel. Cnoidal electron hole propagation: Trapping, the forgotten nonlinearity in plasma and fluid dynamics. *Phys. Plasmas*, 19:020501, 2012.

[2] B. D. Fried and R. W. Gould. Longitudinal ion oscillations in a hot plasma. *Phys. Fluids*, 4:139, 1961.

[3] I. B. Bernstein, J. M. Greene, and M. D. Kruskal. Exact nonlinear plasma oscillations. *Phys. Rev.*, 108:546, 1957.

[4] H. Schamel. Stationary solitary, snoidal and sinusoidal ion acoustic waves. *Plasma Phys.*, 14:905, 1972.

[5] T. H. Dupree. Growth of phase-space density holes. *Phys. Fluids*, 26:2460, 1983.

[6] D. Lynden-Bell. Statistical mechanics of violent relaxation in stellar systems. *Mon. Not. R. astr. Soc.*, 136:101, 1967.

[7] I. H. Hutchinson. Electron holes in phase space: What they are and why they matter. *Phys. of Plasmas*, 24:055601, 2017.

[8] D. Mandal and D. Sharma. Adiabatic electron response and solitary wave generation by trapped particle nonlinearity in a hydrogen plasma. *Phys. Plasmas*, 21:102107, 2014.

[9] D. Mandal and D. Sharma. Nonlinearly interacting trapped particle solitons in collisionless plasmas. *Phys. Plasmas*, 23:022108, 2016.

[10] H. Schamel, D. Mandal, and D. Sharma. On the nonlinear trapping nature of undamped, coherent structures in collisionless plasmas and its impact on stability. *Phys. Plasmas*, 24:032109, 2017.

[11] L. D. Landau. On the vibrations of the electronic plasma. *J. Phys. U.S.S.R.*, 10:25, 1946.

[12] N. G. van Kampen and B. U. Felderhof. *Theoretical Methods in Plasma Physics*. North Holland Co., Amsterdam, 1967.

[13] K. Saeki, P. Michelsen, H. L. Pécseli, and J. J. Rasmussen. Formation and coalescence of electron solitary holes. *Phys. Rev. Lett.*, 42:501, 1979.

[14] G Petraconi and H. S. Maciel. Formation of electrostatic double-layers and electron-holes in a low pressure mercury plasma column. *J. Phys. D: Appl. Phys*, 36:2798, 2003.

[15] S. Kar, S. Mukherjee, G. Ravi, and Y. C. Saxena. Possible excitation of solitary electron holes in a laboratory plasma. *Phys. of Plasmas*, 17:102113, 2010.

[16] H. Matsumoto, H. Kojima, T. Miyatake, Y. Omura, M. Okada, I. Nagano, and M. Tsutsui. Electrostatic solitary waves (ESW) in the magnetotail: BEN wave forms observed by GEOTAIL. *Geophys. Res. Lett.*, 21:2915, 1994.

[17] R. E. Ergun, C. W. Carlson, J. P. McFadden, F. S. Mozer, L. Muschietti, I. Roth, and R. J. Strangeway. Debye-scale plasma structures associated with magnetic-field-aligned electric fields. *Phys. Rev. Lett.*, 81:826, 1998.

[18] J. S. Pickett, L.-J. Chen, S. W. Kahler, O. Santolík, D. A. Gurnett, B. T. Tsurutani, and A. Balogh. Isolated electrostatic structures observed throughout the Cluster orbit: relationship to magnetic field strength. *Annales Geophysicae*, 22:2515, 2004.

[19] J. S. Pickett, J. D. Menietti, D. A. Gurnett, B. Tsurutani, P. M. Kintner, E. Klatt, and A. Balogh. Solitary potential structures observed in the magnetosheath by the Cluster spacecraft. *Nonlin. Processes Geophys.*, 10:3, 2003.

[20] J. S. Pickett, S. W. Kahler, L. J. Chen, R. L. Huff, O. Santolík, Y. Khotyaintsev, P. M. E. Décréau, D. Winningham, R. Frahm, M. L. Goldstein, G. S. Lakhina, B. T. Tsurutani, B. Lavraud, D. A. Gurnett, M. André, A. Fazakerley, A. Balogh, and H. Rème. Solitary waves observed in the auroral zone: the Cluster multi-spacecraft perspective. *Nonlin. Processes Geophys.*, 11: 183, 2004.

[21] H. L. Berk, B. N. Breizman, J. Candy, M. Pekker, and N. V. Petviashvili. Spontaneous hole-clump pair creation. *Phys. Plasmas*, 6:3102, 1999.

[22] M. Lesur and P. H. Diamond. Nonlinear instabilities driven by coherent phase-space structures. *Phys. Rev. E*, 87:031101, 2013.

[23] M. Lesur, P. H. Diamond, and Y. Kosuga. Nonlinear current-driven ion-acoustic instability driven by phase-space structures. *Plasma Phys. Controlled Fusion*, 56:075005, 2014.

[24] B. Eliasson and P. K. Shukla. Formation and dynamics of coherent structures involving phase-space vortices in plasmas. *Phys. Reports*, 422:225, 2006.

[25] H. Schamel. Stationary solutions of the electrostatic Vlasov equation. *Plasma Phys.*, 13:491, 1971.

[26] A. A. Vlasov. On the kinetic theory of an assembly of particles with collective interaction. *J. Phys. U.S.S.R*, 9:25, 1945.

[27] E. Fijalkow. A numerical solution to the Vlasov equation. *Comp. Phys. Communications*, 116:319, 1999.

[28] N. A. Krall and A. W. Trivelpiece. *Principles of Plasma Physics*. San Francisco Press Inc., San Francisco, 1986.

[29] P. K. Kaw and J. M. Dawson. Laser-induced anomalous heating of a plasma. *Phys. Fluids*, 12:2586, 1969.

[30] K. Nishikawa and Chin-Sheng Wu. Effect of electron trapping on the ion-wave instability. *Phys. Rev. Lett.*, 23:1020, 1969.

[31] E. Ott and R. Sudan. Nonlinear theory of ion acoustic waves with Landau damping. *Phys. Fluids*, 12:2388, 1969.

[32] T. M. O'Neil. Collisionless damping of nonlinear plasma oscillations. *Phys. Fluids*, 8:2255, 1965.

[33] H. Schamel. Role of trapped particles and waves in plasma solitons- theory and application. *Physica Scripta.*, 20:306, 1979.

[34] H. Schamel and S. Bujarbarua. Solitary plasma hole via ion-vortex distribution. *Phys. Fluids*, 23:2498, 1980.

[35] F. F. Chen. *Introduction to Plasma Physics*. Springer Science & Business Media, 2012.

[36] H. Schamel. Hole equilibria in Vlasov-Poisson systems: A challenge to wave theories of ideal plasmas. *Phys. Plasmas*, 7:4831, 2000.

[37] T. M. O'Neil and F. V. Coroniti. The collisionless nature of high-temperature plasmas. *Rev. Mod. Phys*, 71:S404, 1999.

[38] K. Saeki and H. Genma. Electron-hole disruption due to ion motion and formation of coupled electron hole and ion-acoustic soliton in a plasma. *Phys. Rev. Lett.*, 80:1224, 1998.

[39] H. L. Berk, C. E. Nielsen, and K. V. Roberts. Phase space hydrodynamics of equivalent nonlinear systems: Experimental and computational observations. *Phys. Fluids*, 13:980, 1970.

[40] B. D. Scott. Introduction to turbulence in magnetized plasmas. In A. Dinklage, Thomas Klinger, Garrit Marx, and L. Schweikhard, editors, *Plasma Physics: Confinement, Transport and Collective Effects*, chapter 8. Springer, Berlin Heidelberg, 2005.

[41] L. D. Landau and E. M. Lifshitz. *Fluid Mechanics, Course of Theoretical Physics*, volume 6. Pergamon Press, Amsterdam, 1959.

[42] W. L. Kruer. *The Physics of Laser Plasma Interactions*, volume 73. Addison-Wesley Publishing Co., Redwood City, CA, USA, 1988.

[43] F. L. Hinton and R. D. Hazeltine. Theory of plasma transport in toroidal confinement systems. *Rev. Mod. Phys.*, 48:239, 1976.

[44] L. McLerran. The physics of the quark-gluon plasma. *Rev. Mod. Phys.*, 58:1021, 1986.

[45] H. Schamel. Particle trapping: A key requisite of structure formation and stability of Vlasov-Poisson plasmas. *Phys. Plasmas*, 22:042301, 2015.

[46] T. H. Dupree. Theory of phase space density granulation in plasma. *Phys. Fluids*, 15:334, 1972.

[47] N. G. van Kampen. On the theory of stationary waves in plasmas. *Physica*, 21:949, 1955.

[48] N. J. Zabusky and M. D. Kruskal. Interaction of "solitons" in a collisionless plasma and the recurrence of initial states. *Phys. Rev. Lett.*, 15:240, 1965.

[49] D. J. Korteweg and G. de Vries. On the change of form of long waves advancing in a rectangular canal and a new type of long stationary waves. *Phil. Mag.*, 39:422, 1895.

[50] J.-M Grießmeier and H. Schamel. Solitary holes of negative energy and their possible role in the nonlinear destabilization of plasmas. *Phys. Plasmas*, 9: 2462, 2002.

[51] A. V. Gurevich. Distribution of captured particles in a potential well in the absence of collisions. *Soviet Physics JETP*, 26:575, 1968.

[52] H. Schamel. Kinetic theory of phase space vortices and double layers. *Physica Scripta.*, T2/1:228, 1982.

[53] H. Schamel. Electron holes, ion holes and double layers: Electrostatic phase space structures in theory and experiment. *Phys. Rep.*, 140:161, 1986.

[54] A. Luque and H. Schamel. Electrostatic trapping as a key to the dynamics of plasmas, fluids and other collective systems. *Phys. Rep.*, 415:261, 2005.

[55] J. Korn and H. Schamel. Electron holes and their role in the dynamics of current-carrying weakly collisional plasmas. Part 1. Immobile ions. *J. Plasma Phys.*, 56:307, 1996.

[56] J. Korn and H. Schamel. Electron holes and their role in the dynamics of current-carrying weakly collisional plasmas. Part 2. Mobile ions. *J. Plasma Phys.*, 56:339, 1996.

[57] B. Lefebvre, L.-J. Chen, W. Gekelman, P. Kintner, J. Pickett, and *et al.* Laboratory measurements of electrostatic solitary structures generated by beam injection. *Phys. Rev. Lett.*, 105:115001, 2010.

[58] W. Fox, M. Porkolab, J. Egedal, N. Katz, and A. Le. Laboratory observation of electron phase-space holes during magnetic reconnection. *Phys. Rev. Lett.*, 101:255003, 2008.

[59] A. A. Kabantsev, J. H. Yu, R. B. Lynch, and F. F. Driscoll. Trapped particles and asymmetry-induced transport. *Phys. Plasmas*, 10:1628, 2003.

[60] P. I. John and Y. C. Saxena. Propagation of ion acoustic solitons in plasma density gradients. *Phys. Letters A*, 56:385, 1976.

[61] J. D. Moody and D. F. Driscoll. Rarefaction waves, solitons, and holes in a pure electron plasma. *Phys. Plasmas*, 2:4482, 1995.

[62] P. L. Colestock and L. K. Spentzouris. The future of accelerator physics: The Tamura Symposium. In *AIP Conf. Proc.*, number 356, Austin, TX, 1996.

[63] M. Blaskiewicz, J. Wei, A. Luque, and H. Schamel. Longitudinal solitons in bunched beams. *Phys. Rev. ST Accel. Beams*, 7:044402, 2004.

[64] D. Boussard. Lecture notes on phys. In *Proc. Joint US-CERN Acc. School, Texas, 1986*, volume 296, page 289, Berlin, 1987. Springer.

[65] R. J. Pasquinelli. In *Proc. PAC 1995, Dallas,TX*, page 2379, Piscataway, NJ, 1995. IEEE.

[66] F. L. Scarf, L. A. Frank, K. L. Ackerson, and R. P. Lepping. Plasma wave turbulence at distant crossings of the plasma sheet boundaries and the neutral sheet. *Geophys. Res. Lett.*, 1:189, 1974.

[67] S. D. Bale, P. J. Kellogg, D. E. Larsen, R. P. Lin, K. Goetz, and R. P. Lepping. Bipolar electrostatic structures in the shock transition region: Evidence of electron phase space holes. *Geophys. Res. Lett.*, 25:2929, 1998.

[68] H. Matsumoto, X. H. Deng, H. Kojima, and R. R. Anderson. Observation of electrostatic solitary waves associated with reconnection on the dayside magnetopause boundary. *Geophys. Res. Lett.*, 30:1326, 2003.

[69] J. Pickett, L.-J. Chen, R. L. Mutel, I. W. Christopher, O. Santolík, G. S. Lakhina, S. V. Singh, R. V. Reddy, D. A. Gurnett, B. T. Tsurutani, E. Lucek,

and B. Lavraud. Furthering our understanding of electrostatic solitary waves through Cluster multispacecraft observations and theory. *Adv. Space Res.*, 41:1666, 2008.

[70] D. B. Graham, Yu. V. Khotyaintsev, A. Vaivads, and M. André. Electrostatic solitary waves and electrostatic waves at the magnetopause. *J. Geophys. Res.: Space Phys.*, 121:3069, 2016.

[71] F. S. Mozer, O. A. Agapitov, A. Artemyev, J. L. Burch, R. E. Ergun, B. L. Giles, D. Mourenas, R. B. Torbert, T. D. Phan, and I. Vasko. Magnetospheric multiscale satellite observations of parallel electron acceleration in magnetic field reconnection by fermi reflection from time domain structures. *Phys. Rev. Lett.*, 116:145101, 2016.

[72] L. Andersson, R. E. Ergun, J. Tao, A. Roux, O. LeContel, and *et al.* New features of electron phase space holes observed by the THEMIS mission. *Phys. Rev. Lett.*, 102:225004, 2009.

[73] C. Norgren, M. André, A. Vaivads, and Y. V. Khotyaintsev. Slow electron phase space holes: Magnetotail observations. *Geophys. Res. Lett.*, 42:1654, 2015.

[74] D. M. Malaspina, L. Andersson, R. E. Ergun, J. R. Wygant, J. W. Bonnell, and *et al.* Nonlinear electric field structures in the inner magnetosphere. *Geophys. Res. Lett.*, 41:5693, 2014.

[75] I. Y. Vasko, O. V. Agapitov, F. Mozer, A. V. Artemyev, and D. Jovanovic. Magnetic field depression within electron holes. *Geophys. Res. Lett.*, 42:2123, 2015.

[76] D. M. Malaspina, D. L. Newman, L. B. Willson III, K. Goetz, P. J. Kellogg, and K. Kerstin. Electrostatic solitary waves in the solar wind: Evidence for instability at solar wind current sheets. *J. Geophys. Res.: Space Phys.*, 118: 591, 2013.

[77] A. Mangeney, C. Salem, C. Lacombe, J.-L. Bougeret, C. Perche, and *et al.* WIND observations of coherent electrostatic waves in the solar wind. *Ann. Geophys.*, 17:307, 1999.

[78] J. D. Williams, L.-J. Chen, W. S. Kurth, D. A. Gurnett, M. K. Dougherty, and A. M. Rymer. Electrostatic solitary structures associated with the november 10, 2003, interplanetary shock at 8.7 au. *Geophys. Res. Lett.*, 32:L17103, 2005.

[79] L. B. Wilson III, C. A. Cattell, P. J. Kellogg, K. Goetz, K. Kersten, and *et al.* Large-amplitude electrostatic waves observed at a supercritical interplanetary shock. *J. Geophys. Res.: Space Phys.*, 115:A12104, 2010.

[80] Adnane Osmane, Drew L. Turner, Lynn B. Wilson III, Andrew P. Dimmock, and Tuija I. Pulkkinen. Subcritical growth of electron phase-space holes in planetary radiation belts. *The Astrophysical Journal*, 846:1–9, 2017.

[81] K. V. Roberts and H. L. Berk. Nonlinear evolution of a two-stream instability. *Phys. Rev. Letters*, 19:297, 1967.

[82] R. L. Morse and C. W. Nielson. One-, two-, and three-dimensional numerical simulation of two-beam plasmas. *Phys. Rev. Letters*, 23:1087, 1969.

[83] P. H. Shakanaka. Formation and interaction of ion-acoustic solitary waves in a collisionless warm plasma. *Phys. Fluids*, 15:304, 1972.

[84] V. L. Krasovsky, H. Matsumoto, and Y. Omura. Interaction dynamics of electrostatic solitary waves. *Nonlinear Proc. Geophysics*, 6:205, 1999.

[85] H. Schamel and A. Luque. Non-linear growth of trapped particle modes in linearly stable, current-carrying plasmas - A fundamental process in plasma turbulence and anomalous transport. *Space Sci. Rev*, 121:313, 2005.

[86] M. Lesur, Y. Idomura, and X. Garbet. Fully nonlinear features of the energetic beam-driven instability. *Phys. Plasmas*, 16:092305, 2009.

[87] P. Petkaki, M. P. Freeman, T. Kirk, C. E. J. Watt, and R. B. Horne. Anomalous resistivity and the nonlinear evolution of the ion-acoustic instability. *J. Geophys. Res.*, 111:A01205, 2006.

[88] M. Lesur, K. Itoh, T. Ido, S. I. Itoh, Y. Kosuga, M. Sasaki, S. Inagaki, M. Osakabe, K. Ogawa, A. Shimizu, K. Ida, and the LHD experimental group. Nonlinear excitation of subcritical fast ion-driven modes. *Nucl. Fusion*, 56: 056009, 2016.

[89] H. L. Berk, B. N. Breizman, and M. Pekker. Numerical simulation of bump-on-tail instability with source and sink. *Phys. Plasmas*, 2:3007, 1995.

[90] Y. Kosuga and P. H. Diamond. Drift hole structure and dynamics with turbulence driven flows. *Phys. Plasmas*, 19:072307, 2012.

[91] P. H. Diamond, S. I. Itoh, and K. Itoh. *Modern Plasma Physics*. Cambridge University Press, Cambridge, UK, 2010.

[92] B. Eliasson and P. K. Shukla. Formation and dynamics of coherent structures involving phase-space vortices in plasmas. *Phys. Reports*, 422:225, 2006.

[93] B. Eliasson and P. K. Shukla. Dynamics of electron holes in an electron-oxygen-ion plasma. *Phys. Rev. Lett.*, 93:045001, 2004.

[94] R. C. Davidson. *Methods in Nonlinear Plasma Theory*. Academic Press, 1965.

[95] T. Umeda. A conservative and non-oscillatory scheme for Vlasov code simulations. *Earth Planets Space*, 60:773, 2008.

[96] C. Z. Cheng and G. Knorr. The integration of the Vlasov equation in configuration space. *J. Comput. Phys.*, 22:330, 1976.

[97] M. Shoucri and R. R. J. Gagne. Numerical solution of the Vlasov equation by transform methods. *J. Comput. Phys.*, 21:238, 1976.

[98] R. Z. Sagdeev. Cooperative phenomena and shock waves in collisionless plasmas. *Reviews of Plasma Physics*, 4:23, 1966.

[99] A. Hasegawa. *Plasma Instabilities And Nonlinear Effects*. Springer, Berlin Heidelberg, 1975.

[100] R. J. Taylor, D. R. Baker, and H. Ikezi. Observation of collisionless electrostatic shocks. *Phys. Rev. Lett.*, 24:206, 1970.

[101] A. Hasegawa and T. Sato. Existence of a negative potential solitary-wave structure and formation of a double layer. *Phys. Fluids*, 25:632, 1982.

[102] T. Sato and H. Okuda. Ion-acoustic double layers. *Phys. Rev. Lett.*, 44:740, 1980.

[103] T. W. Johnston, Y. Tyshetskiy, A. Ghizzo, and P. Bertrand. Persistent subplasma-frequency kinetic electrostatic electron nonlinear waves. *Phys. Plasmas*, 16:042105, 2009.

[104] G. R. Smith and N. R. Pereira. Phase-locked particle motion in a large-amplitude plasma wave. *Phys. Fluids*, 21:2253, 1978.

[105] J. L. Tennyson, J. D. Meiss, and P. J. Morrison. Self-consistent chaos in the beam-plasma instability. *Physica D*, 71:1–17, 1994.

[106] I. Y. Dodin, P. F. Schmit, J. Rocks, and N. J. Fisch. Negative-mass instability in nonlinear plasma waves. *Phys. Rev. Lett.*, 110:215006, 2013.

[107] P. Rosenau and J. M. Hyman. Compactons: Solitons with finite wavelength. *Phys. Rev. Lett.*, 70:564, 1993.

[108] A. Fratalocchi, C. Conti, G. Ruocco, and S. Trillo. Free-energy transition in a gas of noninteracting nonlinear wave particles. *Phys. Rev. Lett.*, 101: 044101, 2008.

[109] A. R. Osborne. Behavior of solitons in random-function solutions of the periodic korteweg-de vries equation. *Phys. Rev. Lett.*, 71:3115, 1993.

[110] A. Costa, A. R. Osborne, D. T. Resio, S. Alessio, E. Chrivì, E. Saggese, K. Bellomo, and C. E. Long. Soliton turbulence in shallow water ocean surface waves. *Phys. Rev. Lett.*, 113:108501, 2014.

[111] I. Y. Dodin and N. J. Fisch. Adiabatic nonlinear waves with trapped particles. I. General formalism. *Phys. Plasmas*, 19:012102, 2012.

[112] R. R. Lindberg, A. E. Charman, and J. S. Wurtele. Self-consistent langmuir waves in resonantly driven thermal plasmas. *Phys. Plasmas*, 14:122103, 2007.

[113] J. M. Grießmeier, H. Schamel, and R. Fedele. Kinetic theory of periodic holes in debunched particle beams. *Phys. Rev. ST Accel. Beams*, 5:024201, 2002.

[114] S. B. Bujarbarua and H. Scahamel. Theory of finite-amplitude electron and ion holes. *J. Plasma Physics*, 25:515–529, 1981.

[115] B. D. Fried and S. D. Conte. *The Plasma Dispersion Function*. Academic Press, New York, 1961.

[116] Milton Abramowitz and Irene A. Stegun. *Handbook of Mathematical Functions with Formulas, Graphs, and Mathematical Tables*. Dover, New York, ninth dover printing, tenth gpo printing edition, 1964.

[117] D. J. Tetreault. Growth rate of the clump instability. *Phys. Fluids*, 26:3247, 1983.

[118] C. Mouhot and C. Villani. On Landau damping. *Acta. Math.*, 207:29–201, 2011.

[119] C. Villani. Particle systems and nonlinear Landau damping. *Phys. Plasmas*, 21:030901, 2014.

[120] J. Wesson. Landau damping. *Phys. Plasmas*, 22:022519, 2015.

[121] G. Belmont, F. Mottez, T. Chust, and S. Hess. Existence of non-Landau solutions for langmuir waves. *Phys. Plasmas*, 15:052310, 2008.

[122] R. H. Berman, D. J. Tetreault, T. H. Dupree, and T. Boutros-Ghali. Nonlinear instability and saturation of linearly stable current-carrying pair plasmas. *Phys. Rev. Lett.*, 48:1249, 1982.

[123] R. H. Berman, D. J. Tetreault, and T. H. Dupree. Simulation of phase space hole growth and the development of intermittent plasma turbulence. *Phys. Fluids*, 28:155, 1985.

[124] A. Luque, H. Schamel, B. Eliasson, and P. K. Shukla. Nonlinear instability and saturation of linearly stable current-carrying pair plasmas. *Phys. Plasmas*, 12:122307, 2005.

[125] Yu. V. Khotyaintsev, A. Vaivads, M. André, M. Fujimoto, A. Retinò, and C. J. Owen. Observations of slow electron holes at a magnetic reconnection site. *Phys. Rev. Lett.*, 105:165002, 2010.

[126] H. Schamel. Theory of solitary holes in coasting beams. *Phys. Rev. Lett.*, 79:2811, 1997.

[127] H. Schamel. Phase space vortices in unbunched beams in synchrotrons. *Phys. Scr. Vol.*, T75:23, 1998.

[128] H. Schamel and R. Fedele. Kinetic theory of solitary waves on coasting beams in synchrotrons. *Phys. Plasmas*, 7:3421, 2000.

[129] H. Karimabadi, V. Roytershteyn, H. X. Vu, Y. A. Omelchenko, J. Scudder, W. Daughton, A. Dimmock, K. Nykyri, M. Wan, and D. Sibeck *et al.* The link between shocks, turbulence, and magnetic reconnection in collisionless plasmas. *Phys. Plasmas*, 21:062308, 2014.

[130] F. Anderegg, C. F. Driscoll, D. H. E. Dubin, and T. M. O'Neil. Wave-particle interactions in electron acoustic waves in pure ion plasmas. *Phys. Rev. Lett.*, 102:095001, 2009.

[131] N. N. Bogolyubov. *Problem of a Dynamical Theory in Statisical Physics*. State Technical Press, Moscow, 1946.

[132] M. Born and H. S. Green. *A General Kinetic Theory of Liquids*. Cambridge, London, 1949.

[133] J. G. Kirkwood. The statistical mechanical theory of transport processes I. General theory. *J. Chem. Phys.*, 14:180, 1946.

[134] J. G. Kirkwood. The statistical mechanical theory of transport processes II. Transport in gases. *J. Chem. Phys.*, 15:72, 1947.

[135] J. Yvon. *La théorie des fluides et l'équation d'état: actualités scientifiques et industrielles*. Hermann et Cie, Paris, 1935.

[136] H. Schamel. Stability of electron vortex structures in phase space. *Phys. Rev. Lett.*, 48:481, 1982.

[137] H. Schamel. Comment on "undamped electrostatic plasma waves" [phys. plasmas 19, 092103 (2012)]. *Phys. Plasmas*, 20:034701, 2013.

[138] F. Valentini, D. Perrone, F. Califano, P. Veltri, P. J. Morrison, and T. M. O'Neil. Undamped electrostatic plasma waves. *Phys. Plasmas*, 19:092103, 2012.

[139] F. Valentini, D. Perrone, F. Califano, P. Veltri, P. J. Morrison, and T. M. O'Neil. Response to "comment on 'undamped electrostatic plasma waves'" [phys. plasmas 20, 034701 (2013)]. *Phys. Plasmas*, 20:034702, 2013.

[140] Y. W. Hou, Z. W. Ma, and M. Y. Yu. Trapped particle effects in long-time nonlinear Landau damping. *Phys. Plasmas*, 18:082101, 2011.

[141] Y. W. Hou, M. X. Chen, M. Y. Yu, B. Wu, and Y. C. Wu. Excitation and evolution of finite-amplitude plasma wave. *Phys. Plasmas*, 22:122101, 2015.

[142] L. Davies, R. Lüst, and A. Schlüter. The structure of hydromagnetic shock waves. *Zeitschrift für Naturforschung A*, 13a:916–936, 1958.